11-20-2015

Multidimensional Waveform Shaping in Multicarrier Systems

Ertugrul Guvenkaya
University of South Florida, ertugrul@mail.usf.edu

Multidimensional Waveform Shaping in Multicarrier Systems

by

Ertuğrul Güvenkaya

A dissertation submitted in partial fulfillment
of the requirements for the degree of
Doctor of Philosophy
Department of Electrical Engineering
College of Engineering
University of South Florida

Major Professor: Hüseyin Arslan, Ph.D.
Richard D. Gitlin, Sc.D.
Nasir Ghani, Ph.D.
Yao Liu, Ph.D.
Erdem Bala, Ph.D.

Date of Approval:
September 23, 2015

Keywords: Artificial noise, asymmetric pulse shaping, OFDM, PAPR reduction, sidelobe suppression

DEDICATION

To our martyrs.

ACKNOWLEDGMENTS

First, I would like to thank my advisor Dr. Hüseyin Arslan for his guidance, encouragement, and support throughout my study. I wish to thank Dr. Richard D. Gitlin, Dr. Nasir Ghani, Dr. Yao Liu, and Dr. Erdem Bala for serving in my committee and for offering valuable suggestions. I hope to be able to benefit from their profound knowledge and experience in the future, as well.

It has been a privilege to have the opportunity to do research as a member of the Wireless Communications and Signal Processing (WCSP) group at USF. I would like to thank my friends Ali Görçin, Alphan Şahin, M. Bahadır Çelebi, Anas Tom, M. Harun Yılmaz, Z. Esad Ankaralı, Ali Fatih Demir, Emre Seyyal and Emre Arslan for their support as friends and productive discussions as colleagues.

Special thanks to Alphan Şahin for his vigorous support and fruitful discussions. I would like to appreciate Ali Görçin's brotherhood, which I believe is another benefit of my PhD years. Also, I owe much to Yılmaz and Arslan families for their great hospitality which minimized the longing to my family and Turkish food.

Last, but by no means least, I would like to express my deepest gratitude to my parents Fatma Güvenkaya and Yaşar Güvenkaya and my dear sisters Şüheda and Asude Büşra for their unconditional support throughout these years. Especially, it is not possible to thank my beloved future wife, Büşra, enough for her unconditional love and her prayers. I am very grateful for having such a wonderful family. May Allah (swt) reward them all with blessings for ever.

TABLE OF CONTENTS

LIST OF TABLES

LIST OF FIGURES

ABSTRACT

Constantly increasing demand for wireless communications in various applications has always led to new ways of modulating the radio frequency (RF) carrier signal by advancing waveform structure throughout generations. Although communication data rates are limited by the theoretical capacity, specific signaling designs for the signal that experiences natural and artificial effects in the transmission medium such as multipath fading channel, hardware impairments and multiuser environment promised better solutions in providing improved wireless access to various type of users and networks. Besides communication capacity, broadcasting nature of radio signals poses the information security as another main concern in wireless communications. In this dissertation, new advanced methods for improving signal statistics in multiple domains are studied. Instead of focusing on a single aspect, the waveform design approaches studied in this dissertation tackle with improving the orthogonal frequency-division multiplexing (OFDM)-based signaling in multiple perspectives such as out-of-band (OOB) emission reduction, peak-to-average-power ratio (PAPR) reduction, and secure transmission with minimum or no effect at the receiver side. Various concepts are coherently exploited while achieving aforementioned goals with minimal cost such as unexplored spaces in the signal space like (CP), guard band, multipath fading; multivariate nature of the multicarrier signals; time spreading and location uniqueness of the wireless channels. The proposed techniques are analyzed theoretically and performance results are presented including related previous works in the literature. It is worth noting that the methods presented in the dissertation can be easily applicable to conventional OFDM systems thanks to having no or minimal change in the receiver structure.

CHAPTER 1:

INTRODUCTION

From smoke signals to transatlantic high definition video calls, wireless communication has been an essential part of both individuals and societies since the beginning of human history. Despite being an old practice, present understanding of wireless communication has been established with the experiments of Nicola Tesla that showed the possibility of energy transmission and telecommunication of information with radio frequency (RF) signals [1]. Then an half century later, Shannon [2] paved the way in exploring the limits of information transmission. Until today, emerging technological advances in computing devices and widespread use of wirelessly communicating user equipments that run data-demanding applications created a large amount of capacity requirement for wireless networks forcing the limits. In addition, recently arising application areas such as sensor networks, advanced metering, vehicular networks, remote health monitoring and data collection systems that benefit from wireless information transmission expanded the definition of user from *person* to *thing*. Thus, in todays world, communication scenarios include machine-to-machine and machine-to-person along with person-to-person. As expected, all of these new connections correspond to dramatic increase in the demand for wireless communication system resources, which is limited to available RF spectrum. Key factors in meeting these requirements in physical and network layer perspectives are high efficiency modulation/transmission techniques and dense frequency reuse, respectively.

Increasing the data rate yields using broader signal bandwidths. In order to maintain the scalable equalization complexity in frequency selective wireless channels, wideband transmission has been achieved via the use of multicarrier transmission [3–6]. Along with the efficient discrete Fourier transform (DFT) algorithms [7], practical implementation of frequency domain equalization (FDE) paved the way for orthogonal frequency-division multiplexing (OFDM): an orthogonal multicarrier

communication technique that can overcome many of the problems that emerge with the high data rate communications, most importantly multipath delay spread. OFDM and its variations are used as the signaling method for various communication standards including broadcasting standards such as Digital Audio Broadcasting (DAB) [8] and Terrestrial Digital Video Broadcasting (DVB-T2) [9], wired internet access technologies like Very-high-speed digital subscriber line 2 (VDSL2) [10] and Broadband over Power Line (BPL) [11] for asymmetric digital subscriber line (ADSL)-based and power line communications, respectively. More popularly, IEEE 802.11a/g/n/ac family of wireless local area network (WLAN) schemes use OFDM as their physical layer (PHY) transmission technique [12]. Good results in the WLAN networks encouraged the standard bodies to use OFDM in metropolitan-area networks (MAN) IEEE 802.16 (also known as Worldwide Interoperability for Microwave Access (WiMAX)) [13] and then fourth generation (4G) cellular networks (Long Term Evolution (LTE)) [14]. Finally, OFDM-based multicarrier solutions are also the strongest candidate for cognitive radio (CR) networks for its flexible spectral utilization and high reconfigurability [15].

While utilizing wider bandwidths, existence of many other users and various technologies that seek for new resources does not allow widening the signal spectrum in order to minimize the interference. However, conventional OFDM systems suffer from high out-of-band (OOB) spurious emission. In addition, high number of independently modulated subcarriers in OFDM creates large dynamic range in signal amplitude. Thus, high spreading along power domain causes signal distortion when it is subject to a nonlinear process such as power amplification at the transmitter. Considering these multiple constraints on multiple domains, advanced waveform design and signal manipulation methods should be able to deal with multiple of these issues jointly.

Due to broadcasting nature of the radio waves, wireless communication provides many benefits such as seamless connectivity, reduced infrastructure cost, support of mobility, and flexibility in communication range. Besides these advantageous, wireless transmission may lead to security vulnerabilities because of the lack of physical boundaries preventing the eavesdroppers, i.e., malicious receivers, from capturing the transmitted message. Thus, security in wireless communication has become one of the main concerns along with capacity requirements. Interestingly, multipath fading feature of the wireless channels inherently provides some signature properties due to ran-

dom scattering nature of the physical propagation environment. Thus, while designing transceiver algorithms and shaping waveform for signal quality purposes, the unique properties of the wireless channel can be exploited to secure the information transmission.

1.1 Scope of the Dissertation

The scope of this dissertation is to design multicarrier waveforms by focusing on reducing the spreading of the signal on multiple domains for enhancing signal quality and achieving physical layer security for data confidentiality. The chapters include performance results of the proposed schemes and comparisons with the available methods in the literature.

1.2 Contributions

Figure 1.1 depicts the domains and main concepts that are studied in this dissertation including the name of chapters that cover the regarding concepts. The focus and the main contributions of this research include the following perspectives.

1.2.1 Waveform Shaping in Time and Frequency Domains

In this research, we primarily focus on time and frequency domains while designing the multicarrier waveform with OFDM kernel. A windowing technique which provides optimal time-frequency containment and maximal adjacent-channel interference (ACI) rejection for OFDM-based systems is introduced. Instead of using a single pulse shape function for all subcarriers, multiple functions are considered in order to maximize the time-frequency containment of the OFDM waveform. The main strategy is to concentrate the spectrum of windowing functions into a given bandwidth while achieving maximum suppression in the out-of-band region. This is achieved by employing prolate-based windowing functions that provide optimal spectral concentration for time-limited pulse shapes. The windowing functions are designed per-subcarrier basis in order to exploit available concentration band for each subcarrier. In addition, the proposed concept is considered for the receive filtering in the presence of ACI. It is shown that the optimal spectral concentration property also maximizes ACI rejection for OFDM receivers. The contributions can be itemized as

- The design of optimum spectral concentration in a given guard band for minimum ACI suppression by introducing per-subcarrier windowing function design
- Optimum joint time-frequency concentration for pulse shaped OFDM that maximizes spectral efficient under a given spectral mask to be complied
- For given spacing between adjacent channels, achieving maximum ACI rejection with utilization of per-subcarrier receiver windowing for OFDM receivers

1.2.2 Waveform Shaping in Time and Frequency Domains with Wireless Channel

In this research, multipath channel and resulting delay spread profile are taken into account while performing waveform shaping in time and frequency. In OFDM systems, suppressing the OOB emission with pulse shaping comes with price. The expense emerges in designing the transition between consecutive symbols. The price can be either reduction of spectral efficiency (SE) with symbol extension for better transition, or introduction of inter-symbol and inter-carrier interference due to reduced cyclic prefix (CP) size. Under this concept of work, we propose a time-asymmetric and per-subcarrier pulse shaping method to minimize the introduced interference without sacrificing SE and OOB performances. Although time-asymmetric pulse reduces the interference due to shortened CP by exploiting the asymmetry in channel delay profile, it causes spectral growth. Thus, the time-asymmetry of the pulse shaping function is gradually increased for the inner subcarriers that have wider spectral room to OOB region. A generalized Kaiser window with adjustable time-asymmetry is introduced to the provided framework. Subcarrier specific interference and mean bit error rate (BER) are derived as a function of the employed per-subcarrier pulse shaping and channel delay profile. Analytical and simulation results showed that proposed technique achieves superior BER performance while achieving the same level of OOB suppression of pulse shaping and SE of conventional OFDM without pulse shaping. The specific contributions on this study can be given as

- Concept of time-asymmetric pulse shaping for OFDM subcarriers is introduced in order to reduce the inter-symbol interference (ISI)/inter-carrier interference (ICI).

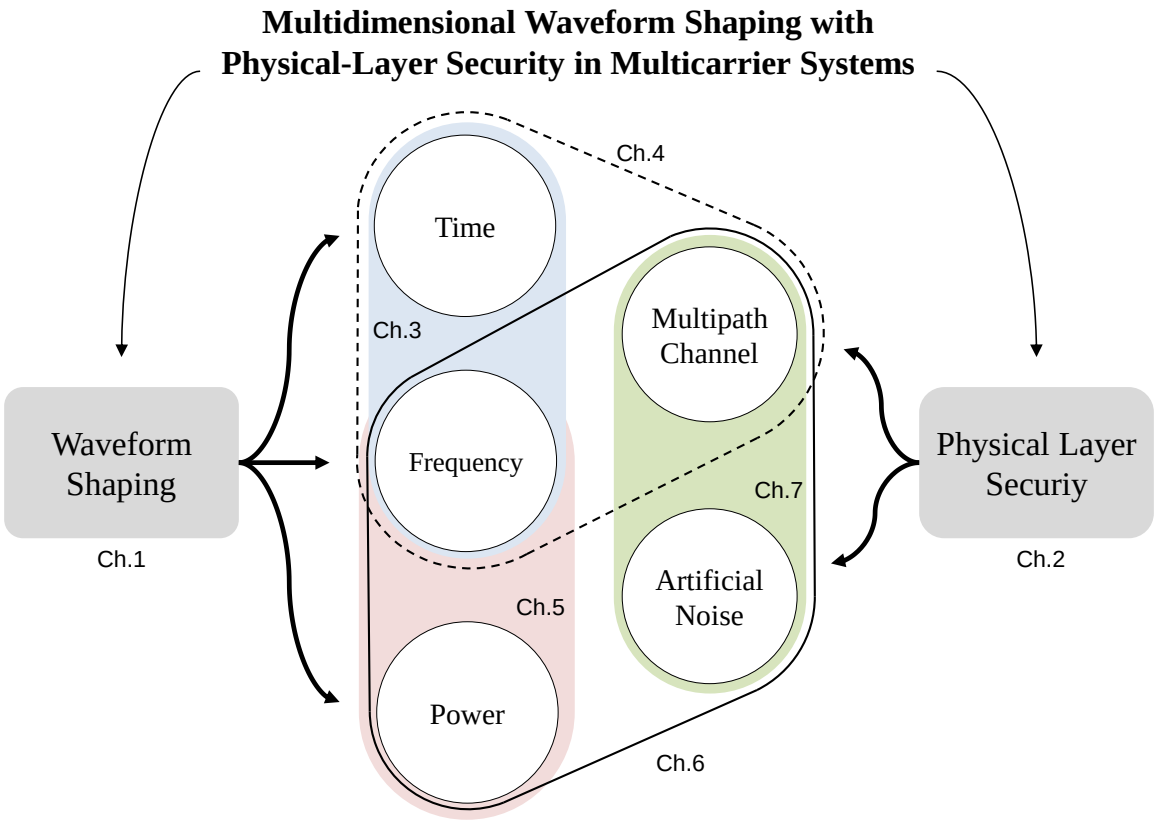

Figure 1.1 Outline of the dissertation that includes the domains and concepts that are studied. The chapters regarding to associated concepts are also highlighted.

- A practical and closed-form pulse shaping function with adjustable time-asymmetry is introduced as generalized Kaiser window (GKW).
- ISI/ICI - OOB trade-off in spectrally efficient pulse shaping is mitigated with per-subcarrier design of the time-asymmetric waveform that minimizes introduced interference while maintaining both OOB emission and SE.

1.2.3 Waveform Shaping in Frequency and Power Domains

In this research item, the dynamic range, peak-to-average power ratio (PAPR), of OFDM waveform is introduced into the waveform design criteria. It is known that OFDM waveform has its own drawbacks that affect application in practice: high OOB radiation and high PAPR. In this approach, a three-stage technique for the joint reduction of OOB radiation and OOB, therefore

minimizing the spectral regrowth after the power amplifier as well as signal distortion is proposed. In the first and the second stages, the OFDM data vector is partitioned into contiguous blocks that are naturally suited for PAPR reduction using partial transmit sequences (PTS). Since edge blocks/subcarriers have more impact on the OOB radiation, each edge block is further divided into smaller interleaved sub-blocks, and optimized phase rotations are applied to each sub-block to suppress the spectral sidelobes. Following the frequency domain techniques, optimum phase rotation for the time domain OFDM symbol is calculated to achieve smoother transition with the previous symbol, which further reduces the OOB spectrum. The proposed method improves the joint containment in frequency and power dimensions, along which the OFDM signal suffers from high spreading. The contributions in this part of the dissertation can be summarized as

- Joint sidelobe suppression and PAPR reduction with interleaved-block phase adaptation and PTS which coherently works for enhancing the transmitted signal quality in the presence of practical limitations
- Three stage method in mutually exclusive manner provides flexible implementation with minimal phase computation

1.2.4 Waveform Shaping in Frequency and Power Domains with PHY Security

This approach includes improvement on both waveform quality in all domains and the PHY security jointly. A signal superposition scheme is proposed that reduces OOB with satisfying symbol continuity, reduces PAPR while there is no adverse affect at the receiver since the superposed component is aligned with the null-space at the receiver. In addition, the superposed alignment component acts as artificial noise (AN) and distorts the received signal at eavesdroppers. The scheme incorporates multipath channel and N-continuous OFDM structure. By exploiting the inevitable guard periods between OFDM symbols, i.e., CP, the correction component which maintains symbol continuity is aligned with the CP duration after passing through the multipath channel. Thus, the proposed method enables disturbance-free data subcarriers at the receiver while maintaining the continuity of OFDM symbols. This is achieved by the generalization of conventional N-continuous with using more degrees-of-freedom stemming from the CP duration. In addition to

continuity, the remaining degrees-of-freedom is used for reducing PAPR of the transmitted symbol. As it eliminates the interference on the data symbols caused by the correction term, it yields no modification at OFDM receiver, which makes the proposed scheme backward-compatible to conventional OFDM receivers. However, unintended receivers, i.e., eavesdroppers, will experience high interference since the correction term is not aligned with their channel that is unique to the location. This corresponds to AN and provides secure transmission in the PHY layer.

- Joint sidelobe suppression, PAPR reduction and PHY layer security in OFDM systems that does not suffer from data rate reduction and adverse affect on legitimate receivers
- Closed form solution for the OOB reduction without loss in spectral efficiency and received signal quality
- Along with aligning the correction term with channel and CP duration, N-continuity is achieved without a need for additional processing at the receivers such as adaptive decoding

1.2.5 Waveform Design for PHY Security Using Fade-Avoiding Artificial Noise

In this research, frequency selectivity of the wireless channels are exploited for providing secure transmission. The random nature of fading channels is an enabling factor for achieving secrecy against eavesdropping. An adaptive transmission scheme in which the faded subchannels of the legitimate channel are not used for conveying information is introduced. Thus, capacity reduction in legitimate channel is minimized while causing a reduction of the eavesdropper channel capacity proportional to the unused subchannels. Besides improving communication secrecy with the intelligent subchannel usage, populating the unused subchannels with artificially-generated noise that further disturbs the eavesdropper's reception is proposed. Since each receiver has its own channel state information (CSI) but not other's, eavesdroppers cannot discard the distortion which is integrated into the transmitted signal as a function of the legitimate pair's CSI. Positive secrecy capacity and outage probabilities are provided as well as error performance example in a communication scenario. It is showed that while careful usage of the subchannels in frequency

selective channels improves the secrecy, introducing the fade-filling noise creates an error floor for the malicious nodes. The contributions on this approach can be itemized as

- Derivation of outage secrecy capacity for introduced subchannel deactivation scheme
- Creating pseudo nullspace in single-input single-output (SISO) channels with adaptive faded subchannel deactivation
- Integration of AN with fade avoiding subchannel usage for enhanced security

1.3 Dissertation Outline

As it is also depicted in Figure 1.1, this dissertation consists of eight chapters in which the Chapter 1 provides introduction and a short overview of the multicarrier waveforms. In Chapter 2, we present a comprehensive overview of PHY-layer security metrics, concepts and techniques before introducing PHY-layer security approaches in waveform design in Chapters 6 and 7. In Chapter 3, waveform shaping dealing in time and frequency domains via a windowing technique which provides optimal time-frequency containment and maximal ACI rejection for OFDM-based systems is presented. Then in Chapter 4, the second order statistics of the multipath channel is introduced into the waveform design by proposing a time-asymmetric and per-subcarrier pulse shaping method to minimize the introduced interference without sacrificing SE and OOB performances in OFDM systems. After the first two approaches that are based on designing the pulse shape in OFDM system without manipulating the data symbols, the rest of the dissertation includes data-dependent techniques where the waveform improvement is achieved by manipulating the data symbols in some form. In Chapter5, a joint sidelobe and PAPR reduction scheme with block-based phase rotation is presented that impacts both frequency and power domains. Then, the security is introduced into the multi-functional waveform design in Chapter 6 where CP-aligned N- continuity with PAPR reduction and PHY security with AN is proposed. In Chapter 7, a secure transmission method that considers frequency selective fading as a degree of freedom to insert AN into the transmission is presented. Finally, Chapter 8 concludes the dissertation along with discussion of possible future research areas.

CHAPTER 2:
PHYSICAL-LAYER SECURITY CONCEPTS AND METRICS IN SIGNAL TRANSMISSION

2.1 Introduction

The communication between distant entities requires exposing the message to outside world in some form of signal transmission. When the physical propagation medium between the transmitter and receiver is not perfectly secured, information transmission comes with confidentiality issues. That is, the transmitted signal is subject to be captured by an unintended third entity with not so good intention, i.e., eavesdropper. Security risk in the propagation can be due to protocol-based such as shared medium, or physical phenomenons such as wireless propagation of radio waves. In particular to wireless systems, although broadcasting nature of the radio waves provides benefits such as connectivity, support of mobility, and flexibility in communication distance, wireless transmission leads to security vulnerabilities due to the lack of physical boundaries preventing the eavesdroppers from capturing the transmitted message.

The key of achieving secure communication to put the eavesdropper at a relative disadvantage compared to legitimate receiver [16]. This can be performed by some cooperation between transmitter and receiver such as encryption/decryption, which has been a widespread method for securing the data in both storage and transmission phases. The other approach is to exploit the discrepancies in the physical characteristics of the propagation environment. Namely, nonidentical observations of the transmitted signal by the legitimate and illegitimate receivers, e.g., via wireless channel, location, and antenna configurations can be the enabling factor for secure communication.

Fundamentals of the secure communication are laid by Shannon [16]. Perfect secrecy in communication is defined as the condition that observation of the signal by an eavesdropper does

not provide any information about the secret message without any assumption on processing power and time. Shannon showed that this is achievable only if the secret key that is used for encryption is at least as large as the message itself. One time pad cryptography is a well-known example of perfect secure system [17]. This result is based on the assumption that the legitimate receiver and eavesdropper have identical observation on the signal. In other words, Shannon's limit is for the cryptographic approaches where all receiver nodes access the same signal without any additional effect [18]. The fact that cryptographic techniques reside in the upper layers of the communication stack supports this assumption since the data is assumed to be acquired from lower layer in an error-free manner [19].

When propagation medium is wireless channel, it is known that the signals captured by legitimate receiver and eavesdropper pass through different paths and experience distinct imperfections. After decades of Shannon's results, the secrecy under this condition was studied by Wyner [20]. Wire-tap channel is defined where the wire-tapper, i.e., the eavesdropper in wireless case, experiences a degraded version of the legitimate receiver's channel. Wyner revealed that it is possible to conduct a perfectly secure communication without using secrecy keys, but only when the main channel is relatively better than the eavesdropper's channel. Hence, the information theoretic notion of perfect secrecy has started the era of physical layer (PHY)-security, which is based on exploiting any form of physical characteristics in the nature of signal propagation in favor of legitimate nodes.

The path that Shannon and Wyner have opened in the secure communication constructs the theoretical limits on the secrecy of the systems. In other words, they follow the information-theoretic principles that generally deal with *how much one can secure the communication*, rather than *how to do it*. That is, practical aspects of the secure communication systems are also crucial along with the theoretical limits, which include the secure transmission techniques, assumptions on the systems nodes, and the practical metrics.

In this paper, we make a comprehensive review for the fundamental stages of information transmission and corresponding requirements from the PHY layer security perspective in the presence of eavesdropper. These stages and requirements are explained by representing the information

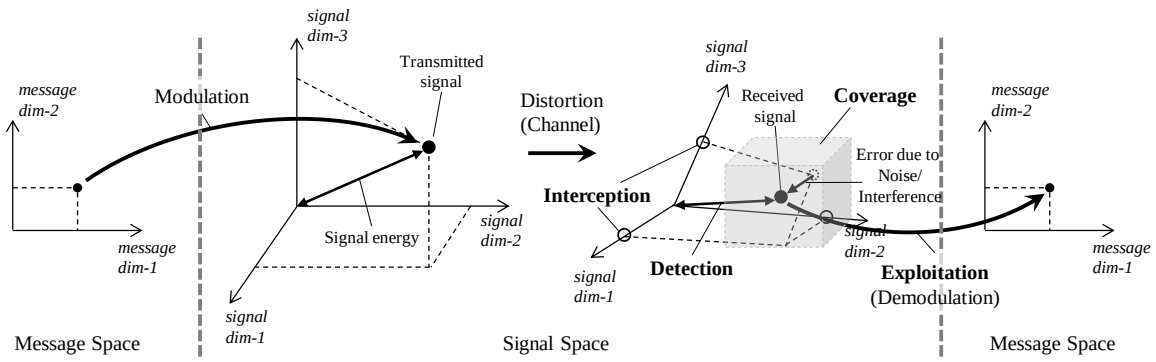

Figure 2.1 Information transmission consists of mapping operations from message space to signal space at transmitter, channel effect with distortion via warping the signal space and addition of noise, and mapping back to message space at the receiver.

and the signals as points in the multidimensional message and signal spaces [2]. While eavesdropper can satisfy some of the requirements via having prior knowledge about the signal properties, the presented framework covers any type of knowledge level during the signal reception. Then, fundamental performance metrics for evaluating the security level along the mentioned stages are surveyed. We cover both information theoretic considerations and practical measures including both existing approaches and recent considerations.

It is convenient to note here the names of the entities in communications with the secrecy concern. We adopt *Alice* as legitimate transmitter that intends to send the secret message to the legitimate receiver, namely *Bob*. Then, the third node, which is assumed to be a passive eavesdropper Eve, aims to obtain the secret message content. The outline of the paper is as follows: In Section 2.2, we present the fundamental steps to be completed for an arbitrary eavesdropper. Then, main performance metrics for the security, including both information theoretic and practical measures are surveyed in Section 2.3. Finally, conclusions are given in Section 2.5.

2.2 Reception Stages with Eavesdropper

Information transmission can essentially be modeled as a series of transform operations. It includes mapping the information in message space to a waveform into the signal space at the transmitter, and the reverse operation at the receiver [2]. As illustrated in Figure 2.1, this well-

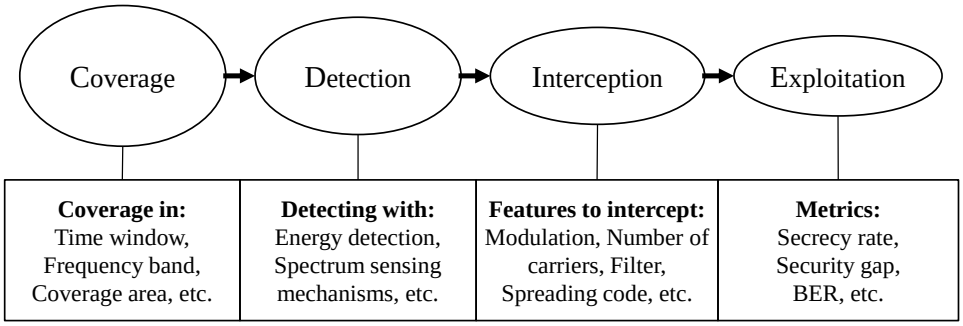

Figure 2.2 Stages of the overall reception mechanism at the eavesdropper.

known representation can also be applied in the presence of an eavesdropper. When the security is concerned in transmission, making the de-mapping operation a hard task for the eavesdropper becomes one of the main requirement along with effective transmission between the legitimate pair.

As an adversary receiver, eavesdropper can posses different levels of prior knowledge on the legitimate signal transmission. For instance, Eve can have as much information as the legitimate receiver including transmission time, frequency, bandwidth, transmit filter, modulation format. On the other hand, she can have less information about the signal, e.g., only the spectral location and bandwidth, in other scenarios. Depending on the situation in this spectrum of knowledge levels, an eavesdropper has to satisfy certain conditions and pass through stages for a successful signal reception. In this section, we review the four main requirements, which an eavesdropper should already satisfy or attain via additional algorithms, as depicted in Figure 2.2: Coverage, Detection, Interception, and Exploitation. Some examples for each stage are also summarized in the figure.

2.2.1 Coverage

Transmitter's main operation is to map the source information in the message space to the a particular signal in the signal space. Thus, a signal is represented as a point in the multidimensional space as shown in Figure 2.1. This can also be regarded as electrospace, where each axis denotes time, frequency, space, code, etc.

The first requirement for an eavesdropper is the having the sufficient capability for capturing the transmitted signal. That is, the reception window of Eve needs to cover the signal of interest. As an example, the time window that eavesdropper is active must cover the frame of

signal observed at the reception after passing through the channel. In addition to time, another domain of coverage is the spectrum. Receiver spectral window that is determined by the carrier frequency and the bandwidth should cover the transmitted signal band. In the multidimensional notion, this translates into the condition that Eve's reception subspace, illustrated as shaded region in Figure 2.1, should include the point which represents the signal after the channel. By satisfying this condition, eavesdropper can make observations that can result in a detection of the secret message. For the eavesdroppers with prior knowledge on signal properties regarding to coverage, this requirement is naturally satisfied via adjusting the reception parameters accordingly.

2.2.2 Detection

Knowing that the possible region of the signal under interest are covered, the next step is to decide if the signal is actually transmitted or not. The detection operation is a common problem in communication, specifically in cognitive radio (CR) systems that requires detection of other users' presence in the network via spectrum sensing mechanisms [21]. In general, detection can be connected to the energy of the signal that receiver examines via energy detection. In that respect, the detection performance is connected to the distance between the point representing the signal and the origin in the message space, which is illustrated in Figure 2.1. Note that the power of the signal along a particular dimension in the signal space, compared to other dimensions, can be significantly different for transmitted and the received signal. This is because of the warping effect of wireless channel on the signal space. For instance, consider a broadband signal passing through a frequency-selective channel that can be represented as multiple orthogonal subchannels with flat fading [22]. In this case, each subchannel becomes a dimension in signal space in Figure 2.1, and selective fading on each subchannel creates the effect of warping. Thus, the overall energy of the received signal determines the detectability of the existence of the signal in the presence of additional effects that create uncertainty in the exact position. That is, channel distortion is critical with noise and interference. The closer the point is located to the origin at Eve (and the farther for Bob), the lower probability for eavesdropper (the higher probability for Bob) to come with a successful binary decision about the signal's presence.

2.2.3 Interception

After detection, further information about the transmitted signal is required for a reliable reception. The transmit filter type, modulation format, number of subcarriers for multicarrier signaling, utilized code sequence for spread spectrum signals are examples of signal features that the eavesdropper needs to intercepted for a reliable decoding of the message. In other words, having prior knowledge on these properties can be considered as Eve having possible locations of the points in the multidimensional space. After detecting the signal covered by the receiver, these interception parameters provide the knowledge of all possible points that the signal resides in the signal space. The exact location of the corresponding point among other possibilities indeed provides the information content of the digitally modulated message. In spread-spectrum signals as an example, the knowledge of the spreading code clears the confusion of the receiver except possible locations in finite alphabet signal map, e.g., quadrature amplitude modulation constellation points.

2.2.4 Exploitation

The final stage is essentially a regular demodulation process with the assumption that all information about the signal is known except the modulated information. Hence, the exploitation of the signal at the end can be the decoding of the intercepted signal where conventional demodulation process, i.e., de-mapping the point in the signal space into message space as in Figure 2.1, occurs. The success in this stage is directly related to the amount of disturbance on the actual signal due to noise and interference. Thus, the aim in the secure transmission is to make the signal observed at eavesdropper more noisy while keeping the distortion at the legitimate receiver minimum. As an example, a common technique is the insertion of artificial noise in the transmitted signal [23], by exploiting the dimension reduction at the receiver. The additional distortion component, artificial noise (AN), is selected from the nullspace of the intended receiver's channel, and hence, it disappears after passing through the wireless channel of the legitimate receiver. This eliminates the adverse effect on the reception performance for Bob. However, since AN is not aligned to the nullspace of the eavesdropper's channel, it creates uncertainty on the actual location of the transmitted signal. The concept of AN is illustrated in Figure 2.3 in a 2×1 multiple-input single-output (MISO)

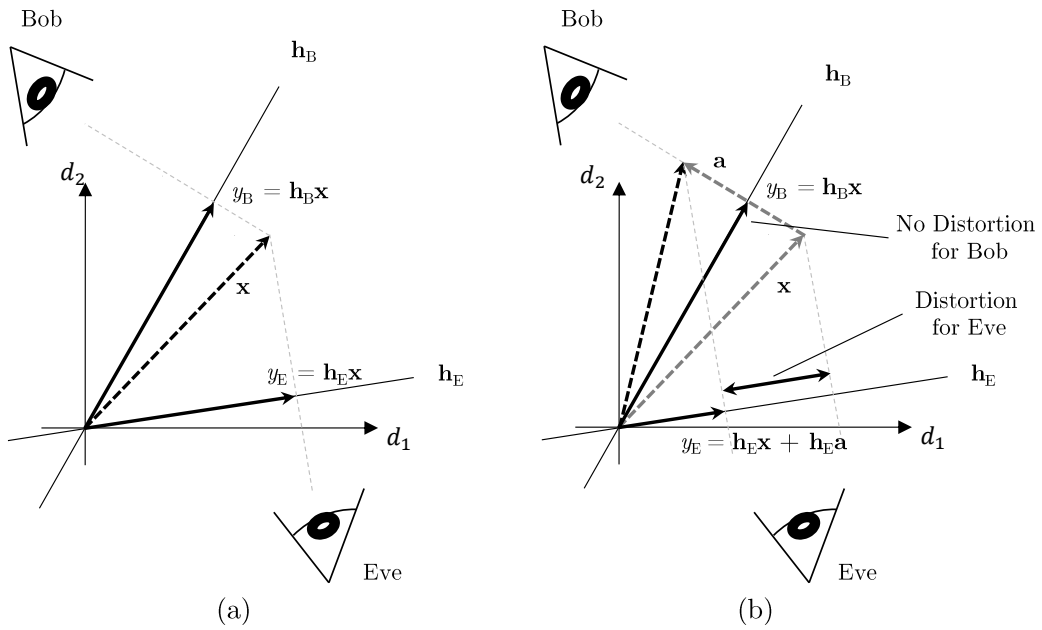

Figure 2.3 (a) 2×1 MISO communication system where two dimensional transmitted signal $\mathbf{x}$ is mapped to one dimensional received signals y_B and y_E along the direction channels $\mathbf{h}_\mathrm{B}$ and $\mathbf{h}_\mathrm{E}$, respectively. (b) Artificial noise component $\mathbf{a}$ is selected along the orthogonal direction to the channel of Bob. Thus, the additional distortion is not observable by the legitimate receiver while it causes distortion at illegitimate receiver Eve.

transmission where the transmitter has more antennas than each receiver in order to achieve a nonzero nullspace for the channels. In other words, a the receiver with single antenna, combination of the signals from two transmit antennas corresponds to dimension reduction in the signal space from 2 to 1. Thus, the two dimensional signal in $d_1 - d_2$ plain is mapped to a point in one dimensional space. Then, after the channel, the main aim is to introduce additional distortion on the signal observed by Eve. In other words, as two observers of the transmitted message in the signal space, indented receiver exploits the signal effectively while for the eavesdropper's demapping operation is much more challenging due to additional uncertainty on the observed signal from her perspective.

In general, the secrecy of the communication is measured from the exploitation perspective. This is because Eve is assumed to posses the same level of prior knowledge on the signal. Thus, the discrepancy between Bob and Eve is observable in the last stage. In the following sections, we will discuss the fundamental metrics to measure the security in the system.

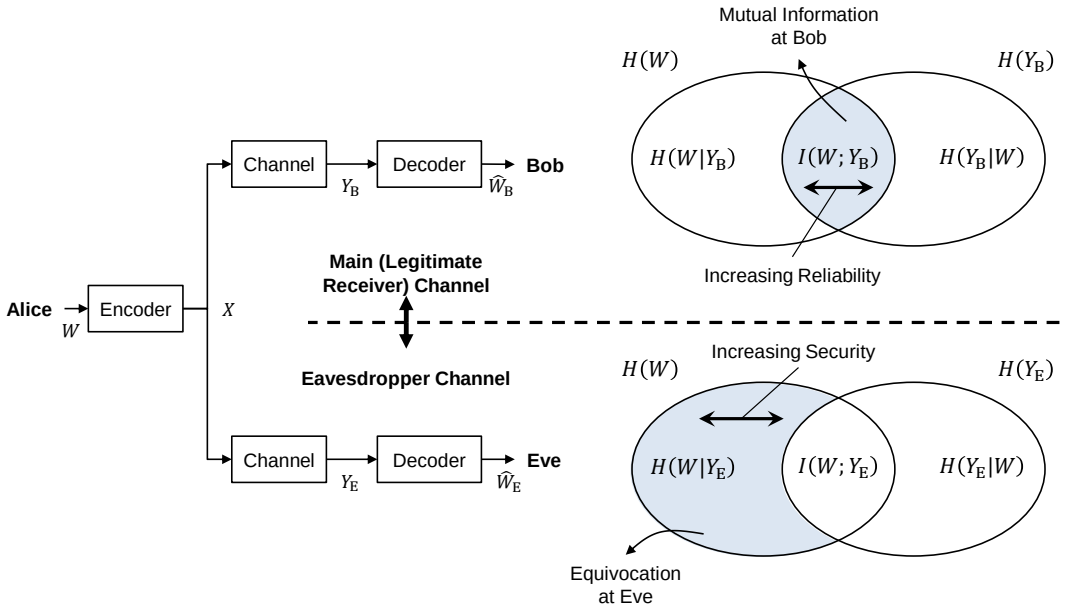

Figure 2.4 Information-theoretic measures. The main aim is to increase the mutual information in main channel for reliability, while minimizing the mutual information (maximizing the equivocation) at Eve for security. Secrecy rate is the difference between mutual informations, which is desired to be maximized.

2.3 Performance Metrics

Either for investigation of the limits of secrecy in a given system, or for evaluation of level of secrecy for a proposed scheme as well as for maximizing it, some numerical metrics have been developed most of which are adopted, or derived from the conventional communication metrics such as channel capacity, signal-to-noise ratio (SNR), and bit error rate (BER). The measures for the secrecy of the system can be considered under two main categories. The first type is information theoretic measures that do not specify a certain communication signaling and protocol, but generally consider the limits of the secrecy which is independent of the applications and underlying procedures. The second type is based on practical measures where the secrecy level is quantified by the metrics that can be observed in practical communication scenarios.

2.3.1 Information-Theoretic Measures

2.3.1.1 Equivocation and Secrecy Rate

The principles of secret communication in information-theoretic sense is constructed by the Shannon's definition for information content, i.e., entropy, which quantifies the unpredictability of a signal as a random variable [24], and defined as

$$H(W) = \mathrm{E}[I(W)] = \mathrm{E}[-\ln(P(W))]. \tag{2.1}$$

where $I(W)$ describes the information content of W. The relations between the information theoretic terms and the secrecy of the communication is illustrated in Figure 2.4. For main channel, the mutual information between the message and received signal, $I(W;Y_{\mathrm{B}})$, is the amount of information that Bob obtains about the message W by observing the received signal Y_{B}. This quantifies the reliability in the communication in terms of data rate, maximum of which is known to be the channel capacity [24]. For the eavesdropper channel, conditional entropy of the message W given that the received signal Y_{E} is known quantifies the amount of information needed to describe the message W. This is also referred as *equivocation*, $H(W|Y_{\mathrm{E}})$, that corresponds to the confusion of eavesdropper on the received signal. Clearly, increasing the equivocation at Eve improves the security of the message. In other words, the unpredictability of Y_{E}, that is not originated from the message W, is the result of independent distortions on the signal such as noise and interference. Hence, increasing the level of distortion on Eve's corresponds to increasing the amount of information needed to determine W from Y_{E}.

Therefore, the main goal in designing the communication system with secrecy constraints is to increase the mutual information between the transmitter and legitimate receiver which stands for the reliability in communication, while maximizing the uncertainty at the eavesdropper which paves the way for the security objectives. In other words, by using the identity that the total entropy of the signal is constituted by the mutual information and the equivocation at Eve, i.e., $H(W) = I(W;Y_{\mathrm{E}}) + H(W|Y_{\mathrm{E}})$, the parameter that is desired to be maximized is the *secrecy rate*

defined as

$$R_s = I(W; Y_{\mathrm{B}}) - I(W; Y_{\mathrm{E}}). \tag{2.2}$$

The maximum achievable secrecy rate over input distributions for the transmitted signal X, which is a function of the coding process, is given as the *secrecy capacity*. That is, the secrecy capacity can be represented as

$$C_s = C_{\mathrm{B}} - C_{\mathrm{E}}. \tag{2.3}$$

where C_{B} and C_{E} are the capacity of the Alice-Bob and Alice-Eve channels [20, 25, 26].

2.3.1.2 Secrecy Outage Probability

Randomness of the physical environment due to uncertainty in some factors such as the locations of nodes, shadowing and multipath-fading effect changes the signals observed by each node in a random manner. Thus, the aforementioned metrics become random variables as well. In such situations, statistical measures are generally adopted to represent the randomness of the environment itself on top of the information. For example, the secrecy outage probability can be defined as the probability that the instantaneous secrecy capacity falls below a target secrecy rate R_s^{t}, as

$$P_{\mathrm{out}}(R_s^{\mathrm{t}}) = P(C_s < R_s^{\mathrm{t}}). \tag{2.4}$$

In such environments that the randomness in the system parameters does not allow a deterministic secrecy metric, the performance of the system can be measured via outage probability [25], which is the better the lower for a given secrecy rate target.

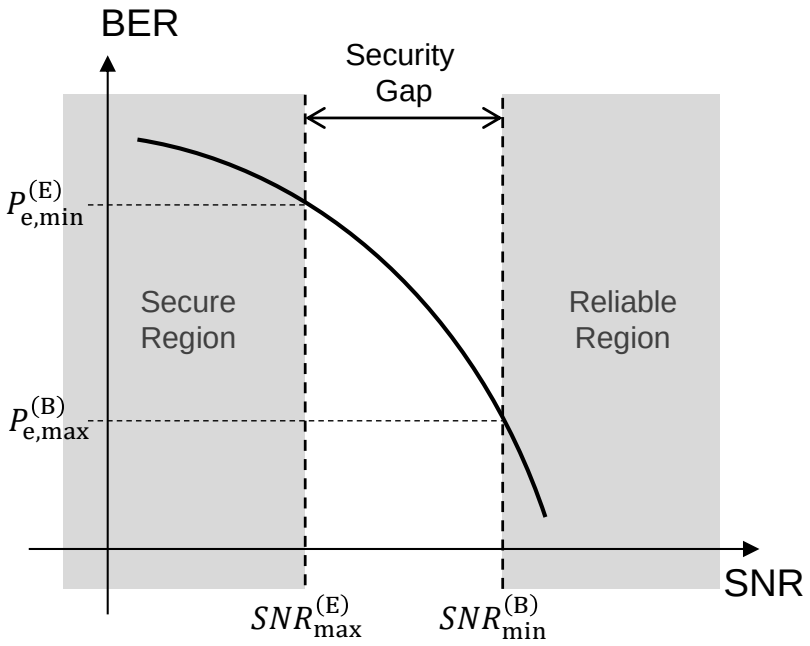

Figure 2.5 Security gap when both receivers are assumed to have identical BER performance.

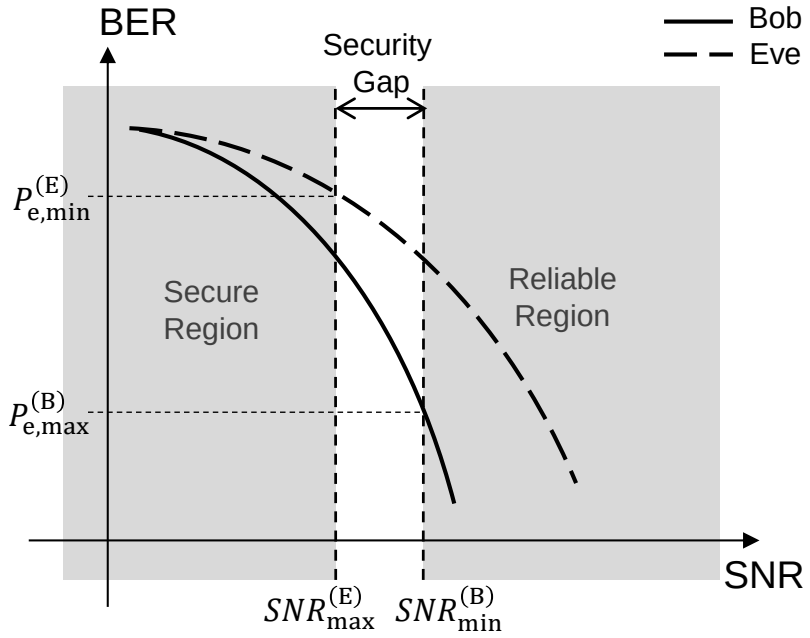

Figure 2.6 Generalized security gap when the Bob and Eve have different BER performances.

2.3.2 Practical Measures

2.3.2.1 Security Gap

Although secrecy capacity is a common metric for security of the communication, it is difficult to realize and measure in practical communication scenarios where non-Gaussian codes and finite block lengths are used. This is also the main reason for not having practical codes with finite length that achieve the secrecy capacity. Thus, although the fact that both the secrecy capacity and equivocation rate provide important estimates of secrecy, when practical coding and modulation schemes are adopted, the metrics that can be mapped to easily measurable parameter, e.g., BER, emerge as valuable alternatives of measuring the security. After several decades of information-theoretic notion, a practical approach to determine a quantitative measure, *security gap*, is introduced in [27] and [28]. Although it does not address the information theoretic measure, the security gap quantifies the secrecy level of the communication environment based on BER performances at Bob and Eve, which is much easier to analyze in practice. The security gap is defined as

$$S_{\mathrm{g}} = SNR_{\mathrm{min}}^{(\mathrm{B})} - SNR_{\mathrm{max}}^{(\mathrm{E})}, \tag{2.5}$$

which is the difference between the minimum SNR level of Bob to achieve reliable reception and the maximum SNR at Eve that guarantees a certain level of BER, which is generally desired to be close to 0.5. As illustrated in Figure 2.5, two regions; reliability region where Bob operates with a certain maximum BER, $P_{\mathrm{e,max}}^{(\mathrm{B})}$, and secure region where Eve is desired to operate not to achieve a certain BER, $P_{\mathrm{e,min}}^{(\mathrm{E})}$, that can provide sufficient information about the original message. In other words, the gap between these two SNR levels denotes the channel quality advantage that Bob has to have over Eve for satisfying the practical notion of the secrecy in transmission.

In order to reduce the security gap for given reliability and security requirements, it is clear that the steepness of the BER curve needs to be increased. In other words, a remarkable increase in BER even with a small degradation in Eve's channel is desirable. Introducing coding with puncturing [27, 28] and non-systematic coding with scrambling [29–32] are common approaches for increasing the steepness of BER curve resulting in smaller security gap.

As it can be seen in Figure 2.5, identical BER performance profile for both legitimate receiver and the eavesdropper is generally assumed while determining the security gap. However, the error rate performance can possess different characteristics due to different perceptions of Bob and Eve. This can be due to natural effects such as different fading statistics with distinct multipath distribution for two receivers, e.g., line-of-sight (LOS) and non-LOS [33], or artificial effects such as AN differently effecting legitimate and illegitimate receivers [23]. Thus, the concept of security gap can be extended into general case where Bob and Eve experience different BER vs SNR characteristics. Note that since we consider fading, the SNR in the generalized case corresponds to mean SNR. As it is illustrated in Figure 2.6, the security gap is determined by the SNR levels as a functions of Bob's and Eve's own environmental conditions. It is worth noting that the security gap with this consideration can even be negative. In other words, the conditions that make secure communication possible when even Eve has better SNR than Bob can be represented in terms of the security gap.

2.3.2.2 Bit Error Rate

Being a widespread measure of reliable communication, BER can also be used to quantify the security performance within a practical point of view. While various functions of BER can be set, a simple cost function as an example can be defined as

$$Cost = \frac{P_{\mathrm{e}}(\text{desired receiver})}{\min\left(P_{\mathrm{e}}(\text{undesired recevier})\right)} \tag{2.6}$$

which is a parameter to be minimized for increasing the security in the system. In the concept of directional modulation [34, 35], the arguments of the error probabilities in (2.6) is considered for desired and undesired direction, respectively.

2.3.2.3 Low Probability of Interception (LPI) / Detection (LPD)

Considering the stages discussed in Section 2.2 as random events with associated success probabilities, the probability of a transmitted signal to be exploited by an eavesdropper can be

given as

$$P(E) = P(E|I)P(I|D)P(D|C)P(C) \tag{2.7}$$

where $P(C)$ denotes the probability of coverage, $P(D|C)$, $P(I|D)$, and $P(E|I)$ are the conditional probabilities of; detection given that the signal is covered, interception given that the signal is detected, and exploitation given that the signal is intercepted, respectively. The task of PHY security techniques is minimizing the probability of exploitation, $P(E)$, via decreasing its one or more probability components, i.e., multiplicands in (2.7).

- *Probability of interception:* The probability that an eavesdropper locates this point, i.e., probability of interception, is another parameter for the security measure. As a general term, the interception can be considered in time-frequency dimension for spread-spectrum techniques [36, 37] where the waveform features such as spreading or hopping sequence becomes the key for successful interception for eavesdropper. In directional signal transmission schemes, this can be in the space domain where the eavesdropper has to intercept in terms of angular location to be able to extract the message. When the mapping operation is tied to the multipath fading channel response, the knowledge of channel state information (CSI) between the transmitter and legitimate receiver can open the path to interception [38] in which the transmission is subject to LPI. Thus, in wireless systems where most of the parameters are random variables, the LPI on a domain based on the security technique stands for a general measure for the level of security. Functionally, probability of interception is analogous to the mutual information between the legitimate transmitter and eavesdropper, which is also desired to be minimized for achieving positive secrecy from the information-theoretic viewpoint [16].

- *Probability of detection:* The term low-probability-of-detection (LPD) is commonly defined as the probability of correctly detecting the presence of communication between the legitimate pair. In other words, LPD is a function of covertness of the communication that is taking place [39], and commonly referred with the concept of spread-spectrum where the power

density of the signal is decreased with spreading and directional transmission techniques where the signal power for undesired directions is reduced [40].

2.4 PHY Techniques Against Eavesdropping

2.4.1 Time/Frequency-Based Techniques

This section is devoted to the techniques that are based on signal manipulations in time/ frequency domain that does not exploit the degrees of freedom provided by the spatial domain, or the wireless channel.

2.4.1.1 Spread-Spectrum LPI/LPD Approaches

In contrast to effort of sending the information by packing into a small area in time/frequency grid, spreading the information along a wide band provide lowering the density of signal energy in a given band. Although the spread spectrum (SS) possess various benefits such as robustness against jamming [36], frequency diversity [41], the motive in the eavesdropping threads is the signal covertness with low-probability-of-interception (LPI) and low-probability-of-detection (LPD). While LPD property comes from the energy spreading possibly making power density to fall under the noise level of the eavesdropper, pseudorandom sequence that is used to spread the information signal to a wideband provides the LPI for the signal [42]. In other words, the coordinates of the point in the signal space is determined by the spreading sequence which is assumed to be known only by the legitimate pairs, and hence acts as a shared secret key [36].

When the wideband information transmission is considered, benefits of SS reduces due to reduced space for spreading gain for a given available bandwidth for transmission [40, 43]. Although the individual symbols can be under the noise level that makes it hard to detect via energy detection based methods, evaluation of second [44] or higher order statistics [45] such as qumulant [46] and kurtosis [47], and determining the likelihood to Gaussian distribution by negentropy [48] makes it possible to detect the existence of spread spectrum signals. On top of the signal detection, the secret key property is subject to be exposed because the direct-sequence multiplication using the same sequence reveals some weaknesses in terms of blind estimation where the spreading codes generated

by linear-feedback shift register (LFSR) may be estimated by eavesdroppers from their received signals [49]. Thus, LPI and LPD of spread spectrum signal is effective on eavesdroppers having no information about the spreading sequence which can hardly hold in practical scenarios [50].

2.4.1.2 Coding Techniques

Secrecy analysis from information-theoretic perspective presents that there exist some coding schemes achieving perfect secrecy with the rate of secrecy capacity [20]. However, no practical schemes with finite code length is known to achieve the secrecy capacity. Thus, investigation of practical coding schemes taking into account the secrecy constraints has been a recent approach [27–32]. For instance, low-density parity-check (LDPC) codes are first studied in the context of secure transmission in [27, 28]. To increase rate of BER growth with degrading channel condition, i.e., SNR, puncturing is introduced in the coding process with the price of increase in transmit power. The error amplification characteristic of the scrambling is exploited in [29] that also reduces the power dissipation caused by puncturing. The scheme is then extended with combination with concatenation and HARQ [31], in order to achieve reduced the security gap by which the legitimate receiver has to lead.

The fading channels in which the SNR is a random variable itself is studied in security gap analysis in [32]. The reliability and security thresholds are defined based on the outage probabilities for a desired BER. Main issue in fading case in terms of security gap, as can be inferred from slow decaying BER compared to additive white Gaussian noise (AWGN) case, is that the gap required over a fading channel is quite large. However, as in the AWGN case, the security gap in multipath fading scenarios can be reduced through the use of scrambling [31] and error correction coding [27, 28]. Depending on the application requirements and channel conditions, practical coding schemes can be employed as a standalone solution, or they can be conjugated with existing cryptographic scheme operating on higher layers of the protocol stack [28].

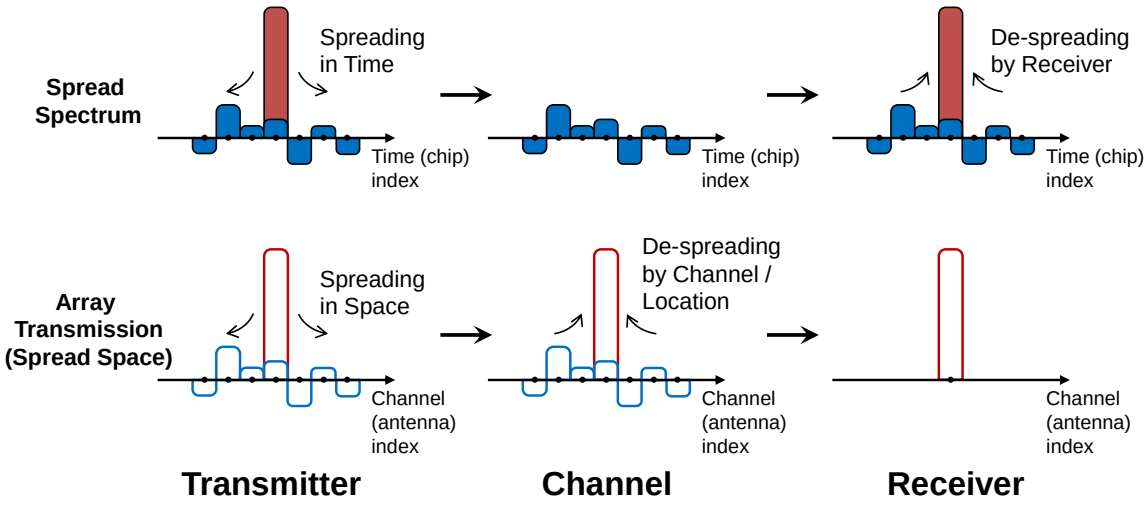

Figure 2.7 While the information is spread along time (of frequency) in SS and de-spread by the receiver, the dimension where the information is spread in array transmission is space in which the de-spreading is inherently done by the channel itself.

2.4.2 Directional Transmission

One of the simplest approaches in dealing with the broadcasting effect in radio frequency (RF) propagation is to introduce directional transmission. Historically, focusing the total radiated energy along a specific direction has been motivated by enhancing the range of communication as well as suppressing the RF power in undesired directions. This inherently helps managing the interference to neighboring systems, i.e., co-channel interference, and finds usage in commercial systems such as cellular to increase frequency reuse in the form of sectorization [41] without introducing new base station towers, and in wireless local area network (WLAN) systems by reducing interference to other networks via transmit beamforming [51].

Considering the challenge in the wireless information transmission security, shrinking the geographical area where the received signal is exploitable plays a critical role in prevention of eavesdropping. Hence, the directional selectivity in the signal transmission has been a well-known countermeasure. Focusing the radiated RF power along a specific direction can be done via various types of antennas such as horn, parabolic, and Yagi antennas [52, 53]. Adaptivity on the antenna radiation pattern and direction becomes crucial when security is the concern. Thus, security-driven directional transmission can be regarded after the advances in phased antenna arrays, which is a

widespread technique known for more than a century [54]. In what follows, the main approaches in providing security in the angular sense are outlined.

2.4.2.1 Array Beamforming

The key idea in array-based directional transmission is to introduce time or phase offset between antenna elements such that the sinusoidal signals add constructively along the desired direction while the combination of the signals from antenna elements occurs destructively, which determines the radiation pattern of the array [55]. In other words, instead of transmitting the signal with a single antenna, the available transmit power is spread across the multiple antennas along with associated weights to align the phase of each path along the same direction for the intended receiver. Spreading the signal in spatial domain indeed shares the same fundamentals as the spread spectrum transmission. As illustrated in upper part in Figure 2.7, the information symbol that can be sent in a short duration for a given system bandwidth is spread across time domain with some associated weights in SS technique[1]. Then, the receiver accumulates the symbol energy by correlating the received signal with the locally available PN sequence. On the other hand, the transmitter spreads the signal energy across space domain in the form of array precoding as given in lower part in Figure 2.7. However, despreading occurs in the RF stage (at the antenna) in contrast to SS case where the despreading occurs in baseband. That is, the *processing gain* of SS is analogous to *array gain* in the array beamforming schemes.

Although the spread spectrum and spread-space (array beamforming) lie on the same base, they differ in practical setting with security consideration. Detecting and decoding the message for an eavesdropper is a matter of having knowledge on the spreading code, which is possible to be estimated blindly even if it is not available. However, for the methods that are strongly tied to the spatial signatures of the intended receiver, e.g., array response, getting in touch with the message requires overcoming the *physical* barriers for the eavesdropper rather than having soft information used in time/frequency basis. That is, an eavesdropper has to be located in the close vicinity with the intended receiver to be able to surpass the PHY security guard.

[1]Note that the spreading can also be considered in frequency domain when we fix the duration of narrowband signal.

The security gain by conventional phased array directional transmission techniques is limited to decreasing the received signal strength along undesired directions. That is, only the power of the signal is suppressed along undesired directions. When we consider the information content, which is conveyed via digital modulation, this corresponds to the shrinking and rotating the constellation in other directions of reception. In other words, although the transmission is directional, the modulation is still omni-directional [56]. Hence, this has no influence on eavesdropper other than capturing lower signal energy. More critically, even though eavesdropper lies on the direction where the power is suppressed, secure transmission would not possible if she is more close to the transmitter enjoying comparable, or even higher, SNR than Bob. Thus, more advanced approaches such as directional modulation has been proposed recently, as reviewed in the next section.

2.4.2.2 Directional Modulation

In order to provide selectivity in the signal pattern on top of the received power as in directional transmission, the techniques that result in selectivity in the modulation structure are studied [34, 57–59] for enhancing the security in the directional sense. Switched-spaced antennas are first introduced to generate directionally-modulated signal in [57]. For a two-antenna case, selection between the antennas is done by a binary code sequence which makes the antenna-level modulation transparent to the wavefront direction. The propagation delay difference between two antennas corresponds to a two-point constellation scheme in which the pattern of modulation points is determined by the direction of the receiver. Also, instead of trying to suppress in one direction, the authors propose focusing the modulation to a desired direction via tapped-delay line antenna array which is driven by a coded sequence with low autocorrelation. By doing so, coherent combination along the desired direction with appropriate delays amplifies the processing gain while non coherent combinations with low autocorrelation suppresses the modulation information in other directions. One physical challenge in directional modulation with the delay-tapped line arrays is that the chip rate required to have a sufficient delay between signals can be very high for a given antenna spacing.

Unlike to actively manipulating multiple antennas via different selections, phases, and delays, one driven antenna accompanied by multiple passive parasitic elements are utilized to distort

the signal along undesired directions [58, 59]. The parasitic elements act as switch or varactor controlled reflectors. Thus, change in the near field characteristics by altering antenna parasitic is used to modulate the signal in the far field. Antenna level modulation with near filed reflections indeed correspond to creating an artificial multipath fading effect in the far field. However the fundamental difference is that the directional fading effect is controlled actively at the transmitter in contrast to regular multipath fading case where no control on the reflections is possible due to randomness of the physical propagation medium. While modulating the signal after power amplifier provides advantage in peak-to-average power ratio (PAPR) by feeding the power amplifier (PA) with unmodulated carrier, one of the main challenges, which originates from the near field nature of the transmission, appears to be high computation and time burden of finding the switching combinations for parasitic elements that result in desired constellation point in the intended direction [34, 59]. Also, since shaping the power spectral density (PSD) of the signal is determined by the symbol transitions, transmitter needs to lower the symbol rate to allocate some of the inter-symbol switching states for shaping the transition.

Simpler methods of introducing directional modulation by using conventional arrays instead of near-field antenna configurations [59] is proposed in [34, 35, 60]. In addition to multi-directional transmission to multiple users by finding appropriate phase shift values for array elements, authors motivate the technique for secure transmission where the constellation is distorted in all directions except that of the desired receiver. In [60], authors use reconfigurable antenna elements, in contrast to phase shifters, each of which has a certain radiation pattern for three modes of operation. Thus, the resulting pattern closely follows the superposition of individual patterns. For achieving desired constellation in the desired direction all states of each element is configured resulting in exhaustive search for each desired direction.

In contrast to phase shifters [34, 35] and switches [57, 60] with multiple antennas, authors in [50] use only two directional beams to be utilized for in-phase and quadrature parts of the signal. Relying on the difference of the radiation patterns of the beams, directional selectivity for the superposed signal is achieved. However, the level of directivity when using two beams is expectedly limited, which is not desired from security perspective.

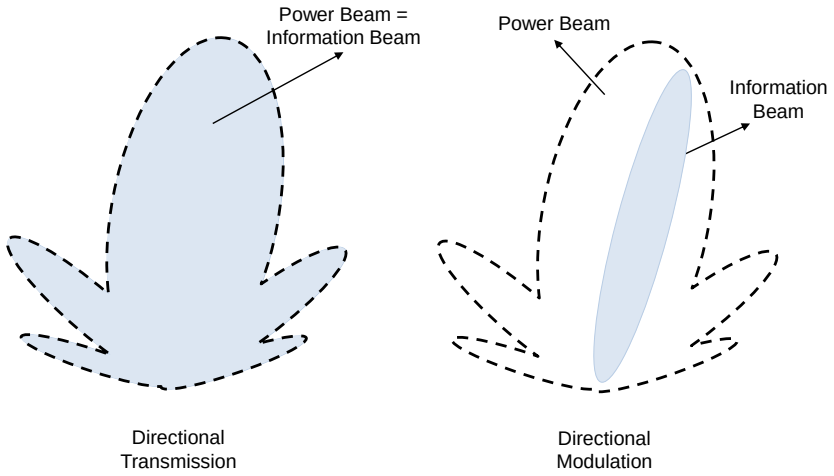

Figure 2.8 Directional transmission vs directional modulation. While the pattern beam and information beam are identical in conventional array beamforming, directional modulation schemes directs the modulation, i.e., information, into desired region that can be different from the radiation pattern of the array.

The LPI property of spread-spectrum technique is enhanced with LPD by combining directional transmission with spread spectrum in [61]. In each chip duration, one antenna subgroup is activated that changes the phase center of the array. Since the index of activated subgroup is determined by the value of corresponding chip, the receiver along the desired direction observes conventional spread spectrum signal. However, the phase values in each chip duration results in arbitrary value due to different phase weights of antennas subgroups along other directions. Therefore, by achieving randomization of spreading code in space domain, an eavesdropper along undesired direction cannot get the processing gain even she has the information about the spreading code used.

A general characteristic in directional modulation techniques is to focus on creating selectivity on the signal constellation. As illustrated in Figure 2.8, the information beam pattern and power beam pattern are separated meaning that the energy higher received signal power does not necessarily mean more information about the message. This distinction is also valid for more advanced versions of array transmission given in the sequel.

With the directional modulation, the structure of the constellation pattern is aimed to be distorted for eavesdroppers along undesired directions. However, for the receivers which can adapt

the symbol-to-bit mapping procedure to decode arbitrary constellation mapping, manipulating the location of the constellation points associated to symbols with directional modulation cannot be effective. That is, this can create weakness where the eavesdropper can perform maximum likelihood (ML)-type detection after determining the distorted constellation blindly or by training with reference symbols. For that reason, selectivity in other dimension in addition to space, i.e., time, is creates the degree of freedom for the aforementioned issue, as discussed in the next section.

2.4.3 Randomized Space-Time Transmission

Communication security is enabled via properly designed selectivity across different dimensions that makes the reception of the signal at the eavesdropper a hard task. For spatial dimension, on top of the selectivity in signal power across direction and modulation, time dimension can also be used as a domain for creating selectivity. That is, the degree of freedom from the antenna redundancy, i.e., having more antennas at transmitter than the receiver, can be used to change the constellation manipulation at the symbol rate. This is performed by randomly updating the array precoding vector (beamforming weights) at the modulation rate, rather than the channel fading rate. [56]

In [62], the conventional phased array systems with main beam is directed towards the intended receiver via progressive phase shifts. However, instead of feeding the array elements with single modulated signal, each element is fed with a Walsh sequence appropriate polarity to construct a pulse position modulation (PPM) signal when the sequences are combined coherently, which happens in desired direction with phased array precoding. For the undesired directions, on top of the distortion on the PPM signal that will be due to noncoherent combination of the Walsh sequences, transmitter randomly remixes the mapping between code sequence and array element to introduce time randomization for undesired direction. Since the array precoding aligns each signal to the same direction, changing the order of antenna does not induce a time variation on the desired direction. Instead of randomizing the effective channel for unintended directions via changing the antenna order with symbol rate, [63] introduces the antenna activation as a way of introducing unpredictable changes in the undesired directions. Since the number of active antennas

is kept constant during transmission, coherent combination on the desired direction does not induce any change in the array response while different antenna subsets in each symbol transmission corresponds to different channel that cannot be traced since the rate is same as the symbol rate. Although the array response at the receiver is a multiplicative effect, the concept of randomized space-time transmission with the randomization rate same as symbol rate is analogous to one-time pad encryption [16] where one pad key corresponds to randomly changing effective channel response.

The nullspace of the multi-antenna channels is exploited to design time-varying transmit beamformers that result in a constant channel to the receiver, but a random time-varying channel for the eavesdropper. The space-time randomization is performed via array precoding in [43, 64–67]. Transmitted signal from each individual antenna is multiplied with such a randomized weight that the effective MISO channel between Alice and Bob will be constant while the effective channel between Alice and Eve is randomized at each symbol transmission. In order to exploit antenna array redundancy as an advancement to zero forcing (ZF)- or eigen-beamforming in the array transmission, the expected transmit power needs to be increased in space-time randomization approaches [43, 64–67]. Although it is considered under the field of AN, the method proposed in [56] corresponds to the time varying beamforming weight randomization. Since the mixing matrix is constant during transmission, conventional AN methods are in principle prone to blind source separation techniques when equipped with sufficient number of receiver antennas to obtain a determined systems of equations.

The uncertainty in time for the undesired direction has been considered as the fourth dimension of the array on top of the first three spatial dimensions in [68]. By just switching some of the antenna elements on and off with a specific rate the received symbol along undesired directions will have additional variation in amplitude and phase independent of the variations due to information symbols. From the frequency perspective, the time modulation creates replicas in the frequency domain whose frequency is determined by the rate of the antenna switching. This needs to be set properly to create aliasing on undesired directions, which is the reason of

distortion. This is called time modulation and this effect is not the case for desired direction creating selectivity/security along direction and time.

2.4.4 Artificial Noise

The space redundancy owing to having more antennas at the transmit than the receiver can be utilized in additive forms of distortion rather than multiplicative as in methods discussed in previous section. That is, introducing the distortion at the transmitter side, referred as AN, which has no or controlled effect on the legitimate receiver in contrast to eavesdropper, is motivated by achieving a guarantied minimum secrecy. This is because the introduced AN creates an interference providing a minimum SNR difference between the legitimate and the illegitimate receiver even if the eavesdropper enjoys better channel quality than the receiver.

The concept of AN is introduced in [69] for array transmission with singe receiver-antenna receivers, and extended to multiple-input multiple-output (MIMO) scenarios in [23, 70] where both receiver and eavesdropper have multiple antennas. Also, the case where multiple eavesdroppers with perfect coordination exist in the environment is considered under the MIMO configuration. In MISO case, the information symbols are first precoded to maximize the SNR at the legitimate receiver. Then, the artificially generated noise vector is inserted into the transmit signal. The noise components are generated such that they cancel each other after passing through the legitimate receiver's MISO channel. That is, the effect of AN is nulled at the receiver while this is not valid for eavesdropper because she experiences a different channel response. The noise components create ambiguity in detecting the actual signal at eavesdropper regardless of her channel quality. Similar to MISO case, AN vector in for MIMO configuration is selected from the nullspace of the MIMO channel between legitimate pair. One critical observation in MIMO case is that guaranteed minimum secrecy is possible when eavesdropper has less antenna than the transmitter so that the degree of freedom from having more antennas at the transmitter, i.e., *antenna redundancy*, is utilized for secure transmission [23]. In [71], the priority for power allocation is given to the intended receiver to satisfy a target signal to interference plus noise ratio (SINR), then the remaining power is

used for distortion of the eavesdropper reception via AN. This strategy corresponds to a suboptimal solution since the reliability and the security, in the form of secrecy rate, is not jointly considered.

Allocating the power for the AN as equal to the information signal power was found to be a simple and a near optimal choice for the non-colluding eavesdropper case in [72]. The AN power needs to be increased when the multiple eavesdroppers coordinate, or one eavesdropper has multiple antennas. Also, the effect of imperfect channel state information (CSI) at the transmitter, which results in leakage of AN into the receivers channel, on the secrecy performance is investigated and showed that as the channel estimation error increases, increasing the AN power is a better choice than increasing the information signal power. [73] further generalized the scenario by optimizing the beamforming directions as opposed heuristic selection in [72], and showed that unlike previous works that aim to null the AN at the legitimate receiver [23, 56, 69–72, 74], the best strategy for optimizing the secrecy rate can include allowing some of the artificial noise components in the channel of intended receivers resulting in new optimal power allocation between the message signal and AN powers [73]. Similar to [71], [75] adopts minimization of the SINR at the eavesdropper with the knowledge of her CSI, rather than maximize the secrecy rate. A motivating property of the AN methods is that the CSI of eavesdropper is not assumed to be known by the transmitter which is the case with passive eavesdropping. More importantly, CSI of legitimate pair is allowed to be known globally since it is not used as a secret key. In [74], AN insertion is applied to the Monopulse Cassegrain antenna where the main signal component and the artificial noise component are separately transmitted by sum beam and two difference beams that have null in the direction where the sum beam is directed. Artificial noise design was studied in [76] for single-input single-output single-eavesdropper (SISOSE) channel with discrete inputs, by assuming an AWGN channel to the Bob and a fast fading channel to the Eve.

Unlike the previous multiple antenna scenarios, [77] introduces the AN concept for single-input single-output (SISO) channels and proposes a time-domain AN design for orthogonal frequency-division multiplexing (OFDM) channel which exploits the freedom provided by the cyclic prefix (CP) to jam the eavesdropper. That is, the AN is inserted into the null space of Toeplitz channel matrix with CP removal which does not affect the legitimate receiver because the CP portion is

already discarded. Also, another approach for frequency selective SISO channels is provided in [78] by taking advantage of the independent frequency selectivity of main and eavesdropper channels. For the single antenna case, the nullspace for SISO channel in which the AN is inserted is considered to be along frequency domain, which was the space domain in multiple antenna-based schemes [23, 69–72, 74].

2.4.5 Channel-Driven Techniques

In multipath scattering environments, the received signal is shown as rapidly decorrelating over a distance of roughly half a wavelength, which is a well-known uniform scattering model by Jakes [79]. In our scenario, this result directly implies that the wireless channel response between Alice and Bob, and the channel between Alice and Eve becomes independently fades as long as Bob and Eve are physically separated by more than a wavelength. Thus, departing form the aforementioned independence, the assumption that Eve is unable to estimate the channel response between Alice and Bob has not been found unrealistic [38, 80–84].

The independent channel fading characteristics for legitimate and illegitimate receivers have been indirectly exploited in various PHY security techniques such as artificial noise and space-time randomization. The concept of using the legitimate channel's response for generating an inherently secret keying variable is proposed in [80] by relying on Jakes findings in both presence and absence of time variation, and its performance is analyzed in [81]. [38] includes the generalization of this concept to MIMO scenarios in the form of space-time secret transmission. Some channel-driven key generation experiments for indoor environments are conveyed in [83].

Instead of explicitly generating the secret key to be employed for cryptologic stages ahead, [82] applies the ideas in [80, 81] to directly manipulate the transmitted signal so that only legitimate receiver receives a clean copy if the signal. Thus, the channel information known to transmitter and client receiver is exploited directly as a form of spatial encryption where the shared private key corresponds to the channel coefficients. Finally, [84] points some critical issues in the usage of channel as a source of secrecy. Especially, the level of secrecy generated from the fading channel

might be limited when the delay spread is short corresponding the low entropy with less number of channel taps to be utilized.

2.5 Conclusions

Securing the information transmission when the medium is wireless is both challenging and, at the same time, provides additional degrees of freedom thanks to different perceptions of the received signal by legitimate receivers and eavesdroppers. Fundamental signal reception stages in secure signal transmission is presented from a different perspective along with the examples. New approaches to the existing performance metrics such as security gap are presented that covers the wider scope of scenarios. The concepts in secure signal transmissions are exemplified with existing PHY layer techniques. The paper puts a step towards understanding the nature of secrecy in wireless communication from different perspectives and exploring new opportunities.

CHAPTER 3:
A WINDOWING TECHNIQUE FOR OPTIMAL TIME - FREQUENCY CONCENTRATION AND ACI REJECTION IN OFDM-BASED SYSTEMS

3.1 Introduction

Orthogonal multicarrier schemes that rely on rectangular pulse shapes, e.g., OFDM, offer prominent features such as robustness against multipath channel and notable flexibility for efficient implementations[1]. Despite their advantages, the use of rectangular pulse shape introduces high spectral leakage in out-of-band (OOB) spectrum due to its sharp transitions in time domain. Similarly, rectangular filters at the receiver capture significant amount of adjacent-channel interference (ACI) from other systems possibly operating asynchronously. One of the common countermeasures for unwanted spectral leakage problem has been replacing the rectangular pulse shapes with smoother filters with good spectral response, commonly referred as filter bank multicarrier (FBMC). A large number of investigations on this strategy exist in the literature. For a comprehensive treatment on this subject, we refer the reader to the surveys in [86–88]. Nevertheless, FBMC may not allow using one-tap equalization for achieving acceptable BER performance in multipath channels and complex equalizers may be needed [89, 90]. Recently, an elegant solution, known as generalized frequency-division multiplexing (GFDM), has been introduced to resolve both equalization and spectral-leakage problem by extending the concept of CP per OFDM symbol to multiple symbols and utilizing smoother filters for each symbol as in FBMC [91]. This structure has its own merits by maintaining the circulant property of the channel matrix for each subcarrier [92]. However, it still introduces abrupt change between consecutive frames, which limits the OOB radiation performance. In addition, increasing the frame size is penalized by the time variation in the channel.

[1]The content of this chapter is published in [85]. Copyright notice for this publication can be found in Appendix C.

Another alternative solution for reducing OOB radiation is known as transmitter windowing technique in which the rectangular pulse shape is smoothed with a specific windowing function. This approach preserves the main structure of OFDM receivers and addresses back-compatibility issues which are important for existing OFDM-based systems. Considering its simplicity and efficient implementation, in this study, we investigate the limits of the windowing approach for OFDM-based schemes to address both spectral leakage and ACI rejection in time-frequency compact manner.

In the literature, it is possible to find numerous windowing approaches for spectral shaping purposes in different cases. In [93], shaping the OFDM subcarriers is proposed for spectrum pooling scenarios where different systems operate at neighboring bands. In order to reduce the interference on adjacent channels, rapid-decaying of OOB spectrum is achieved via windowing approach. Also, by considering the flexible guard band with subcarrier deactivation [93], the trade-off between interference reduction and throughput is presented. In [94], transmitter and receiver windowing are discussed for CR scenarios and the receive windowing is considered for sensing the spectrum occupancy. Transmitter windowing is demonstrated in an OFDM system by dynamically tailoring the properties of spectrum neighbors in a dynamic spectrum access (DSA) configuration [95]. In [96], the authors propose the concept of edge windowing which suggests the use of a longer windowing period accompanied with shorter CP duration for the subcarriers located at the edge of the band. In particular, this approach becomes prominent when various delay spread characteristics of different users are taken into account in multiple accessing scenarios [97]. In [98], windowing approach is also applied at the receiver along with the transmitter windowing in order to suppress spectral leakage and reject ACI. In a recent study [99], a block-emission-mask compliant windowing technique is studied. The duration of time extension for pulse shape function and subcarrier-specific transmit power levels are optimized considering prescribed spectral mask. As a different approach, in [100], the second-order characteristics of the multipath delay spread of multipath channels is considered in windowing design in order to minimize the overhead for a good OOB reduction. This is achieved by designing time-asymmetric pulse shape functions. Besides spectral shaping, the time extension in windowing approaches provide enhanced guarding against inter-symbol interference (ISI). In addition to transmit windowing, another countermeasure

in reducing the OOB leakage is deactivating a certain number of edge subcarriers, which can also be considered in conjunction with windowing [93, 101, 102]. In addition to conventional OFDM waveform structure, there are hybrid multicarrier proposals [103] that combine different concept such as block transmission with CP, windowing for the block edges, circular filtering, and FBMC/offset-QAM (OQAM) in one multicarrier structure.

As it follows from Heisenberg's uncertainty principle, a signal cannot be limited in both time and frequency [104]. Rectangular pulse shape is the extreme case for this phenomena; it has perfect time-localization but poor spectral containment. With transmitter windowing technique as illustrated in Figure 3.1(a), the support in time domain is relaxed for the sake of better spectral concentration. Hence, despite its simplicity, concentration of OFDM signal within a band with windowing approaches brings a loss in spectral efficiency due to extension of symbol duration. However, conventional windowing functions, e.g., raised-cosine (RC) [93, 94, 98], do not provide the optimal solution for time-frequency concentration problem.

In this chapter, we extend the definition of available concentration bandwidth to per-subcarrier basis, which is specific to multicarrier schemes. It is worth noting that inner subcarriers have wider available concentration band, which provide significant relaxation on the design of the windowing function. Considering available concentration bands for individual subcarriers, we introduce a windowing scheme that gives the optimal compaction in frequency for OFDM-based schemes. To this end, the family of discrete prolate spheroidal sequences (DPSS) [105] is adopted for designing windowing functions for individual subcarriers. The proposed method allows asymmetric sidelobe suppression performance by assigning different concentration bands for right and left sides of bands and maximizes the utilization of the available resources in time and frequency for OFDM via windowing approaches. In addition, it is shown that the proposed windowing functions allow maximal ACI rejection in the scenario where there is no time synchronization between desired and interfering transmitters. It is worth noting that since the proposed windowing schemes keep the conventional OFDM kernel, they can be integrated into the prevalent OFDM based systems without a need for substantial modification.

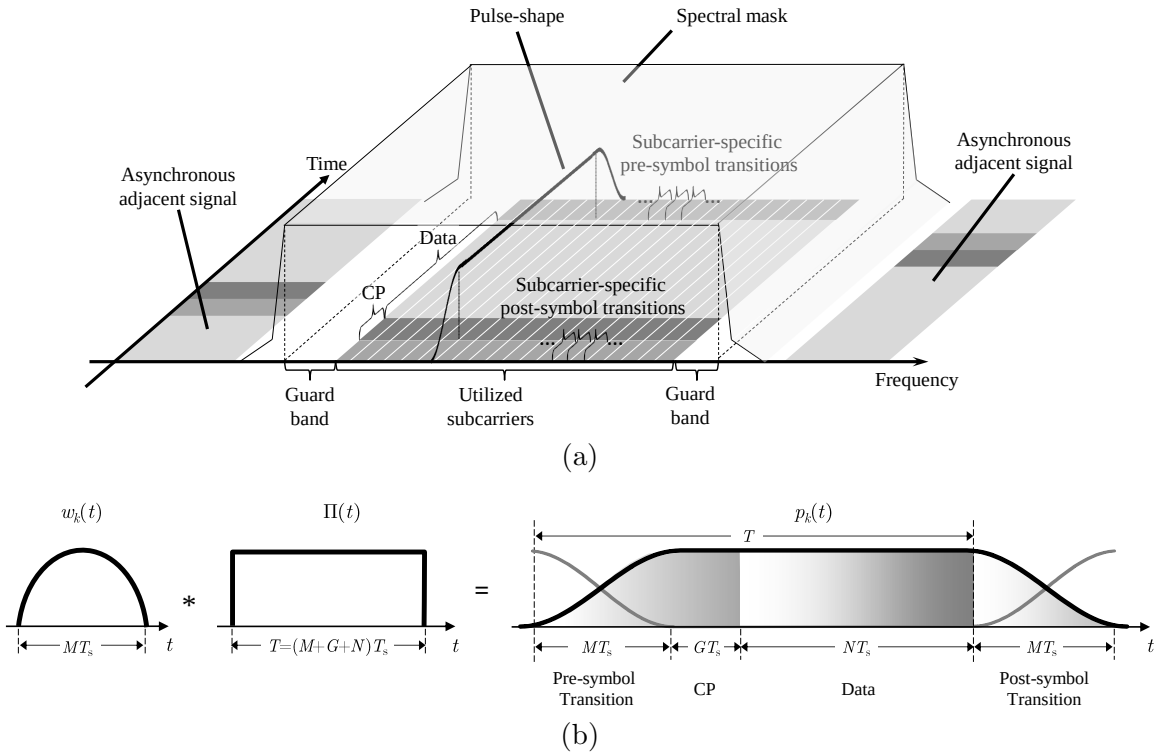

Figure 3.1 (a) The illustration of signal model and aggressors operating at the adjacent channels in time-frequency plane. (b) The illustration of pulse shape generation by convolving the rectangular function with windowing function. This relaxes OFDM symbol in time and provides better spectral concentration.

Remaining of this chapter is organized as follows: The system model is introduced in Section 3.2. The design procedure for optimally concentrated pulse shape function is given in Section 3.3. The application of the proposed pulse shape functions for reducing the spectral leakage of OFDM scheme is investigated in Section 3.4. The optimality of the proposed windowing functions for the ACI rejection is discussed in Section 3.5. The numerical results evaluating the performance of the proposed windowing method are given in Section 3.6 and some concluding remarks are provided in Section 3.7.

The following notation is adopted in this chapter. Matrices [columns vectors] are denoted with upper [lower] case boldface letters (e.g., $\mathbf{A}$ [$\mathbf{a}$]); $*$ denotes the convolution operation; superscripts T and H denote transpose, and conjugate transpose, respectively; $\overline{x}$ denotes the conjugate of a scalar number x; $j = \sqrt{-1}$ is the imaginary unit; $\mathbb{E}_x[y(x)]$ denotes the expectation of $y(x)$ over

the random argument x; $\mathbb{Z}$ denotes the integer number set; and rect(x) is the rectangular function defined as 1 for $|x| < 1/2$ and 0 elsewhere.

3.2 System Model

We consider an OFDM system where windowing functions are utilized at the transmitter for pulse shaping and at the receiver for ACI rejection. For ACI analysis, we adopt a scenario where multiple interfering signals operate at adjacent channels as illustrated in Figure 3.1(a). The victim link and the aggressors operating at the adjacent channels are denoted by ϵ and $i \in \{..., -2, -1, 1, 2, ...\}$, where negative and positive indices indicate the interfering signals located at left and right sides of the band of desired signal, respectively. The baseband OFDM signal of the desired transmitter is given by

$$s^{(\epsilon)}(t) = \sum_{m \in \mathbb{Z}} \sum_{k=-\frac{N_\epsilon}{2}}^{\frac{N_\epsilon}{2}-1} X_{km}^{(\epsilon)} p_{km}^{(\epsilon)}(t), \tag{3.1}$$

where $X_{mk}^{(\epsilon)}$ is the data symbol that modulates the kth subcarrier of mth OFDM symbol, and $N_\epsilon \leq N$ denotes an even number of the activated subcarriers out of N total subcarriers. In (3.1), $p_{km}^{(\epsilon)}(t)$ is the synthesis function associated with the kth subcarrier of mth symbol, which indicates the location and shape of $X_{km}^{(\epsilon)}$ on the time-frequency plane. The synthesis function can be written as

$$p_{km}^{(\epsilon)}(t) = p_k^{(\epsilon)}(t - mT) e^{j2\pi kFt}, \tag{3.2}$$

where $p_k^{(\epsilon)}(t)$ is the subcarrier-specific transmit filter, i.e., pulse shape function, T is the time spacing between consecutive symbols and F is the subcarrier frequency spacing. As it can be seen from Figure 3.1, the symbol spacing includes the transition, CP, and data durations, i.e., $T = (M + G + N)T_\mathrm{s}$ where T_s is the sample duration. While T represents OFDM symbol spacing, the symbol rate is determined by the subcarrier spacing which is reciprocal of the data duration, i.e., $F = 1/(NT_\mathrm{s})$. The signal model in (3.1) is also adopted for the ith adjacent channel signal

given by

$$s^{(i)}(t) = \sum_{m\in\mathbb{Z}} \sum_{k=-\frac{N_i}{2}}^{\frac{N_i}{2}-1} X_{km}^{(i)} p_{km}^{(i)}(t). \tag{3.3}$$

where N_i is the number of subcarriers for ith signal. Similarly, the synthesis function of ith adjacent channel signal is expressed as

$$p_{km}^{(i)}(t) = p_k^{(i)}(t - mT)e^{j2\pi kFt}. \tag{3.4}$$

We assume that the multipath channel between all transmitter and receiver is time-invariant during one OFDM symbol duration. The channel impulse response is characterized as, $h(\tau) = \sum_{\ell=0}^{L-1} a_\ell \delta(\tau - \tau_\ell)$, where L is the total number of multipaths and τ_ℓ is the delay of ℓth path. Each path gain, a_ℓ, is assumed to be independent and identically distributed (i.i.d.) variable where its magnitude follows Rayleigh distribution.

It is assumed that the aggressors on adjacent channels operate independently and there is no time synchronization between them. We define the relative time offset between the victim receiver and the ith aggressor as a random variable of Δt_i, while the frequency separation between channels, i.e., frequency offset, is expressed as Δf_i. After passing through channels, the desired and the interfering signals are combined at the receiver as

$$r(t) = \sqrt{\alpha_\epsilon} \int_\tau h_\epsilon(\tau) s^{(\epsilon)}(t-\tau)\mathrm{d}\tau + \sum_{i\neq 0} \sqrt{\alpha_i} e^{j2\pi\Delta f_i t} \int_\tau h_i(\tau) s^{(i)}(t + \Delta t_i - \tau)\mathrm{d}\tau + z(t), \tag{3.5}$$

where $\sqrt{\alpha_\epsilon}$ and $\sqrt{\alpha_i}$ are large scale channel gains for desired and interfering transmitters. The first term in (3.5) is the received signal of the desired user, the second term corresponds to the sum of the adjacent channel signals, and $z(t)$ is the AWGN. The demodulation at the receiver can be realized by correlating the received signal with corresponding *analysis function* given by

$$q_{lu}^{(\epsilon)}(t) = q_l^{(\epsilon)}(t - uT)e^{j2\pi lFt}, \tag{3.6}$$

where $q_l^{(\epsilon)}(t)$ is the receive filter employed for lth subcarrier. By sampling the output of the correlator, the symbol on the lth subcarrier of uth OFDM symbol is obtained as

$$\hat{X}_{lu}^{(\epsilon)} = \langle r(t), q_{lu}^{(\epsilon)}(t) \rangle \triangleq \int_t r(t) \overline{q_{lu}^{(\epsilon)}(t)} \mathrm{d}t. \tag{3.7}$$

By substituting (3.5) and (3.6) into (3.7), $\hat{X}_{lu}^{(\epsilon)}$ is obtained as

$$\hat{X}_{lu}^{(\epsilon)} = \sqrt{\alpha_\epsilon} X_{lu}^{(\epsilon)} A_{lulu}^{(\epsilon)} + \sqrt{\alpha_\epsilon} \sum_{\substack{m \in \mathbb{Z} \\ m \neq u}} \sum_{\substack{k=-\frac{N_\epsilon}{2} \\ k \neq l}}^{\frac{N_\epsilon}{2}-1} X_{km}^{(\epsilon)} A_{kmlu}^{(\epsilon)} + \sum_{i \neq 0} \sqrt{\alpha_i} \sum_{m \in \mathbb{Z}} \sum_{k=-\frac{N_i}{2}}^{\frac{N_i}{2}-1} X_{km}^{(i)} A_{kmlu}^{(i)} + Z_{lu}. \tag{3.8}$$

In (3.8),

$$A_{kmlu}^{(\epsilon)} = \int_\tau h_\epsilon(\tau) \int_t p_{km}^{(\epsilon)}(t-\tau) \overline{q_{lu}^{(\epsilon)}(t)} \mathrm{d}t \mathrm{d}\tau \tag{3.9}$$

and

$$A_{kmlu}^{(i)} = \int_\tau h_i(\tau) \int_t p_{km}^{(i)}(t + \Delta t_i - \tau) \overline{q_{lu}^{(\epsilon)}(t)} \mathrm{d}t \mathrm{d}\tau. \tag{3.10}$$

Note that (3.9) and (3.10) correspond to the sampled versions of the weighted sum of the ambiguity functions between the synthesis function corresponding to the kth subcarrier of mth symbol and the analysis function corresponding to the lth subcarrier of uth symbol. In other words, they represent the correlation between the transmit and receive filters in time-frequency grid [86, 106]. Finally, relying on the i.i.d. property of the data symbols, the interference power for given channels can be expressed as

$$I_{lu}(\Delta t_i) = \alpha_\epsilon \sum_{\substack{m \in \mathbb{Z}, \\ m \neq u}} \sum_{\substack{k=-\frac{N_\epsilon}{2} \\ k \neq l}}^{\frac{N_\epsilon}{2}-1} \left| A_{kmlu}^{(\epsilon)} \right|^2 + \sum_{\substack{i \in \mathbb{Z}, \\ i \neq 0}} \alpha_i \sum_{m \in \mathbb{Z}} \sum_{k=-\frac{N_i}{2}}^{\frac{N_i}{2}-1} \left| A_{kmlu}^{(i)} \right|^2. \tag{3.11}$$

3.3 Optimally Concentrated Windowing Functions for OFDM Subcarriers

For a particular subcarrier, the pulse shape function can be designed by convolving a rectangular pulse $\Pi(t)$ with a windowing function $w_k(t)$, as also given in [87], by

$$p_k(t) = w_k(t) * \Pi(t), \tag{3.12}$$

where

$$\Pi(t) \triangleq \begin{cases} 1, & (-M-G)T_{\mathrm{s}} \leq t < NT_{\mathrm{s}} \\ 0, & \text{otherwise} \end{cases}. \tag{3.13}$$

The windowing functions satisfy $\int_t w_k(t)\mathrm{d}t = 1$. Therefore, the result of operation in (3.12) takes unit value for CP and data parts while having arbitrary values for the transition periods. As illustrated in Figure 3.1(a), we express the transmit pulse shape function with there different durations: NT_{s} for the main symbol part, GT_{s} for the CP part, and MT_{s} for the pre-symbol as well as post-symbol transition parts of the mth symbol. With this representation, the windowing function in (3.12) completely determines the transient behavior between two symbols, and hence characterizes the spectral response of that particular OFDM subcarrier [87]. Therefore, we consider the design of windowing functions in frequency domain since the shape of the spectrum of OFDM subcarriers is determined via multiplication operation in frequency domain.

Spectral concentration problem for finite duration pulses is well-studied under the family of prolate spheroidal wave functions (PSWF) which offers maximum concentration in time for a band-limited signal, or spectral concentration for a time-limited signal [105]. Herein we consider the optimum real-valued discrete-time windowing function, $w_k[n]$, that concentrates the OFDM subcarrier pulse shape function $p_k[n]$. For a given $p_k[n]$, the ratio of the signal energy in the frequency range $|f| \leq \Omega$, where $\Omega < \frac{1}{2}$, to the total energy is referred as *concentration ratio*. It can be expressed by using discrete-time Fourier transform (DTFT) of the pulse shape function for kth

subcarrier, i.e., $P_{k,M}(f)$, as

$$\lambda_k(M,\Omega) = \frac{\int_{-\Omega}^{\Omega} |P_{k,M}(f)|^2 \,\mathrm{d}f}{\int_{-\frac{1}{2}}^{\frac{1}{2}} |P_{k,M}(f)|^2 \,\mathrm{d}f} \tag{3.14}$$

$$\overset{(a)}{=} \frac{\int_{-\frac{1}{2}}^{\frac{1}{2}} \mathrm{rect}\Big(\frac{f}{2\Omega}\Big) |W_{k,M}(f)C(f)|^2 \,\mathrm{d}f}{\int_{-\frac{1}{2}}^{\frac{1}{2}} |W_{k,M}(f)C(f)|^2 \,\mathrm{d}f} \tag{3.15}$$

$$\overset{(b)}{=} \frac{\int_{-\frac{1}{2}}^{\frac{1}{2}} W_{k,M}(f)\, \Psi_{\Omega}(f) \overline{W_{k,M}(f)} \mathrm{d}f}{\int_{-\frac{1}{2}}^{\frac{1}{2}} |W_{k,M}(f)C(f)|^2 \,\mathrm{d}f}, \tag{3.16}$$

where (3.15) includes the substitution of $P_{k,M}(f) = W_{k,M}(f)C(f)$ into (3.14), in which $W_{k,M}(f)$ and $C(f)$ are the Fourier transforms (FT) of windowing function $w_k[n]$ and $\Pi\,[n]$, respectively. The equality (a) holds due to the rectangular function $\mathrm{rect}\Big(\frac{f}{2\Omega}\Big)$, which limits the integration interval inherently, is plugged in the numerator of (3.14). Thus, the integral limits can be set as $\big[-\frac{1}{2}, \frac{1}{2}\big]$ that will allow time domain representation of the spectral concentration latter. The equality (b) follows the definition of $\Psi_{\Omega}(f) \triangleq C(f)\mathrm{rect}(f/2\Omega)\overline{C(f)}$. Then, by defining $\psi_{\Omega}[n]$ as inverse DTFT of $\Psi_{\Omega}(f)$, (3.16) can completely be represented in discrete time domain as

$$\lambda_k(M,\Omega) = \frac{\sum_{l=0}^{M-1} \sum_{n=0}^{M-1} \overline{w_k[n]} \psi_{\Omega}[n-l] w_k[l]}{\sum_{n=-M-G}^{N+M-1} |w_k[n] * \Pi\,[n]|^2}, \tag{3.17}$$

where the denominator follows the conversion into time domain and the Parseval's theorem. Also, by adopting array representation for the windowing function as $\mathbf{w}_k = [w_k[0], \ldots, w_k[M-1]]^{\mathrm{T}}$, (3.17)

is rewritten in matrix form as

$$\lambda_k(M,\Omega) = \frac{\mathbf{w}_k^{\mathrm{H}} \boldsymbol{\Psi}_\Omega \mathbf{w}_k}{\mathbf{w}_k^{\mathrm{H}} \underbrace{\mathbf{B}^{\mathrm{H}}\mathbf{B}}_{\boldsymbol{\Lambda}} \mathbf{w}_k}, \tag{3.18}$$

where $\boldsymbol{\Psi}_\Omega$ is an $M \times M$ matrix and $\mathbf{B}$ is an $(N+G+M) \times M$ Toeplitz matrix given as

$$\boldsymbol{\Psi}_\Omega = \begin{bmatrix} \psi_\Omega[0] & \psi[1] & \cdots & \psi[M-1] \\ \psi[-1] & \psi[0] & \cdots & \psi[M-2] \\ \vdots & \ddots & \ddots & \vdots \\ \psi[-M+1] & \cdots & \psi[-1] & \psi[0] \end{bmatrix},$$

and

$$\mathbf{B} = \begin{bmatrix} 1 & 0 & \cdots & 0 \\ \vdots & 1 & \ddots & \ddots \\ 1 & \ddots & \ddots & \ddots \\ 0 & 1 & \ddots & \ddots \\ \vdots & \ddots & \ddots & \ddots \\ 0 & \cdots & 0 & 1 \end{bmatrix},$$

respectively. The matrix $\mathbf{B}$ consists of the discrete samples of rectangular function to be convolved with the windowing samples. Therefore, the optimum windowing function that maximizes the spectral containment of kth subcarrier within the range of $[-\Omega, \Omega]$ is obtained as

$$\hat{\mathbf{w}}_k = \arg\max_{\mathbf{w}_k} \frac{\mathbf{w}_k^{\mathrm{H}} \boldsymbol{\Psi}_\Omega \mathbf{w}_k}{\mathbf{w}^{\mathrm{H}} \boldsymbol{\Lambda} \mathbf{w}_k}, \tag{3.19}$$

in which the ratio is known as generalized Rayleigh quotient [107]. By noting that $\boldsymbol{\Lambda}$ is a positive definite matrix, the ratio in (3.19) can be converted to regular Rayleigh quotient [108]. After performing Cholesky decomposition for $\boldsymbol{\Lambda}$ such that $\boldsymbol{\Lambda} = \mathbf{L}\mathbf{L}^{\mathrm{H}}$, we define an invertible transformation

for the windowing vector $\mathbf{w}_k$ as $\mathbf{T} \triangleq \left(\mathbf{L}^{\mathrm{H}}\right)^{-1}$ yielding

$$\mathbf{w}_k = \mathbf{T}\mathbf{z}_k. \tag{3.20}$$

By substituting (3.20) into (3.19), the regularized Rayleigh quotient is obtained as

$$\hat{\mathbf{z}}_k = \arg\max_{\mathbf{z}_k} \frac{\mathbf{z}_k^{\mathrm{H}} \boldsymbol{\Upsilon}_{\Omega} \mathbf{z}_k}{\mathbf{z}^{\mathrm{H}} \mathbf{z}_k}, \tag{3.21}$$

where $\boldsymbol{\Upsilon}_{\Omega} = \mathbf{T}^{\mathrm{H}} \boldsymbol{\Psi}_{\Omega} \mathbf{T}$. Then, the solution for (3.21) reduces to finding the eigenvector of $\boldsymbol{\Upsilon}_{\Omega}$ corresponding to largest eigenvalue by the Rayleigh quotient theorem [107, 108], i.e., largest concentration ratio, satisfying the eigensystem as

$$\boldsymbol{\Upsilon}_{\Omega} \mathbf{z}_k = \lambda_k(M, \Omega) \mathbf{z}_k. \tag{3.22}$$

After determining the vector $\mathbf{z}_k$ that maximizes the concentration ratio λ_k, the windowing function is obtained by the transformation in (3.20). Here, we would like to note that for $\boldsymbol{\Lambda} = \mathbf{I}$, the system corresponds to conventional DPSS problem [105] where there is no flat response of OFDM pulse shape including CP and data durations.

3.4 Transmitter Windowing for OOB Suppression

In this section, the windowing functions that are discussed in Section 3.3 are employed for controlling the OOB leakage of the OFDM. We first present the conventional windowing strategy where the same windowing function is used for all of the subcarriers. We then introduce per-subcarrier windowing scenario where each subcarrier has its own windowing function. This strategy gives the maximum spectral efficiency for an OFDM waveform that complies given constraints. In addition, we consider the spectral mask for the constraint to be satisfied for both scenarios.

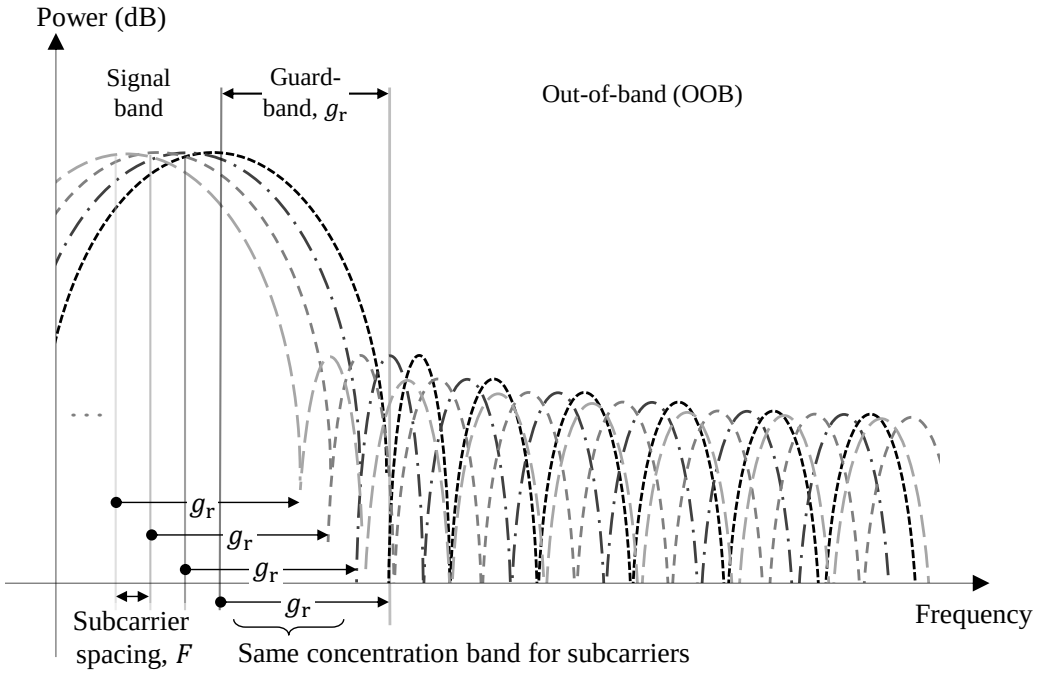

(a)

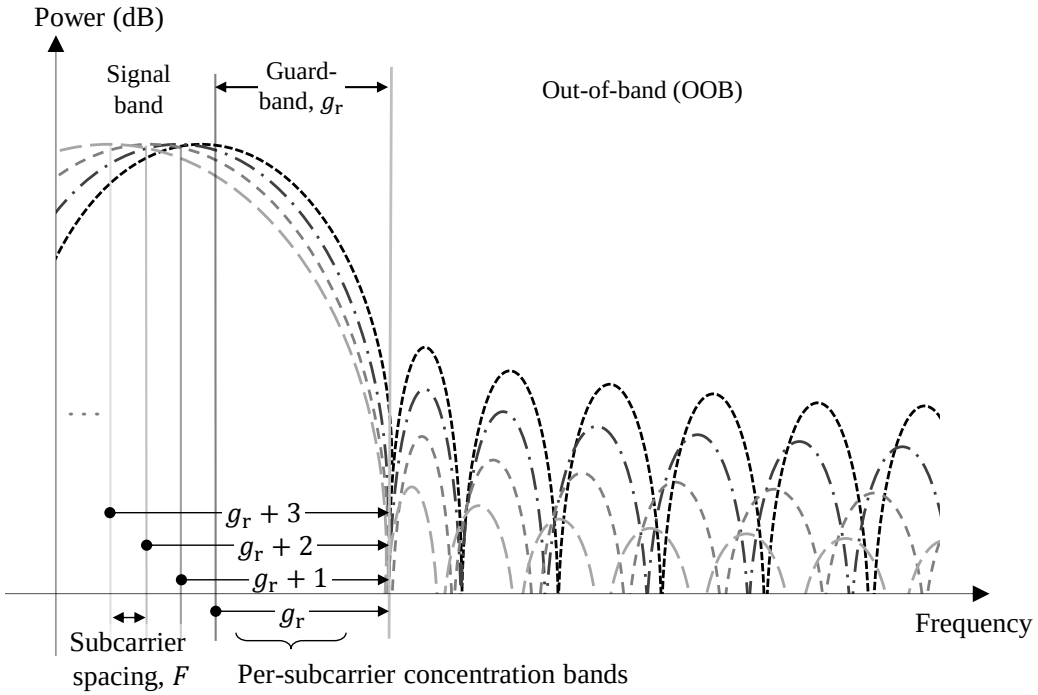

(b)

Figure 3.2 Power spectrum of individual windowing functions. (a)Fixed windowing: All subcarriers are shaped by the same windowing function with a fixed concentration band. (b)Per-subcarrier windowing: Windowing functions are designed in a subcarrier-specific manner and the concentration band for each subcarrier is determined based on its location in frequency.

3.4.1 Fixed Windowing and Per-subcarrier Windowing

In order to suppress the sidelobes of OFDM signal, we exploit the available guard band for individual subcarriers. To this end, we design the windowing function for kth subcarrier as

$$w_k[n] \triangleq w_{\text{op}}\big[M, \Omega_k; n\big], \tag{3.23}$$

where Ω_k is the concentration bandwidth assigned for windowing function of the kth subcarrier, and $w_{\text{op}}\big[M, \Omega; n\big]$ is the windowing function of length M that optimally concentrates the pulse shape function into frequency range $|f| \leq \Omega$ based on (3.19). When the same windowing function is employed for each subcarrier, the available band to concentrate the energy is solely determined by the system guard band, given by

$$\Omega_k = \frac{gF}{1/T_{\text{s}}} = \frac{gF}{NF} = \frac{g}{N}, \tag{3.24}$$

where g is the guard band in terms of subcarrier spacing F. The power spectrum of the individual windowing functions and the combination for right edge of the frequency band are illustrated in Figure 3.2(a). Note that, *windowing functions* are drawn in frequency domain in Figure 3.2 rather than the spectrum of pulse shape functions for the sake of better visualization of the effect of fixed and subcarrier specific concentration bands.

As we relax the spectral concentration constraint of the windowing functions by increasing Ω_k, superior suppression beyond the concentration band is achieved. Therefore, by taking the multicarrier structure of the OFDM waveform into account, this trade-off is utilized to optimize the spectral containment of the overall signal. For this purpose, the available band for each subcarrier is individually exploited. We set the concentration band of each subcarrier as the spectral distance between that subcarrier and the outer boundary of available guard band. This corresponds to assigning individual concentration bands for the windowing functions of each subcarrier as

$$\Omega_k = \frac{1}{N} \min\left(k - \left(\frac{N_\epsilon}{2} + g_{\text{l}}\right), \left(\frac{N_\epsilon}{2} + g_{\text{r}} - 1\right) - k\right), \tag{3.25}$$

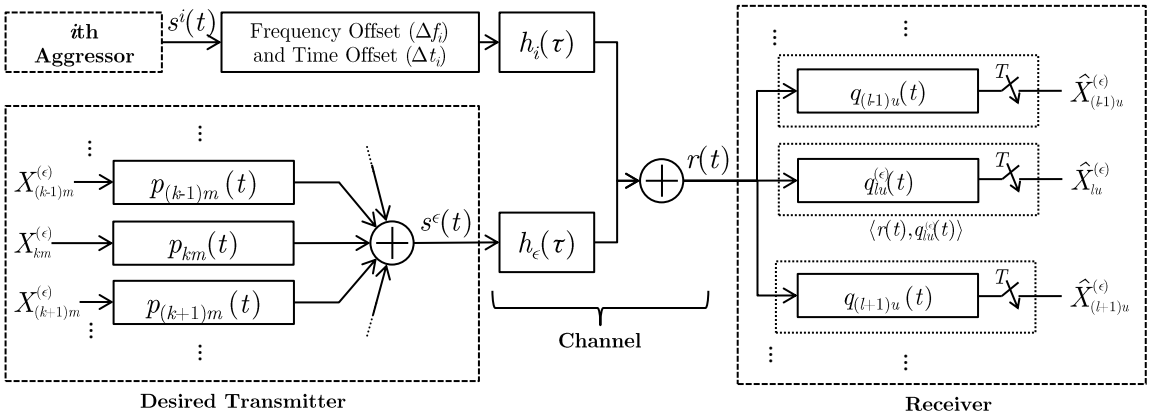

Figure 3.3 Block diagram for the considered scenario. Per-subcarrier windowing is realized by selecting the pulse shapes specific to each subcarrier. The adjacent-channel variables are presented by the index i.

where g_{l} and g_{r} are the left and right guard bands, respectively. Figure 3.2(b) depicts the spectral responses of the windowing functions for each subcarrier. As indicated in (3.25) and shown in Figure 3.2(b), the concentration bandwidth increases for inner subcarriers by one subcarrier-spacing increments. Note that per-subcarrier concentration band configuration in the light of (3.16) and (3.19) individually minimizes the power contribution on the OOB region as shown in Figure 3.2. Considering the i.i.d. property of the information symbols, the total power spectrum of the OFDM becomes the sum of individual subcarrier spectrum. Thus, as independent variables, minimizing the power of each subcarrier in OOB region individually with the proposed per-subcarrier windowing inherently minimizes the total power spectrum as the sum of these variables. Thus, this concentration band assignment eliminates the exhaustive search in finding the optimal solution.

In the scenarios where left and right side of the spectrum host different wireless technologies, different emission requirements on different sides can emerge. Thus, for the cases that allow or require different spectral response in adjacent channels, asymmetric spectral suppression can also be achieved via setting g_{l} and g_{r} in (3.23) differently. For instance, less guard subcarriers, i.e., higher spectral efficiency, can be utilized in the side that can accommodate more spectral leakage.

3.4.2 Design Under a Prescribed Spectral Mask

OOB suppression performance of windowing methods is a function of the level of relaxation in time domain. That is, longer transition duration provides better OOB suppression with the penalty of lowering spectral efficiency. So far we presented the OFDM windowing design that concentrates the signal spectrum into a given band for a given windowing duration MT_{s}. In the following, joint concentration of the OFDM signals in time and frequency, i.e., maximizing the ratio of active area in Figure 3.1(b) to the total region, is considered. When a spectral mask is given, the degrees of freedom that can be selected independently becomes the transition duration (the loss in time domain) and the number of unused subcarriers (the loss in frequency domain). For the frequency utilization, we denote N_ϵ as the number of used subcarriers. Since there is no closed-form expression for the optimum windowing functions, the parameter selection for optimal packing of OFDM symbols can be performed numerically. The problem that seeks for the optimal transition duration and the number of active subcarriers that maximizes the spectrum utilization is then given by,

$$\begin{aligned} (M, N_\epsilon) &= \arg\max_{M,N_\epsilon} \left(\frac{N_\epsilon}{N+G+M} \right), \\ \text{subject to } &\sum_{k=-\frac{N_\epsilon}{2}}^{\frac{N_\epsilon}{2}-1} |W_{k,M}(f-k\Delta f)|^2 \leq S_{\mathrm{mask}}(f) \end{aligned} \tag{3.26}$$

which maximizes the information contained in the given bandwidth limited by the spectral mask, $S_{\mathrm{mask}}(f)$. Since the optimization in (3.26) is an integer program, it can be solved via heuristic methods such as local search around the inequality constraint. First, by fixing one of the parameters, e.g., M, a search over the second parameter can be performed until the inequality holds. Then, a local search over both parameters around the inequality boundary can be performed. This procedure will be discussed in Section 3.6.3 in detail.

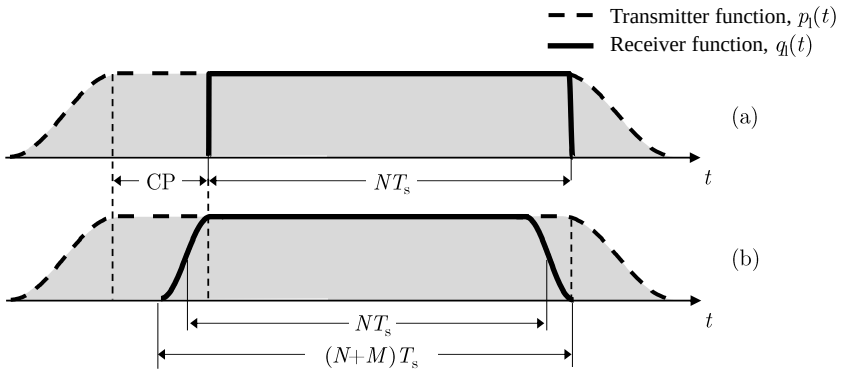

Figure 3.4 Illustration of Nyquist property when receiver windowing is applied. While the rectangular function provides the Nyquist property for OFDM (a), the proper alignment of the windowed receiver function (b) in time maintains the Nyquist property.

3.5 Receiver Windowing for ACI Rejection

In this section, we extend the use of proposed windowing technique for optimal spectral concentration to ACI rejection at the receiver. We exploit the maximum time/frequency concentration property of the proposed windowing functions in Section 3.3 and use it for the rejection of sidelobe components of the aggressors' signals. Receiver windowing has been utilized for OFDM receivers for different purposes such as improving reception against sine spurious [109], minimizing the effect of additive noise and inter-carrier interference (ICI) in the presence of frequency offset [109–113]. In this section, we will focus on the ACI rejection property of the receiver windowing. As it is shown in Figure 3.3, the desired signal that is transmitted via subcarrier specific windowing is received via receiver windowing. Also, the adjacent channel signals exist in the neighboring channels with corresponding frequency spacing, Δf_i, and random time offset Δt_i. The receiver windowing can also be realized in a per-subcarrier manner as shown in Figure 3.3 by employing subcarrier specific receiver window functions.

The time-domain transmitter and receiver functions are illustrated in Figure 3.4. Note that the orthogonality between subcarriers are achieved via the pulse shaping functions with Nyquist criterion. Similar to transmitter pulse shape function, the receiver function is also generated by

convolution of the a receiver windowing function and the rectangular pulse given as

$$q_l(t) = v_l(t) * \Pi_{\mathrm{r}}(t), \tag{3.27}$$

where $v_l(t)$ is the windowing function for the receiver and $\Pi_{\mathrm{r}}(t)$ is the corresponding rectangular function with length NT_{s} different than the transmitter case. This provides the zero-ICI property between the subcarriers. For conventional OFDM reception with no windowing, the rectangular function itself becomes the receiver function as in Figure 3.4(a) with the length of data duration, i.e., $NT_{\mathrm{s}} = 1/F$. For the receiver filtering cases, Figure 3.4(b) shows the function for one of the subcarriers with Nyquist property. In order to avoid ISI, we assume that the guard interval beside windowing duration is long enough to avoid ISI [109, 111].

If the adjacent channel signal is also a OFDM-based signal with the same symbol duration, the timing offset between the desired receiver and the adjacent channel signal becomes a determining factor on the amount of energy that the receive filter, $q(t)$ captures from the interfering signal. Considering Rayleigh fading channel between the adjacent channel signal and the receiver, the argument of the summation in (3.8) that constitute the ACI is an exponentially distributed random variable with means given by

$$\sigma_{\mathrm{s}}^2(k,m,l,u) = \mathbb{E}_h\left[\left|A_{kmlu}^{(\epsilon)}\right|^2\right] = \left|\langle p_{km}^{(\epsilon)}(t), q_{lu}^{(\epsilon)}(t)\rangle\right|^2, \tag{3.28}$$

and

$$\begin{aligned}\sigma_i^2(k,m,l,u,\Delta t_i) &= \mathbb{E}_h\left[\left|A_{kmlu}^{(i)}\right|^2\right] \\ &= \left|\langle p_{km}^{(i)}(t+\Delta t_i), q_{lu}^{(\epsilon)}(t)\rangle\right|^2.\end{aligned} \tag{3.29}$$

where we assume that the maximum excess delay of the channel is negligible compared to pulse duration. In other words, each subcarrier is assumed to be experiencing flat fading channel as it is a valid assumption in OFDM systems. With this assumption along with the i.i.d. property of

the channel tap gains, the dependency of the power delay profile (PDP) on the expected power expressions can be neglected.

As illustrated in Figure 3.1(b), there may be time offset between interfering signal and desired signal. In such cases, both transmit filter and the receive filter jointly plays critical role in the level of ACI rejection. While the receive filter determines the response with shaping the outer transitions, the transmitter pulse shape function of the interfering symbol shaping the transition of the interfering symbols, which falls inside of the receiver window. On the other hand, when two filters are aligned in time, the effect of the transmit filter diminishes, and ACI becomes a function of $q_{lu}^{(\epsilon)}(t)$ and Δf_i. However, since time synchronization is not posed between independent systems, Δt_i is considered to be a random variable uniformly distributed in $(-T/2, T/2)$. Then, the interference contribution is derived by evaluating the expectation over all possible values of Δt_i, which yields

$$\begin{aligned} I_{lu}^{(i)} &= \frac{\alpha_i}{T} \int_{-T/2}^{T/2} \sum_{m\in\mathbb{Z}} \sum_{k=-\frac{N_i}{2}}^{\frac{N_i}{2}-1} \sigma_i^2(k,m,l,u,\Delta t_i) \mathrm{d}\Delta t_i \\ &= \frac{\alpha_i}{T} \sum_{k=-\frac{N_i}{2}}^{\frac{N_i}{2}-1} \sum_{m\in\mathbb{Z}} \int_{-T/2}^{T/2} \left| \langle p_{km}^{(i)}(t+\Delta t_i), q_{lu}^{(\epsilon)}(t) \rangle \right|^2 \mathrm{d}\Delta t_i \qquad (3.30) \\ &= \frac{\alpha_i}{T} \sum_{k=-\frac{N_i}{2}}^{\frac{N_i}{2}-1} \int_f \left| P_k^{(i)}(f - kF - \Delta f_i) \right|^2 \left| Q_l^{(\epsilon)}(f - lF) \right|^2 \mathrm{d}f. \qquad (3.31) \end{aligned}$$

where (3.30) is by the substitution of (3.29). The derivation steps between (3.30) and (3.30) are given in the Appendix A. In (3.31), $Q_l^{(\epsilon)}(f) = V_l^{(\epsilon)}(f)C(f)$ represents the Fourier transform of the receive filter $q_l^{(\epsilon)}(t)$ where $V_l^{(\epsilon)}(f)$ is the Fourier transform of the windowing function utilized at the receiver. As shown in (3.31), the adjacent channel energy on the lth subcarrier is a sum of the correlation between the spectral response of each subcarrier of the interferer and the receive filter utilized for the lth subcarrier. Therefore, the receiver windowing should maintain the correlation terms as low as possible in order to suppress ACI. By defining the PSD of the composite ACI signal

as

$$S^{(i)}(f) \triangleq \sum_{k=-\frac{N_i}{2}}^{\frac{N_i}{2}-1} \left| P_k^{(i)}(f - kF) \right|^2, \tag{3.32}$$

(3.31) can be represented in term of the PSD of interferer signal that yields

$$I_{lu}^{(i)} = \frac{\alpha_i}{T} \int_f S^{(i)}(f - \Delta f_i) \left| V_l^{(\epsilon)}(f) C(f) \right|^2 \mathrm{d}f, \tag{3.33}$$

which shows the impact of windowing function utilized at the receiver. The optimum spectral concentration property of the proposed functions plays an enabling role in minimization of the ACI power given in (3.33). Since the spectrum of proposed windowing function is minimized for the range after the concentration band, the energy captured from the main band of the interfering signal is also minimized when they are utilized as windowing function at the receiver. That is, the proposed functions maximally reject the interference power captured from the adjacent bands. Similar to transmitter case, the interference rejection property for each subcarrier can be maximized considering subcarrier specific receiver windowing. In other words, we adjust the concentration bandwidth of the windowing function of the lth as its distance to the closer edge of the main band of the adjacent signal.

3.6 Numerical Results

In this section, we present the performance of the proposed windowing technique and compare with other methods. We choose the OFDM parameters as $N = 512$ for discrete Fourier transform (DFT) size, $G = 64$ for CP size, and $M = 32$ for the transition duration. Unless otherwise stated, the number of activated subcarriers is set as $N_\epsilon = 300$ and DC subcarrier is disabled.

3.6.1 OOB Emission

In this subsection, the OOB radiation performance of proposed windowing functions with per-subcarrier windowing strategy is investigated and compared with other windowing functions, i.e., RC [98] and Kaiser [114]. Note that conventional RC windowing scenarios that we consider in this chapter corresponds to the OFDM transmitter and receiver windowing scheme presented in [98]. While keeping the structure, we adapt the signal parameters for compariosn with proposed schemes. For the numerical evaluations, various concentration bandwidths are taken into account as $g_{\mathrm{r}} = 12, 24$, and 36. Subcarrier-specific concentration bandwidth for each subcarrier is configured via adjusting its Ω_k-parameter. For each configuration, the proposed per-subcarrier windowing scheme provides superior suppression performance in the outside of the concentration band as shown in Figure 3.5. For instance, while proposed scheme with $g = 12$ provides optimum spectral suppression beyond $f = 162 \times F$, allowing OFDM signal to concentrate its spectral energy within the range $[-186 \times F, 186 \times F]$, i.e., $g = 36$, achieves the minimal OOB emission beyond the specified frequency range.

The ability of frequency-asymmetric implementation of the per-subcarrier windowing is investigated and shown in Figure 3.6. In order to achieve different spectral leakage performance for left and right bands, the concentration bandwidths are set as $g_{\mathrm{l}} = 18$ and $g_{\mathrm{r}} = 36$. This setting results in approximately 30 dB difference in between left and right adjacent bands.

3.6.2 The Effect of Concentration Band

In the following, the effect of concentration range on the spectral leakage is investigated. The ratio of total signal power in the main band to the signal power beyond the concentration band is given as a function of the concentration band in Figure 3.7. Proposed windowing with fixed setting is also considered as a suboptimal solution for the concentration of composite OFDM signal. Since the edge subcarriers have less space for subcarrier specific concentration band, the difference between the fixed and per-subcarrier approach is found to be approximately 5 dB when $g = 25$. Since the proposed schemes maximally exploit the given frequency resources, the OOB leakage performance in fixed and per-subcarrier cases outperforms the RC windowing by around 6

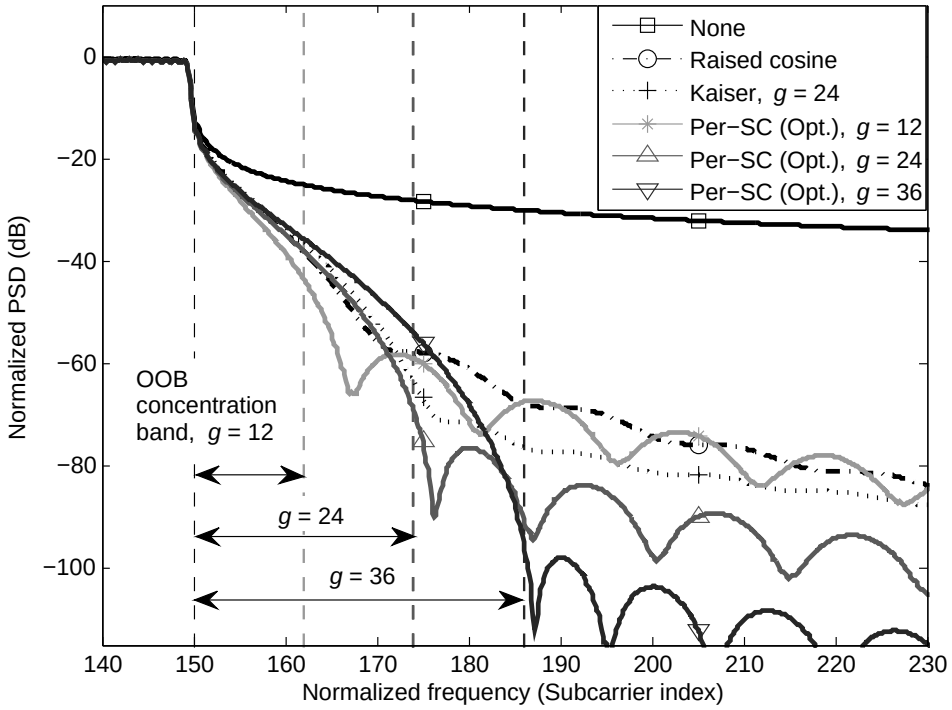

Figure 3.5 OOB leakage for various optimization bands with proposed subcarrier-specific and RC windowing. $N = 512$, $N_\epsilon = 300$, $G = 64$, and $M = 32$.

dB for g values up to 16, which is also the ratio of the windowing duration to the useful symbol duration, i.e., N/M. Beyond this range, the suppression performance increases significantly since the spectral concentration property of the proposed scheme becomes dominant for wider guard bands.

3.6.3 Time-Frequency Concentration with Spectral Constraint

In this subsection, we elaborate the symbol densities of the proposed windowing schemes in the presence of a spectral mask. For simple evaluation, brick-wall type mask is adopted though it is possible to extend it to more complicated mask structures. The width of the mask is set as $256 \times F$ and various suppression levels for OOB are investigated. The objective function in (3.26), which corresponds to the spectral efficiency of the scheme, is given in Figure 3.8 for given windowing size and number of active subcarriers. The feasible region in which the constraint in (3.26) is satisfied is also depicted in Figure 3.8 for the spectral mask with 50 dB suppression level. Similarly, the

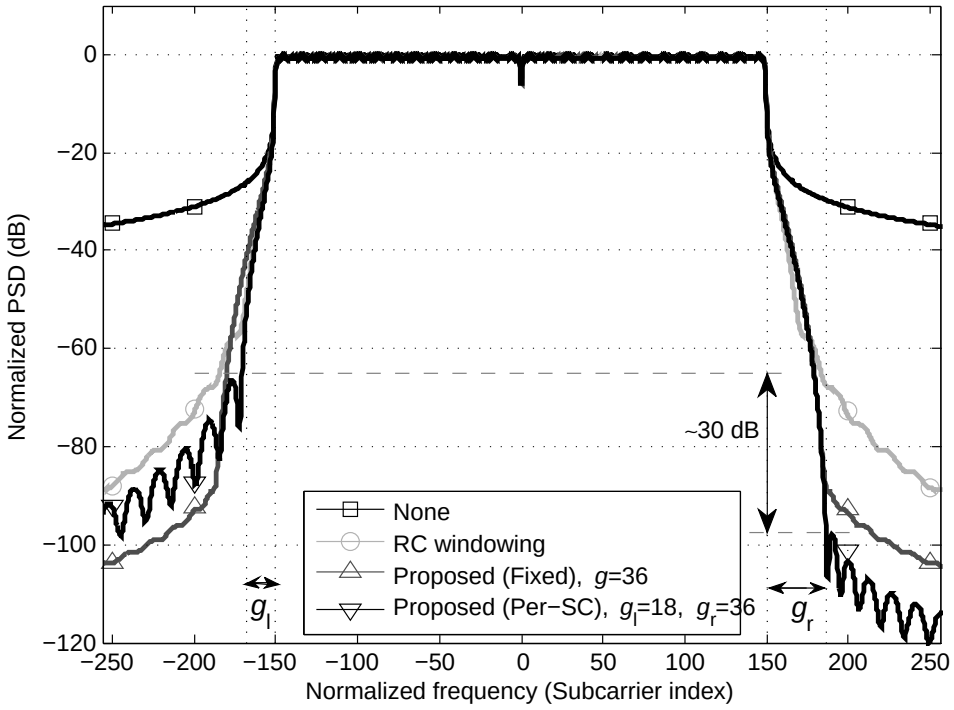

Figure 3.6 Fixed windowing and asymmetric implementation of the per-subcarrier windowing with different left and right guard bands.

objective is also is a monotonic function of two variables M and N_ϵ. Thus, the optimum parameters that maximize the spectral efficiency is heuristically found by first fixing one of the parameters, e.g., M, and searching over the other parameter, i.e., N_ϵ, until the boundary is reached. Then, local search over both parameters around a small region centered at the boundary points can be performed. After determining all of the points near the boundary of the constraint, the one that maximizes the objective function, i.e., spectral efficiency as in Figure 3.8, is obtained.

Table 3.1 reports the spectral efficiency results that are achieved by relaxing both the windowing duration and the number of used subcarriers for maximizing (3.26) while satisfying the corresponding mask. For each suppression level of the spectral mask, the proposed scheme with fixed implementation and per-subcarrier windowing provide greater spectral efficiency compared to conventional windowing scheme by allowing more subcarrier population and/or less windowing size utilization. The improvement in spectral efficiency for per-subcarrier windowing increases from 1.73% to 10.38% compared to RC windowing as deeper spectral suppression is forced, which is

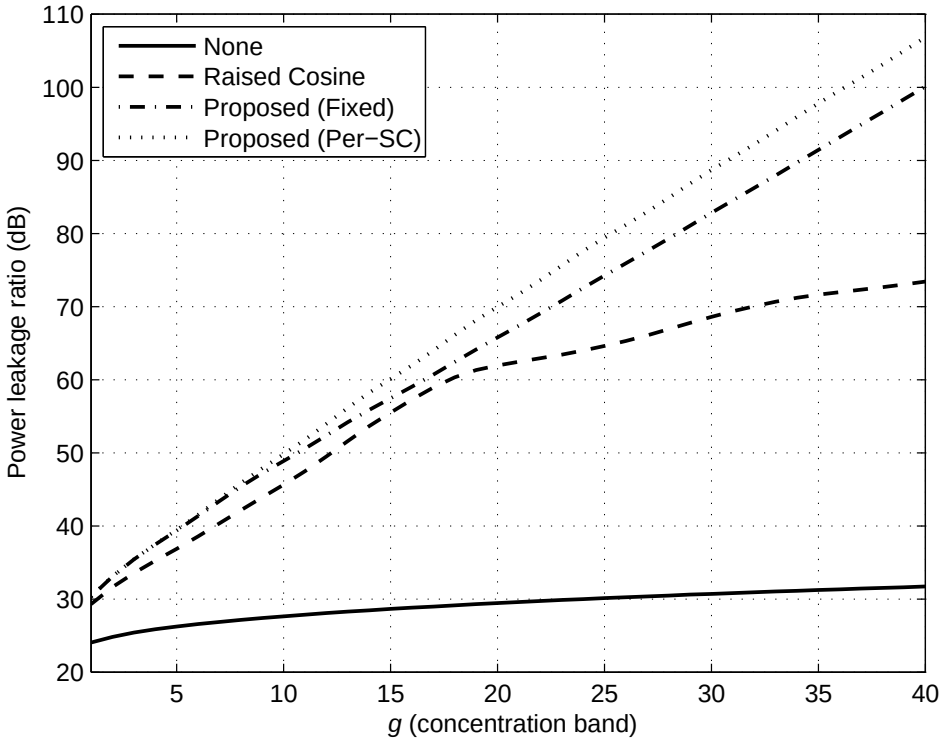

Figure 3.7 Spectral leakage performances for a given concentration band. $N = 512$, $N_\epsilon = 300$, $G = 64$, and $M = 32$.

Table 3.1 Symbol densities for different windowing schemes. $N = 512$, $G = 64$, and $M = 32$.

Suppression level of the spectral mask (dB)	Spectral efficiency (symbols/sec/Hz)				
	RC	Proposed(Fixed)		Proposed(Per-SC)	
			Increase (%)		Increase (%)
50	0.7436	0.7488	0.7	0.7564	1.73
55	0.7296	0.7417	1.66	0.7464	2.31
60	0.6989	0.7324	4.79	0.7370	5.45
65	0.6814	0.7227	6.07	0.7273	6.74
70	0.6512	0.7143	9.69	0.7188	10.38

one of the challenges in DSA scenarios. It is worth noting that the fixed windowing also provides remarkable performance with $\sim 1\%$ degradation compared to per-subcarrier case.

3.6.4 ACI Results

ACI results are evaluated in the presence of an adjacent channel interferer. The guard band between the desired signal and ACI signal is set as $28 \times F$, i.e., $\Delta f_i = 328 \times F$. We assume the

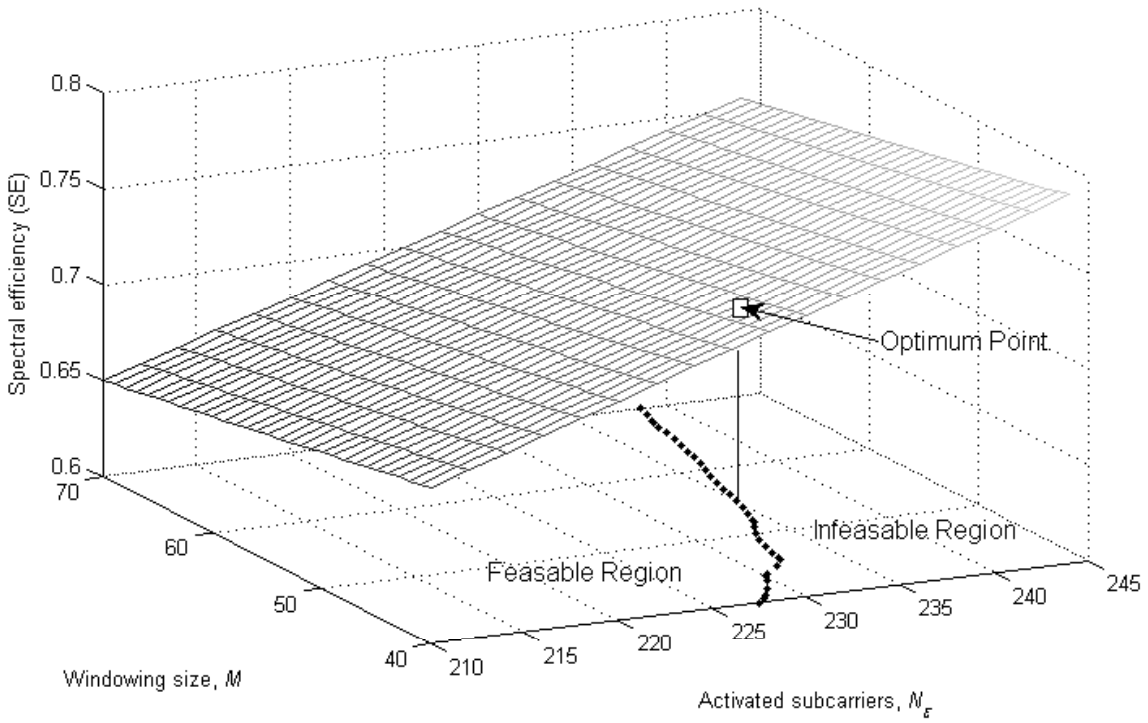

Figure 3.8 The joint optimization of both windowing size and the number of active subcarriers under a spectral mask constraint.

both desired and ACI signals have the same received power, i.e., $\alpha_\epsilon = \alpha_i$ which corresponds to the normalized ACI power. Without loss of generality, the interference power can be scaled up and down depending on the relative channel conditions for the interfering transmitter. Both signals experience Rayleigh fading. Figure 3.9 shows the PSD of ACI signal observed on each subcarrier location at the desired receiver. Three cases are considered including rectangular pulse shaping at ACI transmitter and desired receiver, RC transmit-windowing on ACI signal and receiver-windowing at desired receiver, and subcarrier-specific transmit-windowing at ACI and subcarrier-specific receiver-windowing at desired receiver. As can be observed from the normalized ACI results, proposed subcarrier-specific receiver windowing achieves the best ACI rejection among other windowing scenarios.

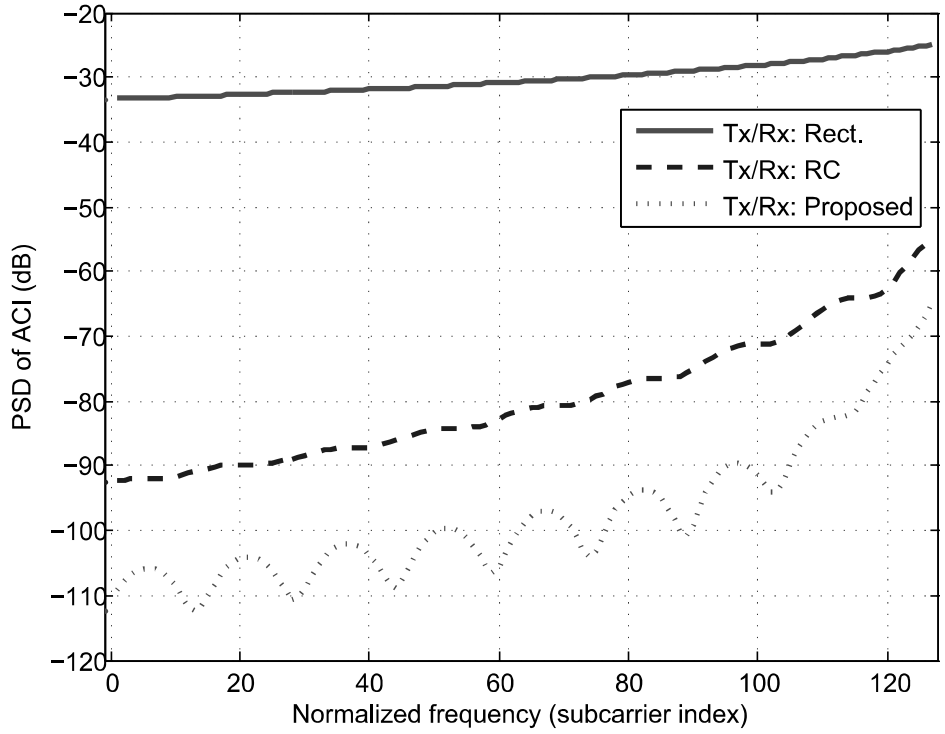

Figure 3.9 Spectral density of adjacent channel interference power for various transmitter and receiver windowing configurations.

3.6.5 Computational Complexity

Achieving the optimum result for spectral concentration with proposed schemes comes with increase in computational complexity. In this section, we present a possible way of generating the OFDM symbols based on the proposed scheme. For the fixed windowing cases, a small increase in the complexity occurs for shaping the transition durations after generating the time domain signal via inverse fast Fourier transform (IFFT). For the per-subcarrier cases, direct implementation based on the signal model in (3.1) requires high number of arithmetic operations. In order to reduce the implementation complexity for per-subcarrier aprroach, generation of CP and main parts (total size of $G + N$) can be performed similar to prevalent schemes with IFFT by utilizing the that there is no modification on these parts as in Figure 3.1(a). Then, the transition parts can be calculated according to pulse shape functions by using direct implementation and appended to the main part. Essentially, when fixed pulse-shaping is utilized for all subcarriers, additional $4M$ real

multiplications are required for symbol transition after obtaining the time domain symbol with inverse fast Fourier transform (FFT). For per subcarrier pulse shaping, however, output of inverse FFT cannot be directly used and hence, a direct implementation is required for the transition part. We evaluate the complexities of different schemes in terms of number of real multiplications per OFDM symbol normalized to that of CP-OFDM based on efficient Split-Radix FFT algorithm [115]. Also, it is worth noting that the computational complexity of the per-subcarrier scheme can also be reduced by dividing the subcarriers into groups, and utilizing a common pulse shape for each group.

We would like to emphasize that the computation of the optimum windowing function is an offline process that requires one-time solution of the Rayleigh quotient. When a change in the OOB requirement occurs, different configurations of asymmetric implementation can be realized by reusing previously computed functions. The only parameter for a windowing function is its concentration band Ω_k. Hence, the functions for inner subcarriers of one configuration can be reused for the outer subcarriers for another configuration, which eliminates new computation for most of the subcarriers for the new setting. Similar to reusing, a lookup table method can also reduce the complexity of the asymmetric implementation with subcarrier specific windowing.

3.7 Conclusions

In this chapter, we evaluate the available guard band in an OFDM scheme per-subcarrier basis, which allows maximal utilization of the spectrum for achieving optimal time-frequency con-

Table 3.2 Complexity comparison of the windowing schemes for $N = 512$, $G = 64$, and $M = 32$

Scenario	Normalized complexity
CP-OFDM	1
Fixed windowing	1.1
Per-SC windowing (Direct implementation)	383.5
Per-SC pulse-shaping (Mixed implementation)	11.6

centration at the transmitter and ACI rejection at the receiver via windowing functions. The proposed windowing strategy considers the locations of subcarriers and exploits the available guard band of each subcarrier. By jointly optimizing the transition duration and number of active subcarriers, the windowing functions that yields maximum spectral efficiency while complying with a prescribed the spectral mask is derived. At the receiver side, we also show that the proposed windowing function can be utilized in order to maximize the ACI rejection capability by exploiting the guard band between desired and ACI signal.

CHAPTER 4:
TIME-ASYMMETRIC AND SUBCARRIER-SPECIFIC PULSE SHAPING IN OFDM-BASED WAVEFORMS

4.1 Introduction

In wireless communications, orthogonal frequency-division multiplexing (OFDM)-based signaling enables efficient wideband transmission by converting frequency-selective fading channel to multiple narrowband flat-fading channels[1]. In addition, flexibility with independent utilization of the subcarriers provides a strong motivation for deployment in cognitive radio (CR) scenarios [116]. Despite its prominent benefits, OFDM waveform suffers from high out-of-band (OOB) emission due to the rectangular transmit pulse.

A simple countermeasure to high OOB emission has been smoothing the symbol transitions via shaping the boundaries of the rectangular transmit pulse [93–96, 98, 101, 102], which is also referred as time domain windowing. Smoother pulse shaping functions for OFDM subcarriers provide suppressed spectral response as opposed to slow decaying sinc-shaped subcarriers. In the literature, shaping the OFDM symbols is proposed in spectrum pooling scenarios [93] to reduce the interference on adjacent channels via rapid decaying of OOB spectrum. Also the authors present the trade-off between interference reduction and throughput by considering the flexible guard band with subcarrier deactivation. Pulse-shaped OFDM is demonstrated in [95] by dynamically tailoring the properties of spectrum neighbors in dynamic spectrum access (DSA) scenarios. In [96], authors proposed using longer transition duration complied with shorter cyclic prefix (CP) for the band-edge subcarriers, and longer CP with shorter transition duration for the inner subcarriers. The motivation in this approach is to reduce the total redundancy by exploiting different mul-

[1]The content of this chapter is published in [100]. Copyright notice for this publication can be found in Appendix C.

tipath delay spread characteristics of the users in orthogonal frequency-division multiple access (OFDMA) scenario. In [98], receiver windowing is also taken into account to reject adjacent-channel interference (ACI) along with the transmit pulse shaping to reduce OOB spectral leakage. In a recent study [99], block-emission-mask compliant pulse shaping technique is studied based on the optimization of the roll-off parameter, which determines the duration of time extension, and subcarrier-specific transmit power.

Spectral suppression with pulse shaping can be achieved at the expense of either degradation of spectral efficiency (SE) or introduction of inter-symbol interference (ISI)/inter-carrier interference (ICI). In the first case, CP is extended and shaped for smooth transition, which keeps zero-ISI/ICI property in multipath channel [93–96, 99]. Despite the interference-free setup with sufficient CP size, increasing the effective symbol duration reduces the OFDM symbol rate and hence SE. In the second approach, which is adopted in [101] and [98], a portion of the existing CP is used for the transition period without conceding the OFDM symbol rate. The drawback in this approach is introducing interference due to multipath components exceeding the reduced CP size. However, the transition period in the second approach still has a partial role on dealing with the multipath components. That is, the transition part can be designed to be effective against the ISI/ICI caused by the insufficient CP size. Thus, with the motivation of maintaining the SE, which is a crucial issue in future wireless communication systems, we tackle the introduced interference in pulse shaped OFDM by using the part of the CP, i.e., adopt the second approach.

In this chapter, we propose time-asymmetric and subcarrier-specific pulse shaping method to minimize the ISI/ICI for a spectrally efficiency and well-localized OFDM waveform. The multipath channel with which the transmitted signal is filtered has a one-sided time response because of the causality. Thus, time-asymmetric pulse shape strengthens the guarding property of the transition duration against delay spread by reducing the effect of multipath components from the previous OFDM symbol falling into the fast Fourier transform (FFT) window of the receiver, and increasing the contribution from the current symbol. Although it is considered for Nyquist pulses in the context of single carrier signals, asymmetric filter design for coping with ISI is studied in [117],

and it is shown that the time-asymmetric Nyquist filter can reduce ISI when the second multipath component is weaker than the first one.

Designing the transmit pulse shape in a time-asymmetric manner worsens the spectral response of the subcarriers for which the trade-off between OOB emission reduction and ISI/ICI mitigation emerges. However, this trade-off can be mitigated by considering the multicarrier nature of the OFDM as a degree of freedom via per-subcarrier pulse-shaping. When the time-asymmetry of pulse shapes for the inner subcarriers is gradually increased, spectral growth can be contained in the signal bandwidth without causing increase in the OOB frequency range. By minimizing the interference caused by insufficient CP, the proposed per-subcarrier asymmetric pulse shaping scheme provides superior bit error rate (BER) performance over conventional schemes. The main contributions of this chapter can be itemized as follows

- Concept of time-asymmetric pulse shaping for OFDM subcarriers is introduced in order to reduce the ISI/ICI. For this purpose, generalized Kaiser window (GKW) is proposed as a practical and closed-form pulse shaping function with adjustable time-asymmetry.

- ISI/ICI - OOB trade-off in spectrally efficient pulse shaping is mitigated with per-subcarrier design of the time-asymmetric waveform that minimizes introduced interference while maintaining both OOB emission and SE. Subcarrier specific interference and mean BER are derived as a function of the employed per-subcarrier pulse shaping and channel delay profile.

It is worth noting that in the proposed OFDM transmission, the modification is performed only on the transition part that is implemented at the transmitter. Therefore, by maintaining the same symbol- and total guard- durations, there is no need a change in existing frame structure and OFDM-based receivers since the transition part is removed at the receiver along with the CP.

The remainder of this chapter is organized as follows: In Section 4.2, the system model is introduced. Then, the interference analysis along with asymmetric design is given in Section 4.3. In Section 4.4, per-subcarrier implementation of the proposed pulse shaping is presented. A novel generalized Kaiser window (GKW) function that allows time asymmetry is introduced into the proposed framework in Section 4.5. In Section 4.6, further discussions on the proposed scheme

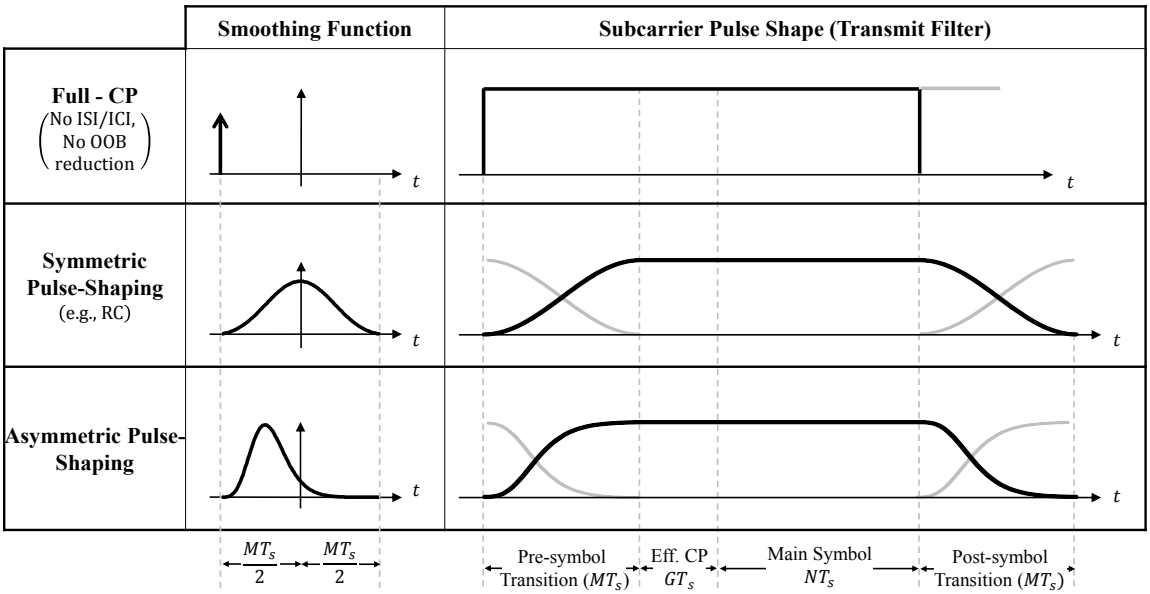

Figure 4.1 Three pulse shaping scenarios with associated smoothing functions. Full-CP where all of the time extension is used for CP, conventional pulse shaping, and time-asymmetric pulse shaping with shortened CP durations for the purpose of maintaining the SE.

are provided. Performance results and comparisons are given in Section 4.7 and finally, conclusions are drawn in Section 4.8.

Notation: Matrices [columns vectors] are denoted with upper [lower] case boldface letters (e.g., $\mathbf{A}$ [$\mathbf{a}$]); calligraphic letters (e.g., $\boldsymbol{\mathcal{A}}$) denote the submatrix of a previously defined matrix (e.g., $\mathbf{A}$); $\{\mathbf{A}\}_{i,j}$ indicates the $(i+1, j+1)$th element of an $N \times M$ matrix $\mathbf{A}$, with $i \in \{0, 1, \ldots, N-1\}$ and $j \in \{0, 1, \ldots, M-1\}$; $\star$ and $\circ$ denote the convolution operation and entrywise matrix product, respectively; superscripts T and H denote transpose, and conjugate transpose, respectively; $\mathbf{0}_{N \times M}$ and $\mathbf{I}_N$ represent the $N \times M$ zero matrix and $N \times N$ identity matrix, respectively; δ_{ij} is the Kronecker delta function, $j = \sqrt{-1}$ is the imaginary unit; and $\mathbb{E}_x[y(x)]$ denotes the expectation of $y(x)$ over the random argument x.

4.2 System Model

We consider a pulse-shaped OFDM system which employs N subcarriers. Instead of one prototype filter for all subcarriers, we define the transmit filter, i.e., pulse shape, for each subcarrier

specifically. Thus, complex representation for discrete-time domain OFDM signal is given as

$$s[n] = \frac{1}{\sqrt{N}} \sum_{m} \sum_{k=0}^{N-1} \gamma_{m,k} w_k \left((n - m\zeta) T_{\mathrm{s}} \right) e^{j \frac{2\pi}{N} k (n - m\zeta)} \tag{4.1}$$

where $\gamma_{m,k}$ is independent and identically distributed (i.i.d.) symbol (e.g., QAM) modulated on the kth subcarrier of the mth OFDM symbol with zero mean and unit variance, i.e.,

$$\mathbb{E}\left[\gamma_{m,k} \gamma_{p,q}^{\mathrm{H}} \right] = \delta_{mp} \delta_{kq}, \tag{4.2}$$

$w_k(t)$ is the pulse shape function for the kth subcarrier, and T_{s} is the sampling duration. Note that (4.1) includes the sampling of the pulse shape function, which is originally defined in continuous time, that represents the discrete time OFDM signal. In (4.1), $\zeta = M + G + N$ denotes the effective symbol size in samples with M and G corresponding to the part of the CP allocated to symbol transition, and the shortened rectangular guard duration referred as effective CP, respectively. Hence, with the given fixed rate OFDM symbol structure as depicted in the last column in Figure 4.1, SE is maintained while performing OOB suppression albeit with the cost of introduced interference with shortened CP of size G. The proposed multicarrier waveform design minimizes this cost to improve BER performance.

As seen in Figure 4.1, pulse-shaping functions have unity response for CP and main symbol durations, and a smoothing response for the transition duration that constitutes the main focus of this chapter. Thus, the pulse shaping function $w_k(t)$ is obtained by convolution of the rectangular pulse, $\mathit{\Pi}(t)$, with the smoothing function $v_k(t)$ that characterizes the pulse shape as

$$w_k(t) = v_k(t) \star \mathit{\Pi}(t), \tag{4.3}$$

where

$$\mathit{\Pi}(t) = \begin{cases} 1, & \left(-\frac{M}{2} - G\right) T_{\mathrm{s}} \leq t < \left(N - 1 + \frac{M}{2}\right) T_{\mathrm{s}}, \\ 0, & \text{otherwise.} \end{cases} \tag{4.4}$$

The smoothing function in (4.3) is normalized in amplitude as $\int_{-MT_s/2}^{MT_s/2} v_k(t)\mathrm{d}t = 1$, in order for the pulse shape function to take the unity response for mentioned parts. For reference, commonly used raised-cosine (RC) pulse shaping is adopted as the conventional case where the smoothing filter can be written as

$$v_{\mathrm{RC}}(t) = \begin{cases} \frac{\pi}{2MT_s}\cos\left(\frac{\pi t}{MT_s}\right), & -\frac{MT_s}{2} \le t < \frac{MT_s}{2}, \\ 0, & \text{elsewhere.} \end{cases} \tag{4.5}$$

Another important property of $w_k(t)$ by virtue of (4.3) and the normalization is the vestigial symmetry with respect to ζT_s. That is,

$$\sum_{m=-\infty}^{\infty} w_k\left((n-m\zeta)T_s\right) = 1, \text{ for } N-\zeta \le n < N. \tag{4.6}$$

The smoothing function characterizes the OFDM signal in terms of OOB emission. As convolution operation in (4.3) implies, the power spectrum of pulse-shaped OFDM subcarrier is determined by the spectrum of the smoothing function along with the sinc type frequency response of the rectangular function.

The transmitted signal passes through a time-variant multipath channel after which the received signal can be given as

$$y[n] = \sum_{\ell=0}^{L-1} h_\ell[n]s[n-\ell] + z[n] \tag{4.7}$$

where L is the number of multipath channel taps, i.e., maximum excess delay (MED), $h_\ell[n]$ is the complex coefficient for ℓth tap, and $z[n]$ is the additive white Gaussian noise (AWGN), respectively. We assume that the channel taps are i.i.d., and fading coefficients are constant during one OFDM symbol. The received signal is then given as

$$y[n] = \sum_{\ell=0}^{L-1} h_\ell s[n-\ell] + z[n], \quad m\zeta \le n < (m+1)\zeta. \tag{4.8}$$

Unless otherwise specified, the power delay profile (PDP) of the multipath channel is considered as exponentially decaying [118] as

$$\Omega(\ell) = \mathbb{E}_h\left[|h_\ell|^2\right] = \Omega_0 10^{-\beta\ell}, \quad \ell = 0, \ldots, L-1, \tag{4.9}$$

where β denotes the decay rate, and $\Omega_0 = \frac{1-10^{-\beta}}{1-10^{-\beta L}}$ is for the normalization of total power of the channel to unity.

4.3 Interference Analysis and Asymmetric Pulse-Shape

In this section, the relationship between the pulse shape and ISI caused by the multipath channel is analyzed by considering a single subcarrier, i.e., $N = 1$. Then the analysis will be generalized to multicarrier case. Following the mentioned setting yields

$$s[n] = \sum_m \gamma_m w\left((n - m\zeta)T_\mathrm{s}\right) \tag{4.10}$$

for transmitted signal where the subcarrier index is omitted[2], i.e., $w = w_0$. The effective OFDM symbol consists of ζ samples (M for transition part, G for effective CP, and N for main symbol). The mth effective symbol can be formulated into vector form as

$$\begin{aligned}\mathbf{s}^m &= \left[s[-M-G+m\zeta], \ldots, s[N-1+m\zeta]\right]^\mathrm{T} \\ &= \gamma_{m-1}\mathbf{1}_\mathrm{p}\mathbf{w} + \gamma_m \mathbf{1}_\mathrm{c}\mathbf{w}\end{aligned} \tag{4.11}$$

[2]Since $N = 1$, the only subcarrier is the DC subcarrier whose subcarrier index is omitted for this section.

where

$$\mathbf{w} = \left[w\left((-M-G)T_{\mathrm{s}}\right), \ldots, w\left((N-1+M)T_{\mathrm{s}}\right)\right]^{\mathrm{T}},$$

$$\mathbf{1}_{\mathrm{p}} = \begin{bmatrix} \mathbf{0}_{M\times\zeta} & \mathbf{I}_{M} \\ \mathbf{0}_{(\zeta-M)\times\zeta} & \mathbf{0}_{(\zeta-M)\times M} \end{bmatrix}, \text{and}$$

$$\mathbf{1}_{\mathrm{c}} = \begin{bmatrix} \mathbf{I}_{\zeta} & \mathbf{0}_{\zeta\times M} \end{bmatrix}$$

denote the vector form of the pulse-shaping function, time-shifter matrix that shifts the pulse shaping function of the $(m-1)$th symbol by ζ, and the indicator matrix that takes the first ζ samples of the pulse shaping associated with the current symbol, respectively. Then, after passing through the multipath channel, the noiseless mth received symbol can be written as

$$\mathbf{y}^{m} = \mathbf{H}\mathbf{s}^{m} \tag{4.12}$$

where $\mathbf{H}$ is an $N \times \zeta$ Toeplitz matrix denoting the convolution of signal with the multipath channel impulse response and CP removal. That is,

$$\mathbf{H} = \begin{bmatrix} h_{M+G} & \cdots & h_0 & 0 & \cdots & 0 \\ 0 & h_{M+G} & \cdots & h_0 & \cdots & \vdots \\ \vdots & \ddots & \ddots & \cdots & \ddots & 0 \\ 0 & \cdots & 0 & h_{M+G} & \cdots & h_0 \end{bmatrix} \tag{4.13}$$

By substituting (4.11) into (4.12), the multipath signal components that fall into the FFT window of the mth symbol can be represented as

$$\mathbf{y}^{m} = \underbrace{\gamma_{m-1}\mathbf{H}\mathbf{1}_{\mathrm{p}}\mathbf{w}}_{\text{undesired}} + \underbrace{\gamma_{m}\mathbf{H}\mathbf{1}_{\mathrm{c}}\mathbf{w}}_{\text{desired}}. \tag{4.14}$$

The first term in (4.14) corresponds to ISI when MED of the channel exceeds the effective CP, i.e., $L > G$. This is because G is the length of shortened CP. In other words, while the multipath

components with smaller excess delay than G are handled by effective CP, the components with larger excess delay than G create ISI as a function of pulse shaping function. In (4.14), the second term includes multipath components of the current symbol. Note that the desired signal is also a function of $\mathbf{w}$, i.e., pulse shape. This effect can be identified by decomposing the desired part as

$$\mathbf{y}^m = \gamma_{m-1}\mathbf{H1}_{\mathrm{p}}\mathbf{w} - \gamma_m\mathbf{H1}_{\mathrm{c}}\left(1-\mathbf{w}\right) + \gamma_m\mathbf{H1}_{\mathrm{c}} \tag{4.15}$$

in which the second term denotes the reduction in the multipath components for the desired signal, and the last term is the expected desired signal without the effect of pulse shaping. By considering a three-tap multipath channel, Figure 4.2 illustrates these two effects on the ISI part (the first term in (4.15)), and the desired signal (the second term in (4.15)). Since we consider one carrier in this section, the effect of pulse shaping on the current symbol remains to be a reduction. However, for multicarrier case, this term also causes ICI between the subcarriers of the current symbol, which is given in the next section.

For a given channel realization, the ISI power can be given as

$$\begin{aligned} P_{\mathrm{I}} &= \mathbb{E}_{\gamma}\left[\left(\gamma_{m-1}\mathbf{H1}_{\mathrm{p}}\mathbf{w}\right)^{\mathrm{H}}\gamma_{m-1}\mathbf{H1}_{\mathrm{p}}\mathbf{w}\right] \\ &= \left(\mathbf{H1}_{\mathrm{p}}\mathbf{w}\right)^{\mathrm{H}}\mathbb{E}_{\gamma}\left[\gamma_{m-1}^{\mathrm{H}}\gamma_{m-1}\right]\mathbf{H1}_{\mathrm{p}}\mathbf{w} \\ &= \left(\mathbf{H1}_{\mathrm{p}}\mathbf{w}\right)^{\mathrm{H}}\mathbf{H1}_{\mathrm{p}}\mathbf{w}, \end{aligned} \tag{4.16}$$

by using (4.2). The vector form of smoothing filter, i.e., $\mathbf{v} = \left[v\left(-MT_{\mathrm{s}}/2\right),\ldots,v(MT_{\mathrm{s}}/2)\right]^{\mathrm{T}}$, is substituted into (4.16) since we design the smoothing filter that determines the pulse-shaping function. For this purpose, the convolution operation in (4.3) is defined in matrix form as $\mathbf{w} = \mathbf{R}\mathbf{v}$, where $\mathbf{R}$ is $(\zeta + M)\times(M+1)$ convolution matrix of the rectangular function. Thus, (4.16) is given in terms of the smoothing function as

$$P_{\mathrm{I}} = \mathbf{v}^{\mathrm{H}}\left(\mathbf{H1}_{\mathrm{p}}\mathbf{R}\right)^{\mathrm{H}}\mathbf{H1}_{\mathrm{p}}\mathbf{R}\mathbf{v}. \tag{4.17}$$

We can further simplify the interference power by considering the structures of convolution matrix $\mathbf{H}$ with zero elements for $i > j$ where $i = \{0, \ldots, N-1\}, j = \{0, \ldots, \zeta - 1\}$, and time-shifter matrix $\mathbf{1}_{\mathrm{p}}$ with zero and identity submatrices. In (4.17), the term that includes the channel, shifting of pulse-shaping function, and the convolution of the smoothing function with rectangular filter can be rephrased as

$$\begin{aligned}\mathbf{H}\mathbf{1}_{\mathrm{p}}\mathbf{R} &= \begin{bmatrix} \mathbf{0}_{M\times\zeta} & \boldsymbol{\mathcal{H}} \\ \mathbf{0}_{(N-M)\times\zeta} & \mathbf{0}_{(N-M)\times M} \end{bmatrix}\mathbf{R} \\ &= \begin{bmatrix} \boldsymbol{\mathcal{H}}\boldsymbol{\mathcal{R}} \\ \mathbf{0}_{(N-M)\times(M+1)} \end{bmatrix}\end{aligned} \tag{4.18}$$

where $\boldsymbol{\mathcal{H}}$ is $M \times M$ submatrix taking the first M rows and M columns of $\mathbf{H}$, and $\boldsymbol{\mathcal{R}}$ is $M \times (M+1)$ submatrix which consists of the last M rows of $\mathbf{R}$. That is, $\{\boldsymbol{\mathcal{R}}\}_{i,j} = 1$ for $i < j$, and 0 elsewhere.

The interference power above is evaluated for a given channel response by expectation over i.i.d. information symbols. Coefficients of the multipath channel are also random variables following a fading distribution, e.g., Rayleigh fading. Therefore, we perform the expectation over the realizations of the channel response. Then, by substituting (4.18) into (4.17), the expected interference power is given as

$$\begin{aligned}\tilde{P}_{\mathrm{I}} &= \mathbb{E}_{\mathbf{H}}\left[P_{\mathrm{I}}\right] \\ &= \mathbb{E}_{\mathbf{H}}\left[\mathbf{v}^{\mathrm{H}}\boldsymbol{\mathcal{R}}^{\mathrm{H}}\boldsymbol{\mathcal{H}}^{\mathrm{H}}\boldsymbol{\mathcal{H}}\boldsymbol{\mathcal{R}}\mathbf{v}\right] \\ &= \mathbf{v}^{\mathrm{H}}\mathbf{D}\mathbf{v}\end{aligned} \tag{4.19}$$

where $\mathbf{D} = \boldsymbol{\mathcal{R}}^{\mathrm{H}}\mathbb{E}_{\mathbf{H}}\left[\boldsymbol{\mathcal{H}}^{\mathrm{H}}\boldsymbol{\mathcal{H}}\right]\boldsymbol{\mathcal{R}}$ is a symmetric matrix whose nonzero elements are monotonically increasing along increasing rows and columns. By invoking that the channel taps are i.i.d., elements of $\mathbf{D}$ can be given in terms of the PDP as

$$\{\mathbf{D}\}_{i,j} = \sum_{\substack{\ell=G+M \\ -\lambda+1}}^{G+M} (\ell + \lambda - G - M)\,\Omega(\ell), \tag{4.20}$$

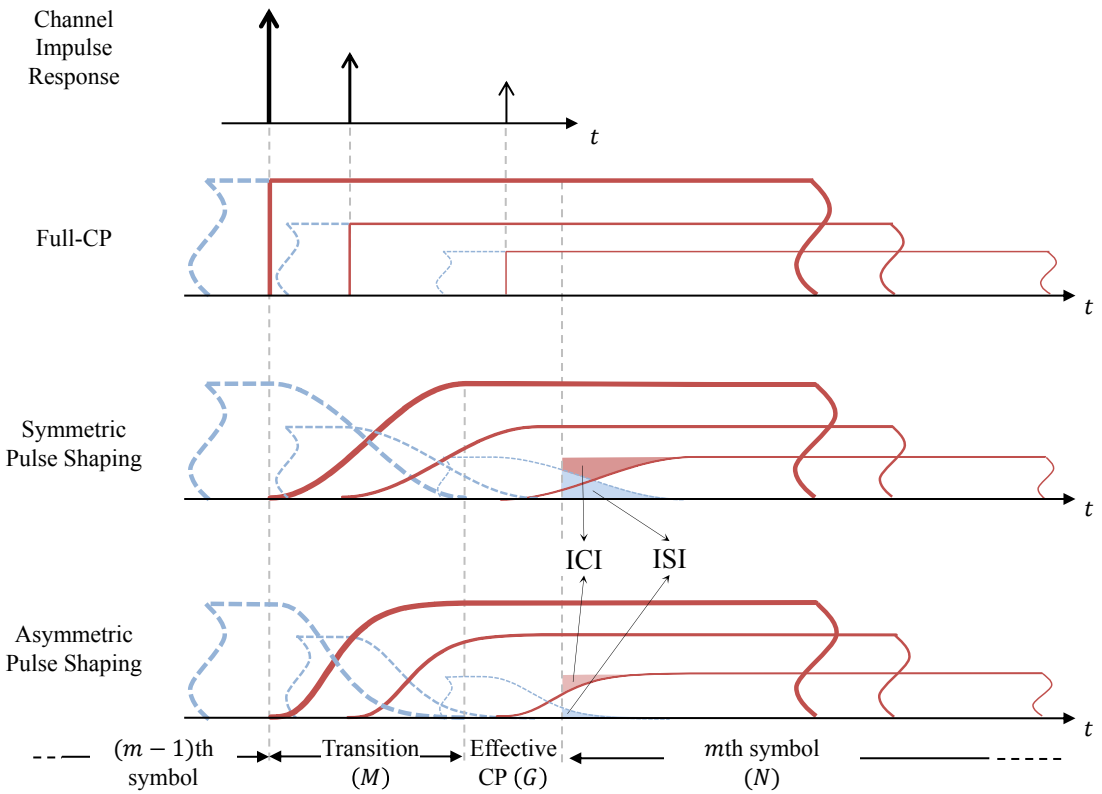

Figure 4.2 OFDM waveform scenarios with 3-tap channel are illustrated by focusing on the symbol transition. While the multipath components do not create interference for full-CP case, the components that exceed the effective CP result in ISI/ICI in pulse shaped OFDM. Time-asymmetric pulse shaping reduces interference contributions.

where $\lambda = \min(i, j)$. Therefore, the relationship between smoothing function and interference power is established in (4.19). Monotonically increasing profile of elements of $\mathbf{D}$ implies that the interference power in the quadratic form in (4.19) reduces as the value of the smoothing function is more concentrated on the earlier indexes (time). Clearly, no interference occurs when $\mathbf{v} = [1, 0, 0, \ldots, 0]^{\mathrm{T}}$, i.e., when CP size is set as $M + G$ without any pulse shaping. As illustrated in Figure 4.1, this case is referred as full-CP with smoothing function corresponding to Dirac delta with a time lag of $-MT_{\mathrm{s}}/2$. Also, conventional (time-symmetric) and asymmetric smoothing functions and associated pulse shapes are depicted in the same figure.

In full-CP case, the smoothing function rejects all multipath components falling into the FFT window at the receiver. For conventional symmetric case, e.g., RC as in (4.5), the asymmetric

profile of the multipath components creating ISI are captured after being weighted with the symmetric smoothing function. The last waveform scenario, which is depicted in the last row in Figure 4.1, is an arbitrarily asymmetric with respect to the time origin. The effect of time asymmetry towards the earlier time brings better ISI rejection capability than that of the conventional case as it can be observed from Figure 4.2. In fact, the proposed asymmetric pulse shaping stands in between two existing OFDM signal structures: Full-CP and conventional (symmetric) pulse shaping. On one hand, full-CP provides perfect interference rejection with extremely asymmetric pulse shape without any spectral shaping. On the other hand, a symmetric pulse shape achieves good spectral shaping but poor guarding against the interference caused by multipath delay spread. As the balancing solution, the asymmetric pulse comes with superior ISI mitigation than the conventional pulse shaping while compromising the spectral shape. It is worth noting that the asymmetry in the time domain for pulse shape has no correspondence to asymmetry in frequency as the real function in time domain has conjugate symmetric response in frequency, and hence symmetric power spectrum however. Thus, we conclude that when a single pulse-shape is considered, it is inevitable to trade between the OOB emission and ISI/ICI for a given SE. In the next section, we show that the interference side of this trade-off can substantially be reduced by taking the multicarrier nature of the OFDM waveform into account.

4.4 Per-Subcarrier Asymmetric Pulse Shaping

Removing the transition and effective CP portions before applying FFT correspond to rectangular receiver filtering, which implies the biorthogonality of the pulse-shaped OFDM similar to CP-OFDM [86]. This removing process provides flexibility in transmit pulse shape design as a degree of freedom when it is coupled with the multicarrier waveform structure. In particular, providing better interference mitigation with time asymmetric pulse shape causes a degradation in OOB performance. By following this fact, time-asymmetry of the pulse of a specific subcarrier can be determined based on the level of contribution of that subcarrier on the OOB emission of the composite signal. Since the band edge subcarriers have greater effect on the spectral emission, symmetric pulse shaping functions can be adopted for the edge subcarriers. Then, by increasing

the time asymmetry for the inner subcarriers for achieving better interference mitigation, the spectral response of the composite signal on the OOB range can be kept minimally affected. Figure 4.3 depicts the subcarrier specific time asymmetry of the proposed OFDM waveform structure in time-frequency plane. Detailed design procedure to obtain pulse shaping parameters for the per subcarrier time-asymmetric waveform will be given in Section 4.5. It is worth noting that the time asymmetry of the pulse shaping function does not imply an asymmetry in the power spectrum. However, the asymmetry in the frequency domain can be achieved via exploiting the subcarrier specific pulse shaping which is regardless of time asymmetry, which out of the scope of this chapter.

Before moving on to the choice of pulse shaping functions in the subcarrier specific manner, in the following, we investigate interference that is caused by multipath delay spread in the presence of multiple subcarriers and subcarrier specific pulse-shaping. Adopting the vector form for the multicarrier case in (4.1), the mth effective OFDM symbol can be written as

$$\mathbf{s}^m = \mathbf{1}_{\mathrm{p}} \left(\mathbf{W} \circ \mathbf{F}_{\mathrm{f}}^{\mathrm{H}} \right) \boldsymbol{\Upsilon}_{m-1} + \mathbf{1}_{\mathrm{c}} \left(\mathbf{W} \circ \mathbf{F}_{\mathrm{f}}^{\mathrm{H}} \right) \boldsymbol{\Upsilon}_m \tag{4.21}$$

where $\boldsymbol{\Upsilon}_m = [\gamma_{m,0}, \ldots, \gamma_{m,N-1}]^{\mathrm{T}}$ is complex information vector for mth OFDM symbol, and $\mathbf{F}_{\mathrm{f}} = [\boldsymbol{\mathcal{F}}_{\mathrm{B}}\ \boldsymbol{\mathcal{F}}_{\mathrm{G}}\ \mathbf{F}\ \boldsymbol{\mathcal{F}}_{\mathrm{A}}]$ with $\boldsymbol{\mathcal{F}}_{\mathrm{B}}$, $\boldsymbol{\mathcal{F}}_{\mathrm{G}}$, and $\boldsymbol{\mathcal{F}}_{\mathrm{A}}$ denoting the submatrices of $N \times N$ discrete Fourier transform (DFT) matrix $\mathbf{F}$ including the columns corresponding to pre-symbol transition, CP, and post-symbol parts, respectively. In (4.21), $\mathbf{W} = [\mathbf{w}_0, \ldots, \mathbf{w}_{N-1}]$ denotes the pulse-shaping matrix with each column corresponding to the pulse for associated subcarrier. After passing through the multipath channel, DFT operation converts the received signal into frequency domain in which the information symbols are defined. Received data vector is then given as

$$\hat{\boldsymbol{\Upsilon}}_m = \mathbf{F}\mathbf{H}\mathbf{s}^m. \tag{4.22}$$

The multipath components exceeding the effective CP result in ICI between the subcarriers of current OFDM signal as well as ISI between consecutive symbols. ISI and ICI are represented

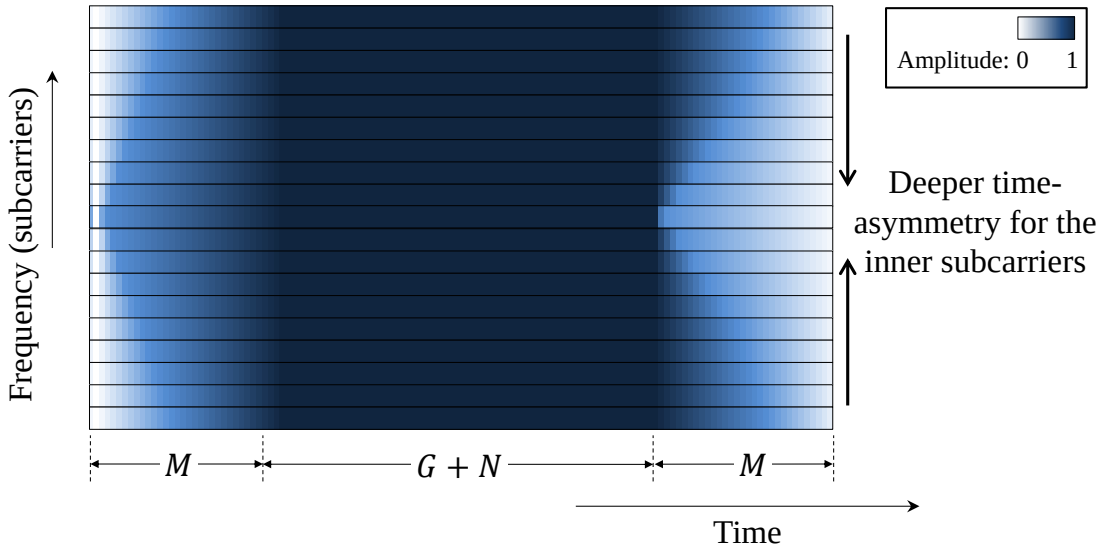

Figure 4.3 Time-frequency structure of the proposed per-subcarrier time-asymmetric pulse shaping functions denoting the values in $\mathbf{W}$. Asymmetry of the subcarrier pulses are gradually increased for inner subcarriers which maintains the spectral response for the OOB range while minimizing ISI/ICI.

by decomposing the received symbol as

$$\hat{\boldsymbol{\Upsilon}}_m = \Delta_{\mathbf{H}} \boldsymbol{\Upsilon}_m + \mathbf{FH1}_{\mathrm{p}} \left(\mathbf{W} \circ \mathbf{F}_{\mathrm{f}}^{\mathrm{H}} \right) \boldsymbol{\Upsilon}_{m-1} - \underbrace{\mathbf{FH1}_{\mathrm{c}} \left((\mathbf{J} - \mathbf{W}) \circ \mathbf{F}_{\mathrm{f}}^{\mathrm{H}} \right) \boldsymbol{\Upsilon}_m}_{\boldsymbol{\Upsilon}_m^{\mathrm{und.}}} \tag{4.23}$$

where $\mathbf{J}$ is all 1 matrix with same size of $\mathbf{W}$, and $\Delta_{\mathbf{H}} = \mathbf{FH1}_{\mathrm{c}} \mathbf{F}_{\mathrm{f}}^{\mathrm{H}} \boldsymbol{\Upsilon}_m$ is the diagonalized channel matrix with diagonal elements representing the channel response at associated subcarrier frequency. In (4.23), the first term is the desired signal, the second and the third terms denote ISI and ICI for $L > G$, respectively.

A closer look into the transmitter operations in (4.23), which corresponds to synthesis of the transmitted signal from the information symbols, yields the term corresponding to ISI as

$$\mathbf{1}_{\mathrm{p}} \left(\mathbf{W} \circ \mathbf{F}_{\mathrm{f}}^{\mathrm{H}} \right) = \begin{bmatrix} \boldsymbol{\mathcal{R}} \mathbf{V} \circ \boldsymbol{\mathcal{F}}_{\mathrm{A}}^{\mathrm{H}} \\ \mathbf{0}_{(N-M) \times N} \end{bmatrix} \tag{4.24}$$

where $\mathbf{V} = [\mathbf{v}_0, \ldots, \mathbf{v}_{N-1}]$. For the ICI term, we use the vestigial symmetric property of the pulse shaping functions to be able to write

$$\mathbf{1}_{\mathrm{c}} \left((\mathbf{J} - \mathbf{W}) \circ \mathbf{F}_{\mathrm{f}}^{\mathrm{H}} \right) = \begin{bmatrix} \boldsymbol{\mathcal{R}} \mathbf{V} \circ \boldsymbol{\mathcal{F}}_{\mathrm{B}}^{\mathrm{H}} \\ \mathbf{0}_{(N-M) \times N} \end{bmatrix} \tag{4.25}$$

The undesired terms in (4.23) are used to obtain the total interference power in multicarrier case as a function of the per-subcarrier smoothing functions. Expectation over i.i.d. information symbols yields

$$\begin{aligned} P_{\mathrm{I}} &= \mathbb{E}_{\boldsymbol{\Upsilon}} \left[\left(\boldsymbol{\Upsilon}_m^{\text{und.}} \right)^H \boldsymbol{\Upsilon}_m^{\text{und.}} \right] \\ &= \mathrm{tr} \left(\left(\boldsymbol{\mathcal{R}} \mathbf{V} \circ \boldsymbol{\mathcal{F}}_{\mathrm{A}}^{\mathrm{H}} \right)^{\mathrm{H}} \boldsymbol{\mathcal{H}}^{\mathrm{H}} \boldsymbol{\mathcal{H}} \left(\boldsymbol{\mathcal{R}} \mathbf{V} \circ \boldsymbol{\mathcal{F}}_{\mathrm{A}}^{\mathrm{H}} \right) \right) \\ &\quad + \mathrm{tr} \left(\left(\boldsymbol{\mathcal{R}} \mathbf{V} \circ \boldsymbol{\mathcal{F}}_{\mathrm{B}}^{\mathrm{H}} \right)^{\mathrm{H}} \boldsymbol{\mathcal{H}}^{\mathrm{H}} \boldsymbol{\mathcal{H}} \left(\boldsymbol{\mathcal{R}} \mathbf{V} \circ \boldsymbol{\mathcal{F}}_{\mathrm{B}}^{\mathrm{H}} \right) \right) \end{aligned} \tag{4.26}$$

Similarly, the expected interference power considering the multipath fading channel is obtained as

$$\begin{aligned} \hat{P}_{\mathrm{I}} &= \mathbb{E}_{\mathbf{H}} \left[P_{\mathrm{I}} \right] \\ &= 2\mathrm{tr} \left(\mathbf{V}^{\mathrm{H}} \mathbf{D} \mathbf{V} \right). \end{aligned} \tag{4.27}$$

It is clear that assigning different transmit filter for each subcarrier results in experiencing different levels of interference, as a function of pulse shape associated to that subcarrier. Therefore, it is necessary to investigate the expected interference power for individual subcarriers. By using the undesired signal vector as the last two terms in (4.23), expected interference power for kth subcarrier can be obtained by determining the mth diagonal element of the covariance matrix as

$$\hat{P}_{\mathrm{I}}(k) = \left\{ \mathbb{E}_{\mathbf{H}} \left[\mathbb{E}_{\gamma} \left[\boldsymbol{\Upsilon}_m^{\text{und.}} \left(\boldsymbol{\Upsilon}_m^{\text{und.}} \right)^H \right] \right] \right\}_{k,k} \tag{4.28}$$

which is a function of the subcarrier specific waveform and the PDP of the multipath channel.

4.4.1 OOB Emission Constraint for Composite Signal

Power spectral density (PSD) of the OFDM signal composed of N pulse-shaped subcarriers with i.i.d. symbols, as in (4.2), can be given as [33]

$$S_s(f) = \sum_{k=0}^{N-1} \left| W_k(f - k'\Delta f) \right|^2 \tag{4.29}$$

where $W_k(f)$ denotes Fourier transform (FT) of $w_k(t)$, and k' denotes the shifted subcarrier index corresponding to the actual location of kth subcarrier in the spectrum, i.e., $k' = k - N$ for $k \geq N/2$, and $k' = k$ otherwise. It is known from (4.3) that $W_k(f)$ is determined by FTs of the smoothing function, $V_k(f)$, and sinc(f). This yields,

$$W_k(f) = \zeta T_{\mathrm{s}} V_k(f) \mathrm{sinc}\left(\zeta T_{\mathrm{s}} f\right). \tag{4.30}$$

For an OFDM signal under consideration, OOB emission compliance is represented by the spectral mask as

$$S_s(f) \leq S_{\mathrm{mask}}(f), \quad f_{\mathrm{l}} \leq |f| \leq f_{\mathrm{u}} \tag{4.31}$$

where $S_{\mathrm{mask}}(f)$ is the spectrum emission mask that the transmitted signal needs to comply, and f_{l} and f_{u} are lower and upper frequency boundaries for the OOB region at both sides of the spectrum.

As mentioned earlier, increasing the robustness of a pulse shape against interference comes with an increase in the spectral sidelobes of corresponding subcarrier, as a function of the level of time-asymmetry. At this point, we exploit the multicarrier structure and the flexibility of designing independent pulse-shaping functions for each subcarrier, or for a set of subcarriers to mitigate this trade-off. In particular, the aim is to aggressively utilize the wider spectral room of inner subcarriers to the OOB region. That is, the spectral growth of time-asymmetric pulse shaping function is managed in such a way that the rise is contained inside the signal band, i.e., $\left[-\frac{N}{2}\Delta f,\ \left(\frac{N}{2} - 1\right)\Delta f\right]$. By doing so, the effect of the introduced asymmetry on the OOB spectrum is avoided. Thus, the design procedure consist of maximizing the asymmetry of pulse shaping function, i.e., minimizing

the interference, subject to a OOB constraint for each subcarrier. It is crucial to note that constraining each subcarrier with a given spectral mask, $S_{\text{mask}}(f)$, results in exceeding the mask after the composition of N subcarriers as in (4.29). To obtain a composite OFDM signal with PSD complying a given spectral mask, we decompose the mask into N components, and use each one for masking associated subcarrier. For this purpose, we employ PSD of RC pulse shaped OFDM signal as the spectral mask, i.e., $S_{\text{mask}}(f) = S_{\text{RC}}(f)$. This choice enables a simple decomposition of the spectrum mask into individual subcarriers as

$$\left|W_k(f - k'\Delta f)\right|^2 \leq \left|W_{\text{RC}}(f - k'\Delta f)\right|^2, f_{\text{l}} \leq |f| \leq f_{\text{u}},\ k' \in \left[-\frac{N}{2}, \frac{N}{2} - 1\right], \tag{4.32}$$

which yields the desired OOB constraint for the composite signal as

$$\begin{aligned} \sum_{k=0}^{N-1} \left|W_k(f - k'\Delta f)\right|^2 &\leq \sum_{k=0}^{N-1} \left|W_{\text{RC}}(f - k'\Delta f)\right|^2 \\ S_{\text{s}}(f) &\leq S_{\text{RC}}(f) \\ &= S_{\text{mask}}(f), \quad f_{\text{l}} \leq |f| \leq f_{\text{u}} \end{aligned} \tag{4.33}$$

In addition, forcing the composite spectrum of the proposed waveform to be less than or equal to that of symmetric pulse shaping inherently provides a fair comparison between the proposed and conventional schemes.

4.4.2 Optimization of Per Subcarrier Pulse Shapes

In the presence of delay spread longer than the reduced CP size, each subcarrier is spoiled by ISI component as a function of the utilized pulse shape, which is given in (4.19). Also, the same pulse function determines the ICI originated from that subcarrier on the other subcarriers of the same symbol. As shown in (4.27), these two interference components have the same power contribution when the vestigial symmetric property presented in (4.6) is satisfied. Performing a minimization on the total interference power in (4.27) does not guarantee a fair distribution of the total interference power among individual subcarriers. Thus, each subcarrier pulse shape needs

to be handled individually to be able to control its contribution on OOB emission as well as the ISI/acici. By also invoking the ISI/ICI equality, we perform the optimization for each subcarrier separately. Similar to objective function, constraint in the optimization is already configured to be per-subcarrier via decomposition of spectral mask as in Section 4.4.1. Thus, by substituting (4.30), the optimization problem can be represented in terms of the smoothing functions as

$$\begin{aligned} &\text{minimize } \mathbf{v}_k^{\mathrm{H}}\mathbf{D}\mathbf{v}_k \\ &\text{subject to } \left|V_k(f-k'\Delta f)\right|^2 \leq \left|V_{\mathrm{RC}}(f-k'\Delta f)\right|^2, \quad f_{\mathrm{l}} \leq |f| \leq f_{\mathrm{u}} \end{aligned} \tag{4.34}$$

for $k = 0, \ldots, N-1$. The problem in (4.34) falls into quadratically constraint quadratic problem (QCQP), which is generally NP-hard [119], and quite hard to solve since the optimization matrix $\mathbf{D}$ is not sparse. In the sequel, we propose a suboptimal closed form solution to asymmetric pulse shaping function design that can be used in the per-subcarrier pulse shaping scheme.

4.5 A Novel Solution to Asymmetric Pulse Design: Generalized Kaiser Window

In order to provide a simple solution for the design of pulse shaping function with flexible asymmetry, we take Kaiser window [114] as reference for generating the smoothing functions. Kaiser functions provide an approximation to the finite-length optimum spectrally concentrated function, which is critical as we consider containing the spectrum of each subcarrier in the signal bandwidth. Also, in its usage as the smoothing functions, its β-parameter allows adjustment of the time asymmetric behavior.[3] Hence, Kaiser window function is generalized by redefining the β-parameter as a function of time. Thus, the *GKW* is given as

$$v_{\mathrm{GKW}}(t) = \begin{cases} \dfrac{I_0\left(\beta(t)\sqrt{1-\left(\frac{2t}{MT_{\mathrm{s}}}\right)^2}\right)}{\int_{-MT_{\mathrm{s}}/2}^{MT_{\mathrm{s}}/2} I_0\left(\beta(\tau)\sqrt{1-\left(\frac{2\tau}{MT_{\mathrm{s}}}\right)^2}\right)\mathrm{d}\tau}, & -\frac{MT_{\mathrm{s}}}{2} \leq t < \frac{MT_{\mathrm{s}}}{2}, \\ 0, & \text{elsewhere,} \end{cases} \tag{4.35}$$

[3] Although generalizing the Kaiser window is considered here, one can also find other asymmetric pulse shape functions to be used in the given framework.

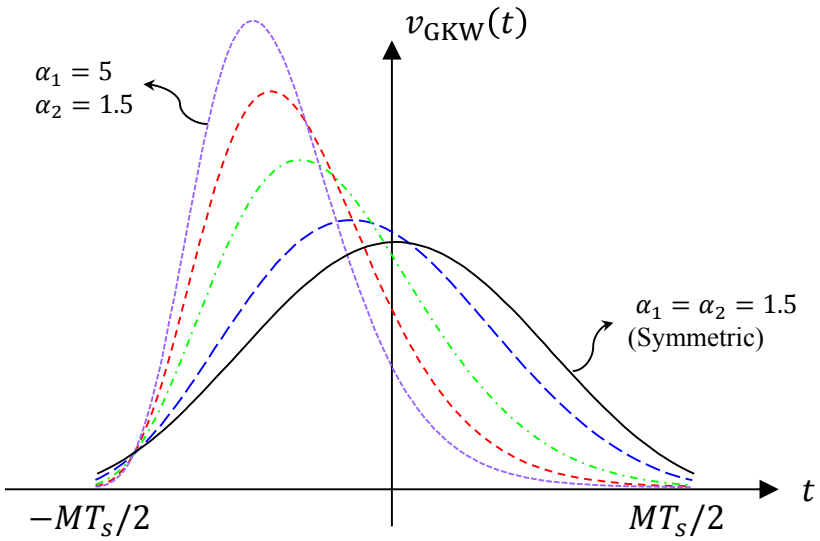

Figure 4.4 Generalized Kaiser windows. For given α_2, e.g., $\alpha_2 = 1.5$, increasing α_1 creates asymmetry in time towards left. From right to left, α_1 is 1.5, 2, 3, 4, and 5, respectively.

where $I_0(t)$ is the zeroth-order modified Bessel function of the first kind, and $\beta(t)$ is the time-variant β-parameter defined as

$$\beta(t) = \pi\alpha_1 \left(\frac{\alpha_2}{\alpha_1}\right)^{\left(\frac{t}{MT_s}+0.5\right)} \tag{4.36}$$

where the parameter pair (α_1, α_2) characterizes the asymmetry of the proposed smoothing function. The GKW-based smoothing function is then rewritten as $v_{\mathrm{GKW}}^{(\alpha_1,\alpha_2)}(t)$.

Since $I_0(x)$ is an exponentially increasing function of x, greater time scaling parameter $\beta(t)$ in (4.35) results in faster growing $v_{\mathrm{GKW}}^{(\alpha_1,\alpha_2)}(t)$. Therefore, selecting $\alpha_1 > \alpha_2$ makes the smoothing function leaning back in time, which is desired for the pulse-shaping function to mitigate the interference caused by delay spread. in In Figure 4.4, GKW functions with different (α_1, α_2) pairs are given. The deeper time-asymmetry is obtained as increasing α_1 for a given α_2. Note that for α_1 and α_2 , i.e., constant β, GKW simplifies to the conventional (symmetric) Kaiser window function with $\beta = \pi\alpha_1 = \pi\alpha_2$.

By introducing GKW in the waveform design, the problem in (4.34) is readily reduces to finding only two parameters, α_1 and α_2, for the smoothing function. In order to reduce the search space for α_1 and α_2, we start the optimization from the edge subcarrier. In other words, since there

is no enough room for spectral growth of the edge subcarrier due to introduced time asymmetry, the PSD of RC pulse, as the constraint for the edge subcarrier, forces the GKW pulse shape to be symmetric similar to RC. Then, the parameters for the kth subcarrier are found as

$$\begin{aligned}\left(\alpha_1^{(k)}, \alpha_2^{(k)}\right) = \arg \min_{\left(\tilde{\alpha}_1^{(k)}, \tilde{\alpha}_2^{(k)}\right) \in \Theta_k} & \left(\mathbf{v}_{\mathrm{GKW}}^{\left(\tilde{\alpha}_1^{(k)}, \tilde{\alpha}_2^{(k)}\right)}\right)^H \mathbf{D} \mathbf{v}_{\mathrm{GKW}}^{\left(\tilde{\alpha}_1^{(k)}, \tilde{\alpha}_2^{(k)}\right)} \\ \text{subject to } & \left| V_{\mathrm{GKW}}^{\left(\tilde{\alpha}_1^{(k)}, \tilde{\alpha}_2^{(k)}\right)}(f - k'\Delta f) \right|^2 \leq \left| V_{\mathrm{RC}}(f - k'\Delta f) \right|^2, \ f_{\mathrm{l}} \leq |f| \leq f_{\mathrm{u}}, \end{aligned} \tag{4.37}$$

where Θ_k denotes the two dimensional local search space for the parameter pair of the kth subcarrier. The local search region represents $\tilde{\alpha}_1^k \in [\alpha_1^{(k+1)} - \theta, \alpha_1^{(k+1)} + \theta]$ and $\tilde{\alpha}_2^k \in [\alpha_2^{(k+1)} - \theta, \alpha_2^{(k+1)} + \theta]$ where θ determines the size of local search space. That is, since the constraint for each subcarrier is incrementally changed from the $(k+1)$th to the kth subcarrier, the best GKW parameter set for the kth subcarrier is searched in the close vicinity of the parameter set found in the $(k+1)$th subcarrier. The design procedure for finding the GKW parameters is summarized in Table 4.1.

Each GKW-shaped subcarrier is masked by the spectral response of RC counterpart in the OOB region. Therefore, the lack of enough degree of freedom for the band edge subcarriers in terms of OOB constrained, (4.37) forces the smoothing function for edge subcarrier to be symmetric similar to the conventional cases. However, as the inner subcarriers with wider guard bands becomes the object of the interference minimization problem in (4.37), α_1 is allowed to increase smoothly in contrast to α_2. Therefore, the interference minimization problem with a given (decomposed) spectral mask results in an OFDM waveform with per-subcarrier pulse shaping along with time

Table 4.1 Procedure for finding GKW parameters.

start
$k = N/2 - 1$
$\alpha_1^{(k)} = 2.5, \ \ \alpha_2^{(k)} = 2.5$
while $k \geq -N/2$
$k = k - 1$
find $\left(\alpha_1^{(k)}, \alpha_2^{(k)}\right)$ by following (4.37)
end

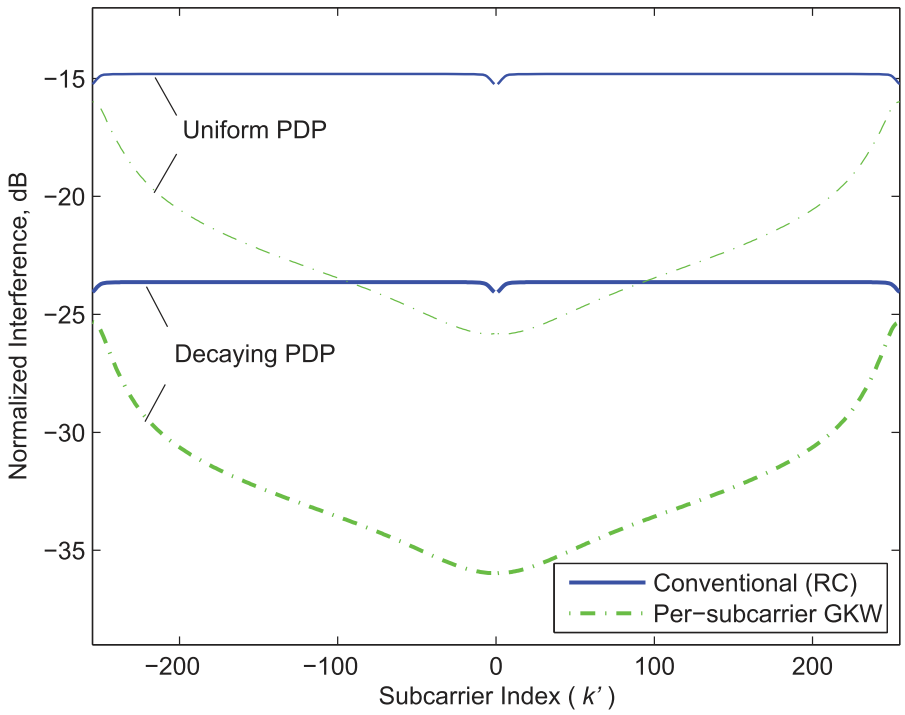

Figure 4.5 Expected interference due to multipath delay spread along subcarriers. Increasing time-asymmetry for the inner subcarriers with GKW-based pulse shapes achieves superior interference mitigation.

asymmetric functions. As also illustrated in Figure 4.3, the pulse shapes for edge subcarriers are more symmetric than the ones for the inner subcarriers.

The nonuniform level of time-asymmetry across the subcarriers directly affects the amount of interference caused by multipath delay spread. That is, ISI/ICI contribution has also nonuniform profile over the subcarriers. In Figure 4.5, expected interference powers per subcarrier given in (4.28) are given for uniform and exponentially decaying PDPs[4]. For the pulse shaping scenarios, per subcarrier GKW setup obtained by (4.37), and conventional symmetric pulse shaping are considered. Parameters for the OFDM waveform are set as $N = 512$, $M = 3G = 3N/16$, and the channel length is set to total redundant period, i.e., $L = M + G$. As seen in Figure 4.5, while RC pulse-shaping experiences uniform interference over subcarriers, increasing asymmetry of the

[4]It is worth noting that PDP of the effective channel might have a transient increase before decaying exponentially once the RF front end components such as bandpass filter are taken into account. However, this transient part can be considered to be covered by the allocated effective CP of size G.

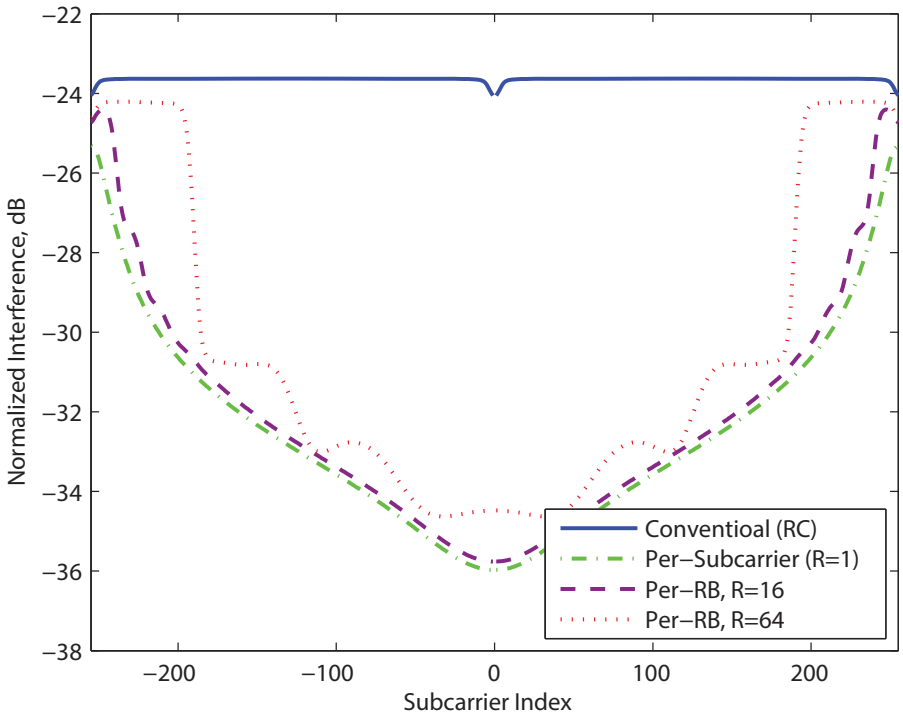

Figure 4.6 Expected interference along subcarriers for various resource block (RB) sizes. Changing the asymmetry of the pulse shaping for every R subcarrier results in a quantized interference profile.

subcarrier pulse shapes with GKW functions provide up to 12 dB less interference power for the inner subcarriers and have similar consequence for edge subcarriers as expected with symmetric configuration. Further improvements by taking nonuniform suppression of interference into account will be noted in the next section.

4.6 Further Notes

4.6.1 Per Resource-Block (RB) Time-Asymmetric Pulse Shaping

Per-subcarrier pulse shaping opportunistically utilizes the spectral room of each subcarrier while minimizing the interference-OOB trade-off. However, high number of subcarriers each shaped with specific pulse shaping function results in an increase in baseband implementation cost, which will be analyzed in the following sections. Thus, we propose a simple approach for this issue by decreasing the number of distinct pulse shapes in the composite OFDM waveform. Instead of employing a pulse shape for each subcarrier, a group of consecutive subcarriers, referred as resource

block (RB), are shaped with a common function. The pulse shape of the RB is determined based on the most critical subcarrier in that RB. In other words, as the spectral constraint in (4.17) implies, outer subcarriers are allowed to have less time asymmetry due to smaller distance to the band edge compared to inner subcarriers. Therefore the pulse shape of RB with R subcarriers is set as pulse shape of the outermost subcarrier in that RB. Apparently, per-RB pulse shaping reduces the resolution along the frequency domain and comes with a slight loss in ISI/ICI mitigation performance. This can be observed from Figure 4.6 in which the interference powers over subcarriers for per-RB asymmetric pulse shaping with various RB sizes are depicted. As can be seen from the figure, changing the pulse shape for every R subcarriers results in a quantized profile for expected interference power.

4.6.2 Improvements for Non-Uniform Interference

Since the edge subcarriers have greater effect on the OOB emission, experiencing a nonuniform degradation along the subcarriers is a common issue in OFDM spectral suppression [97, 120]. In our case, this can be readily addressed by simple countermeasures such as selective modulation/coding across subcarriers. Besides that, user degree of freedom in an OFDMA scenario can also be considered to enhance the error rate performance further, which is also proposed in [97] in the context of edge windowing [96]. In the multiple access scenario, the edge subcarriers/RBs can be assigned to users that experience less time dispersion which can be mapped to the distance of the user to the base station [121].

4.6.3 Complexity

We evaluate the complexities of different schemes in terms of number of real multiplications per OFDM symbol normalized to that of CP-OFDM based on efficient Split-Radix FFT algorithm [115]. Since we keep the receiver side unchanged, there is no additional complexity at the receiver. Since we do not perform any modification on the CP and main parts of the OFDM waveform, generation of these parts (total size of $G+N$) of the composite signal is the same as prevalent schemes with FFT. However, M-sample transition duration requires more effort compared to con-

ventional pulse shaping. Essentially, when one pulse shape is utilized for all subcarriers, additional $4M$ real multiplications after obtaining the time domain symbol with inverse FFT are required for symbol transition. For per subcarrier pulse shaping, output of inverse FFT cannot be directly used and hence, a matrix multiplication is required. In particular, when the symbol generation in (4.21) is considered, the transition part equals to the multiplication of upper submatrix of $\mathbf{W}$ including the first M rows and the input vector.

The results are summarized in Table 4.2. While the generation of per-subcarrier pulse-shaped OFDM schemes requires relatively higher number of real multiplications. However, for per-RB cases, OFDM (or OFDMA downlink) has reduced implementation complexity that decreases with increasing R. Also, when we take into account the uplink cases in OFDMA scenarios, the complexity in per-RB case is directly proportional to number of RB, r, used by the mobile nodes.

4.7 Results

In this section, performance results of the proposed OFDM waveform is evaluated and compared with the performance of the conventional CP-OFDM and OFDM with symmetric pulse shaping. For the three OFDM structures total excess time, hence the SE is fixed, i.e., $\zeta = 5N/4$, (refer Figure 4.1). In CP-OFDM without any OOB emission concern, all of the excess period is allocated for CP (full-CP) while in the two pulse-shaped OFDM waveforms, 3/4 of the excess

Table 4.2 Normalized complexity of the pulse shaping schemes for $N = 512$, $G = 32$, and $M = 96$

Scenario	Normalized complexity		
	OFDM	OFDMA	
		$r = 1$	$r = 2$
CP-OFDM (Full-CP)	1	1	1
Conv. pulse-shaping	1.1	1.1	1.1
Per-SC pulse-shaping	32.9	2.9 ($R = 16$) 8.9 ($R = 64$)	4.9 ($R = 16$) 16.9 ($R = 64$)
Per-RB pulse-shaping	17.9 ($R = 16$) 4.4 ($R = 64$)	1.1	2.2

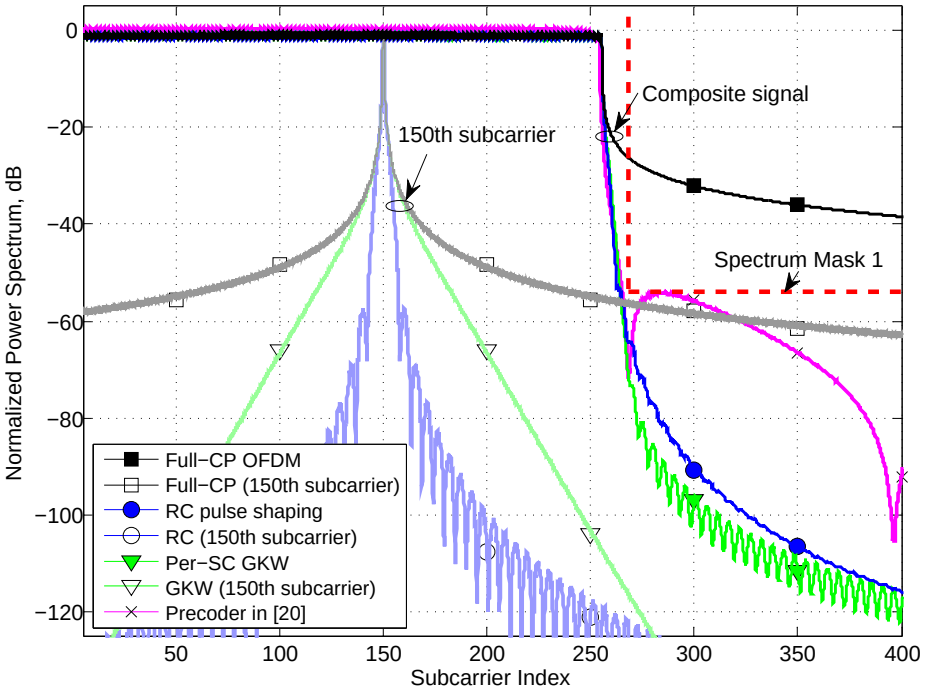

Figure 4.7 Power spectra for three scenarios. Composite signal, contribution of an inner (e.g., $k' = 150$) subcarrier, and the PSD for the precoder in [20] with parameters set to satisfy the Mask 1 are given. Contribution of the inner GKW subcarrier reveals in-band growth due to time-asymmetry, which has no effect in OOB emission.

period is used as transition period, i.e., $M = 3G = 3N/16$. The number of subcarriers N is set to 512 on which 16-QAM modulated symbols are modulated.

Figure 4.7 depicts the PSD of the composite OFDM signals for three cases. The PSD of a single inner subcarrier with index $k' = 150$ is also illustrated to clearly show the effect of time asymmetric pulse shaping on an individual subcarrier spectrum. In the design procedure of GKW waveform in Section 4.5, the frequency response of each subcarrier pulse is constrained by the spectrum of RC pulse that is centered at the same frequency location as given in (4.37). When this is done for each subcarrier, the PSD of the composite signal for per-subcarrier (per-SC) asymmetric GKW becomes constrained by the PSD of the composite OFDM signal with RC pulse shaping in the OOB frequency range. As the result of time asymmetry, the robustness against ISI/ICI for the inner subcarriers comes as in-band spectral growth that has no effect in OOB emission.

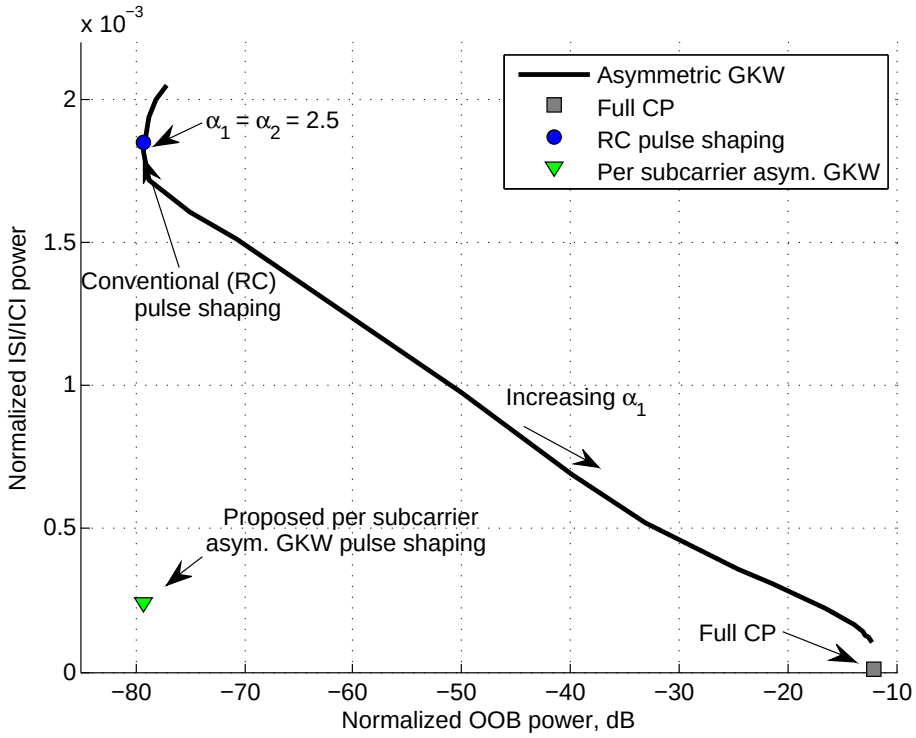

Figure 4.8 The trade-off between OOB power and ISI/ICI as a function of time asymmetry of the pulse shape. The proposed scheme breaks the trade-off with reduced interference by maintaining the OOB performance.

For further comparison, a well known precoding-based OOB emission reduction method [122] is also considered. To have a fair comparison between the pulse shaping methods and the precoding method, the parameters of the precoder are selected such that the same number of active subcarriers will satisfy the spectral mask given in [102], referred as mask 1. For this purpose, the spectral null locations of the precoder in [122] are set to $\{\pm 269.5, \pm 270, \pm 396.5, \pm 397\}$, measured in subcarrier spacing. The precoding that we selected for comparison is a fixed one that does not depend on the transmitted data symbols, so that the implementation is similar to pulse shaping methods for fair comparison. The interested readers are directed to the other studies [123, 124] that include the complexity comparison of pulse shaping methods to the more complex and data-dependent schemes.

The interference mitigation property of the time asymmetric pulse trades the OOB emission. In the following, the trade-off between the OOB suppression and ISI/ICI mitigation is presented.

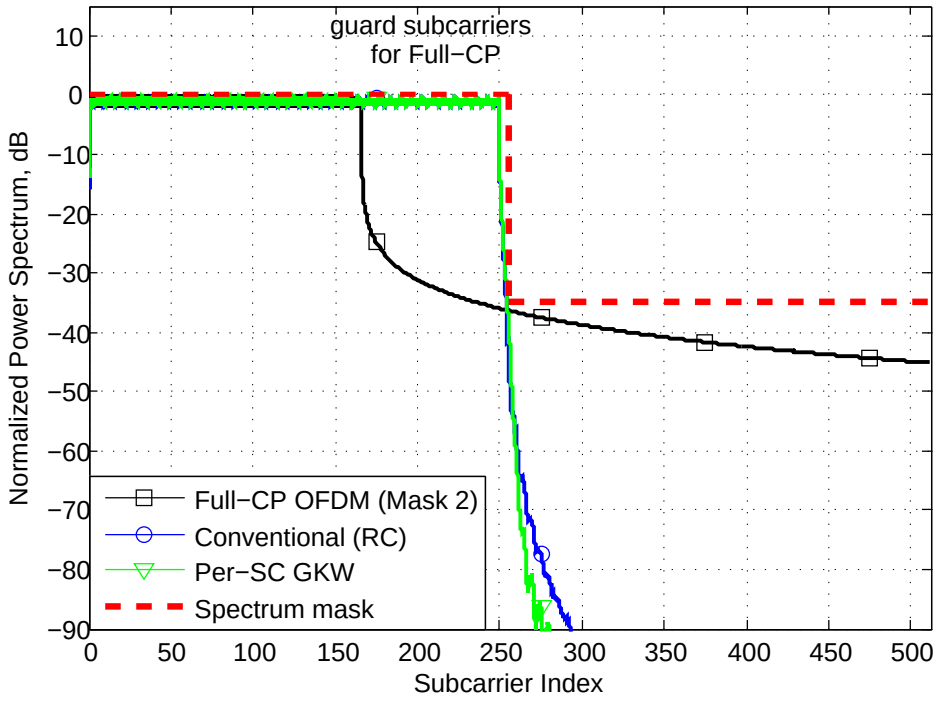

Figure 4.9 PSD results with the mask compliant version of the full-CP case.

Also, our method of per-SC time asymmetry is given. Figure 4.8 shows the operation points of all pulse shaping scenarios in terms of the OOB and interference power. When all subcarriers have the same pulse shape function without any per subcarrier implementation, increasing asymmetry of the GKW pulse shape with increasing α_1 corresponds to reduction in the interference, however increasing the OOB power approaching the one that belongs to the full-CP case. Note that full-CP is an interference-free scheme with the worst OOB performance. The symmetric pulse shaping on the other hand, which is the case for $\alpha_1 = \alpha_2 = 2.5$, or RC pulse shape corresponding the same OOB and interference performance, results in the best OOB suppression while loosing from the interference mitigation capability. Finally, our scheme with subcarrier specific time asymmetry with GKW pulse shapes minimizes the interference power by achieving the same OOB performance of the symmetric pulse shapes. For the per-SC GKW scheme, the parameters found in the optimization given in (4.37) starts from $\left({\alpha_1}^{(k)}, {\alpha_2}^{(k)}\right) = (2.5, 2.5)$ for the edge subcarriers from both sides, i.e., for $k = 255$ and $k = 256$, and ends at $\left({\alpha_1}^{(k)}, {\alpha_2}^{(k)}\right) = (56.8, 0.13)$ at the first subcarriers from both sides, i.e., for $k = 1$ and $k = 511$.

Next, we compare the BER performance of the three waveforms. In order to make a fair comparison, all waveforms have to achieve a certain level of OOB. As it can be observed from Figure 4.7, however, the OOB emission of full CP OFDM is significantly higher and does not have comply the mask. Therefore, some subcarriers in the full-CP case are allocated for guard band so that the PSD can stay within the given mask[5]. After assigning 172 guard subcarriers (i.e., 86 on left and right) for full-CP OFDM that corresponds to 340 activated subcarriers, denoted as N_{S} in Table 4.3, the OOB of full-CP becomes as shown in Figure 4.9 along with the other scenarios. In addition to spectral emission, data rate for three OFDM waveforms should be equal for a fair BER comparison. Since full CP OFDM complying the OOB requirement has fewer active subcarriers, the modulation order is increased from 16-QAM to 64-QAM; with these parameters the data rate becomes 2044 bits per OFDM symbol for all three waveforms.

In the following, we consider the error rate performance by both using the theoretical expected interference powers from (4.28), and performing Monte Carlo simulations. Block fading 6-tap Rayleigh-distributed multipath channel is considered with MED equal to length of the total redundancy, $N/4$. The decaying rate of exponential PDP is set as $\beta = \frac{2}{L-1} = \frac{8}{N}$ so that the last tap is 20 dB below the first tap. For the analytical results, we performed Gaussian approximation for the ISI/ICI component by invoking the central limit theorem. Then, BER for each subcarrier based on the signal to interference plus noise ratio (SINR) is calculated [125] and averaged across subcarriers. For the simulation results, 1,000 OFDM symbols are generated for each channel realization and QAM demodulation is performed after performing frequency domain equalization by using the perfect channel knowledge at the receiver. Then, the BER results from 50 channel realizations are averaged.

In Figure 4.10, BER results are given for three main scenarios as well as the precoder in [122]. Note that since CP completely covers the multipath delay spread in full-CP case without dedicating any resource for smoothing symbol transition (without mask compliance), it corresponds to lower bound in terms BER. The proposed per-subcarrier asymmetric pulse shaping approaches

[5]For comparing the mask compliant version of the full-CP case, we adopt using a relaxed version of the spectrum mask given in [102] since the there is no possibility of satisfying the original version of the mask with 55 dB suppression. Thus, we set the suppression as 35 dB in the relaxed mask and referred as mask 2.

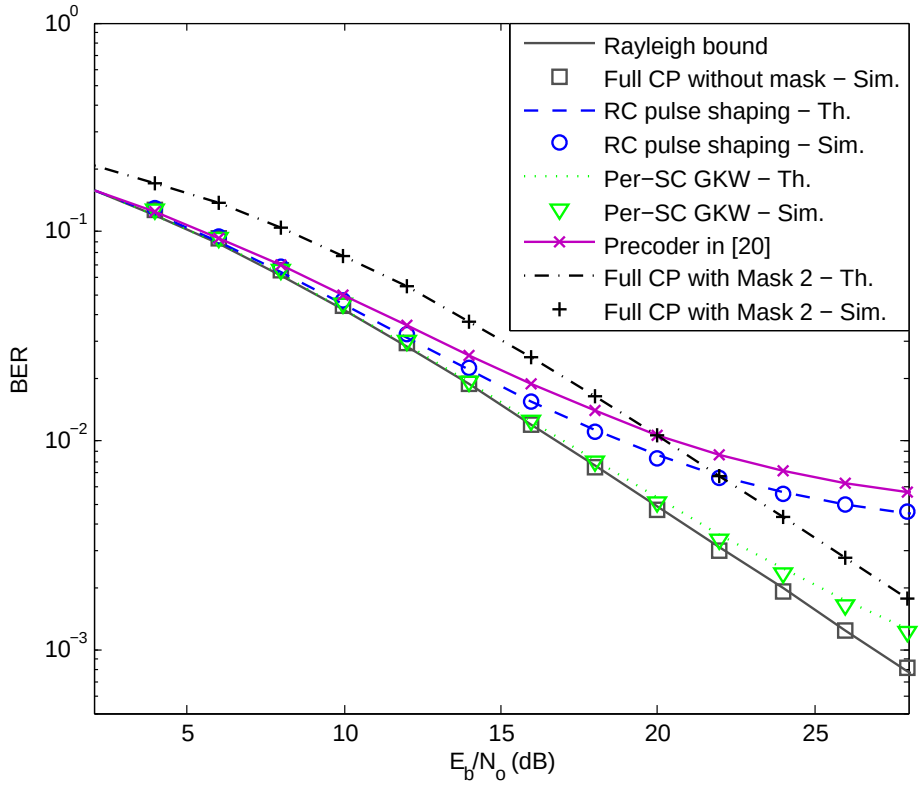

Figure 4.10 BER performance for full-CP case without mask compliance corresponding to error bound, RC pulse shaping, per-subcarrier asymmetric GKW, precoder in [20], and full-CP case with mask compliance via guard subcarriers.

Table 4.3 Parameters for three waveform cases complying the spectrum mask with same data rate

	Spectrum Mask	Modulation	Interference	BER
Full CP	✓($N_S = 340$)	64-QAM	No	↑
RC pulse	✓($N_S = 511$)	16-QAM	↑	↑
Per-SC GKW	✓($N_S = 511$)	16-QAM	↓	↓

the lower limit while achieving the same OOB emission of conventional pulse shaping, i.e., RC. For comparison of the mask compliant version of the full-CP case, as given in Table 4.3, the error rate becomes higher due to increased modulation order. That is, even with a relaxed mask restriction, the per-subcarrier GKW achieves the lowest BER for a given SE and spectral mask. It is worth noting that the BER results for pulse shaping cases (e.g., RC and GKW) belong to the worst cases in terms of channel realizations because the MED is fixed to the length of total guard time

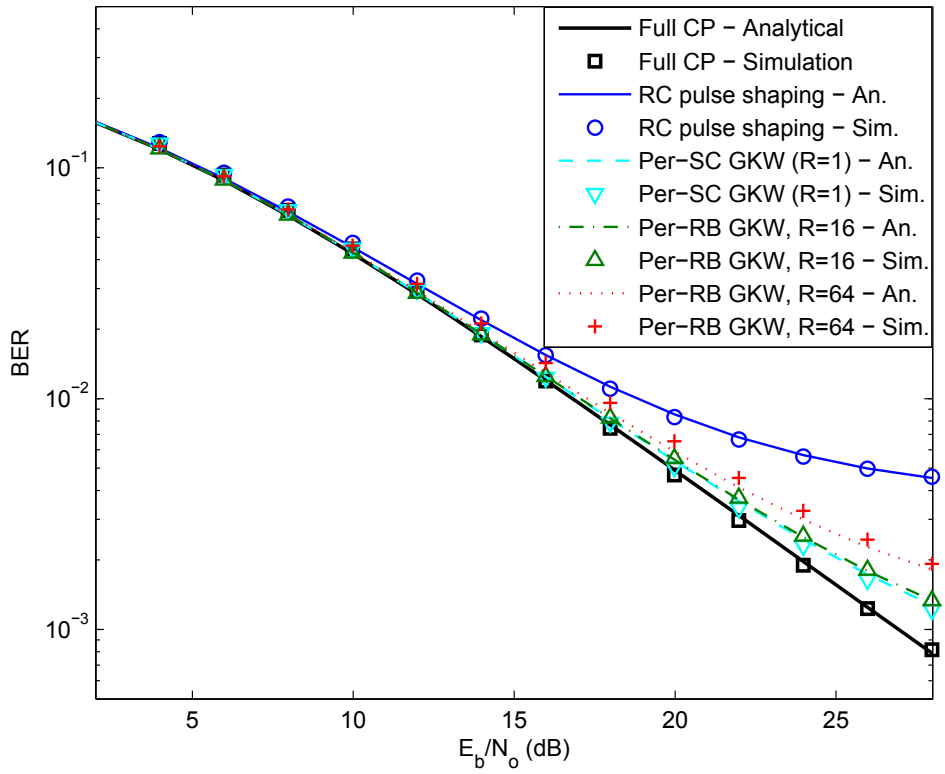

Figure 4.11 BER performances for resource block specific time-asymmetric GKW as a function of the RB size.

(transition and CP). However, statistically, the channel can be shorter than CP, which is generally designed to satisfy the worst MED scenario. On the other hand, the distortion introduced by the precoder on the data symbols in precoding type schemes is not a function of channel, i.e., always exists regardless of the channel condition. For per-RB asymmetric pulse shaping cases, sacrifice from full degree of freedom comes with slight degradation in BER performance compared to per-subcarrier case. As shown in Figure 4.11, BER performance with $R = 16$ is almost the same as that of per-subcarrier case ($R = 1$), while slight degradation is observed for $R = 64$.

The effect of imperfect channel state information at the receiver is also investigated in the proposed framework. The channel estimation error is measured in mean-squared error (MSE) and connected to the received SNR as $MSE = \rho \times SNR$ where ρ corresponds to effective length of the training sequence. The BER results as a function of the quality of the channel information at the receiver are given in Figure 4.12. As it can be observed from the figure, the gain of the proposed

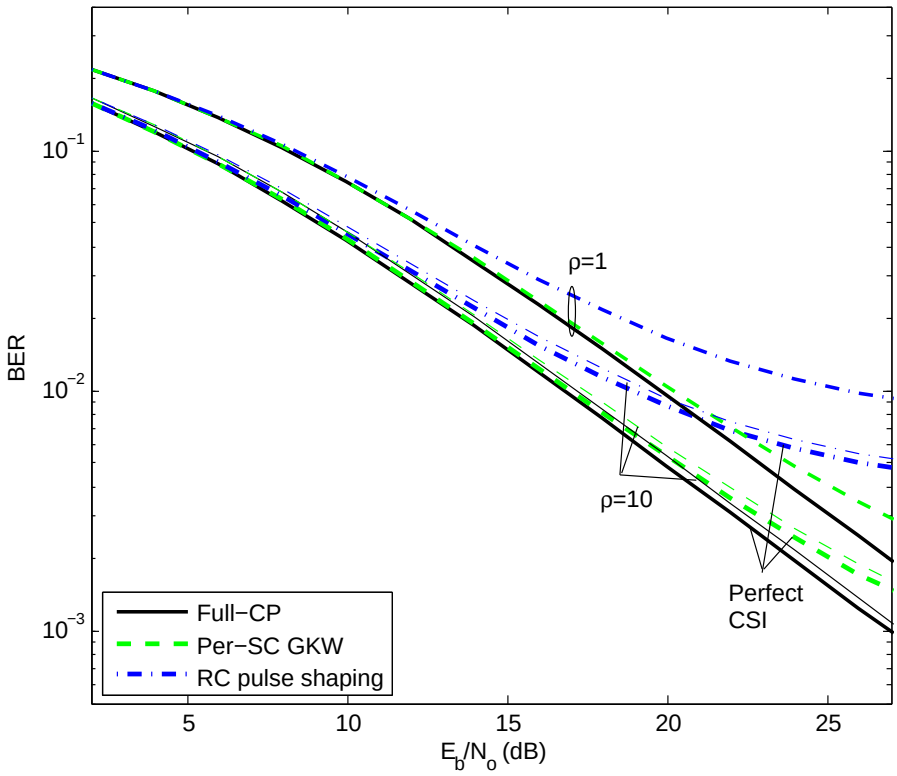

Figure 4.12 BER performances in the presence of imperfect channel state information.

scheme compared to the other scenarios for a given MSE is not affected by the imperfection of the channel information at the receiver.

Finally, we investigate BER performance when selective modulation across subcarriers are performed to mitigate the effect of nonuniform interference profile as shown in Figure 4.6. To illustrate this effect, the inner $N/2$ subcarriers are assigned to 16-QAM while the remaining outer subcarriers (N/4 lower edge and N/4 upper edge) are assigned to QPSK modulation with same symbol power. As shown in Figure 4.13, BER performance with per-subcarrier setting follows that of the full-CP case closer since QPSK is more robust to perturbation.

4.8 Conclusions

Multipath delay spread is introduced as a criterion for pulse shaping design in addition to sidelobe suppression for OFDM-based waveforms. It is shown that by considering the multicarrier

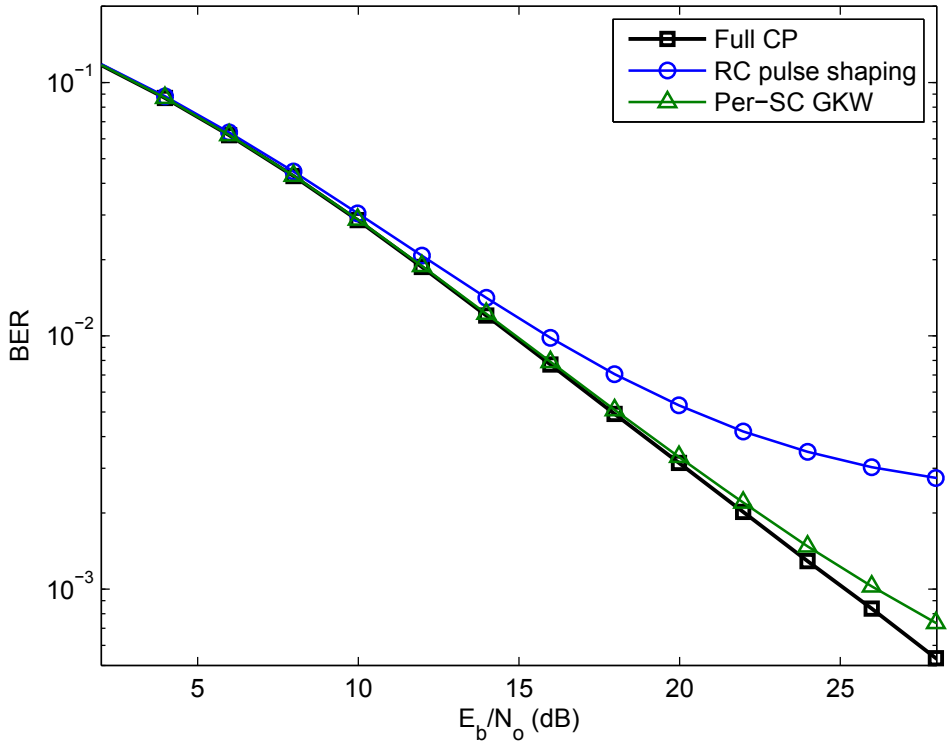

Figure 4.13 BER performances for selective modulation over the subcarriers considering the nonuniform interference profile.

nature of the bi-orthogonal pulse shaped OFDM, employing per-subcarrier and time asymmetric pulse shaping achieves superior interference mitigation while maintaining the same OOB emission reduction performance of the conventional pulse shaping. The proposed scheme efficiently utilizes the time-frequency resource by well-localized and spectrally efficient OFDM transmission while approaching the interference-free BER performance. Also, with RB-specific time-asymmetric waveform configuration, implementation complexity of the subcarrier-specific OFDM waveform is reduced with negligible degradation in BER performance compared to per-subcarrier case.

CHAPTER 5:
JOINT SIDELOBE SUPPRESSION AND PAPR REDUCTION IN OFDM USING PARTIAL TRANSMIT SEQUENCES

5.1 Introduction

Robustness against multipath channels coupled with simple equalization and flexibility in dynamic spectrum usage have made orthogonal frequency-division multiplexing (OFDM) a well accepted signaling scheme in wireless communication systems[1]. Despite its prominent advantages, two of the main drawbacks of OFDM have been considered as major limiting factors in practice: high out-of-band (OOB) radiation and high peak-to-average power ratio (PAPR).

Rectangular transmit pulses trade the spectral containment of the signal due to sharp symbol transitions corresponding to sinc subcarrier spectrum with high sidelobes. Apart from shaping the rectangular transmit pulse to achieve smoother symbol transitions [93], various active techniques have been proposed for suppressing the OOB radiation of rectangularly-shaped OFDM signal. These schemes can be gathered under two main approaches as frequency domain and time domain. In the former, for each OFDM symbol, spectra of individual subcarriers along with the data symbols are taken into account while in the latter, the focus is on smoothing the transitions between consecutive OFDM symbols to suppress the OOB leakage. Dedicating edge subcarriers for sidelobe cancellation [127], mapping the original data sequence to multiple-choice sequences (MCS) and selecting the one that gives the least sidelobe power [128], and projection of the transmitted symbols to force spectral nulls [122] follow the frequency domain criterion, while inserting adaptive symbol transitions based on two consecutive symbols [129] and data distortion to make the emitted

[1]The content of this chapter is published in [126]. Copyright notice for this publication can be found in Appendix C.

signal's phase and amplitude continuous [130] can be considered as techniques that are based on time domain criterion.

Besides the OOB radiation, since an OFDM symbol is a combination of sinusoids with independent amplitudes and phases, the probability of having a high instantaneous power increases, especially when the number of subcarriers is large. This drawback, on one hand, both shortens the communication range and reduces the power conversion efficiency of the transmitter power amplifier (PA) when the mean signal power is reduced due to regulatory other practical limitations. On the other hand, when the mean power is not reduced, operation in the nonlinear region of the radio frequency (RF) components, typically PA, creates both spectral regrowth and self-distortion in the transmitted signal [131]. The techniques which deal with PAPR reduction in OFDM can be found in [132] and references therein. Among these countermeasures, partial transmit sequences (PTS) [133] and selected mapping (SLM) [134] have been promising alternatives.

The aforementioned techniques for reducing OOB radiation give good results for an ideal signal. However, the spectral regrowth effect after the PA restores the suppressed sidelobes of the original signal to a level that is determined by the PA operation characteristics. In other words, when the effect of amplifier is not taken into account, sidelobe suppression techniques become ineffective for the suppressions that falls under the spectral response of the PA. For joint consideration of the two issues, a recent study [135] adopts multiple-choice-based techniques: MCS for sidelobe suppression and SLM for PAPR reduction by refining the objective of MCS that restricts the set of sequences with a sidelobe power constraint, before applying SLM-based PAPR reduction.

In this chapter, we propose a PTS-based joint suppression of spectral sidelobes and the PAPR of the OFDM signal that actively minimizes the spectral leakage and peak power with appropriate phase rotations of partial sequences. Hence, reduction of the spectral OOB leakage and mitigation of PAPR-related drawbacks are collectively accomplished in practice so that the spectral suppression performance will not be degraded due to the existing PAPR of OFDM signal. The proposed scheme consists of three stages all of which are based on shifting the phases of the blocks of subcarriers that constitute the partial transmit sequences. Interleaved blocks of edge subcarriers are first phase shifted for suppression of the combined effect on the OOB, then PTS is

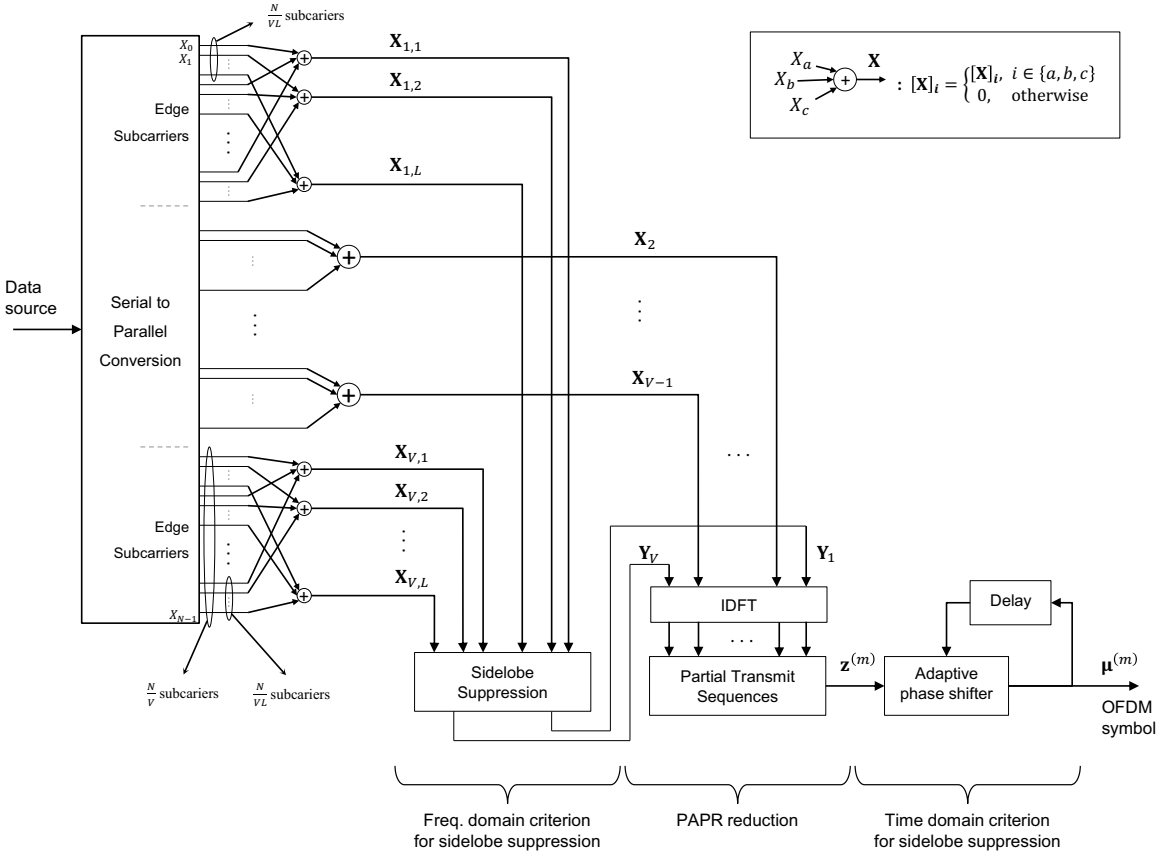

Figure 5.1 Block diagram of three-stage technique. Edge subcarriers are first considered for sidelobe suppression. Then the output is used for PAPR reduction and finally phase transition between consecutive symbols is improved by an optimum phase shift.

performed for PAPR reduction considering the contiguous blocks, and finally, an adaptive phase rotation for the current OFDM symbol is performed to achieve minimal phase transition with the previous symbol. Since the proposed technique is based on the phase-shift for the blocks of subcarriers, both computational complexity for phase computations and the size of information to represent the phase information are kept minimal.

The remainder of this chapter is organized as follows: In Section 5.2, the system model is introduced. Then, the stages of the proposed scheme: frequency domain criterion for sidelobe suppression, PAPR reduction with PTS, and the spectral suppression with a time domain criterion are presented in Sections 5.3, 5.4, and 5.5, respectively. Section 5.6 presents the simulation results for the spectral and PAPR suppression and finally, conclusions are drawn in Section 5.7.

5.2 System Model

N data symbols, $X_k,\ k = 0, \ldots, N-1$, are modulated in each OFDM symbol. Therefore, we consider N-subcarrier OFDM system whose mth discrete time-domain symbol including the cyclic prefix (CP) is written as

$$x^{(m)}(n) = \frac{1}{\sqrt{N}} \sum_{k=-N/2}^{N/2-1} X_{k+N/2}^{(m)} e^{j\frac{2\pi kn}{\rho N}}, \quad -\rho G \leq n < \rho N, \tag{5.1}$$

where $X_k^{(m)}$ is the complex symbol modulated on the kth subcarrier of the mth OFDM symbol, G is the CP size, and ρ is the oversampling ratio. The combination of independent and identically distributed data symbols, $X_k^{(m)}$, increases the probability of observing high PAPR, defined as

$$PAPR^{(m)} = \frac{\max\limits_{0 \leq n < \rho N} |x^{(m)}(n)|^2}{\mathbf{E}[|x^{(m)}(n)|^2]}, \tag{5.2}$$

where oversampling of the time domain symbol by ρ provides better approximation to the true PAPR.

The three-stage algorithm for jointly reducing the OOB radiation and PAPR is depicted as block diagram in Figure 5.1. For all stages, the only operation is a phase rotation of the blocks and subblocks of the data vector $\mathbf{X}^{(m)} = [X_0^{(m)}, X_1^{(m)}, \ldots, X_{N-1}^{(m)}]^T$. For this purpose, two-level partitioning of the data vector is adopted. The higher level is basically splitting $\mathbf{X}^{(m)}$ into V distinct and consecutive blocks $\mathbf{X}_v^{(m)},\ \ v = 1, 2, \ldots, V$ for the PAPR reduction, where each block is independently phase-rotated for minimizing instantaneous peak power. This high level partition is formulated as

$$\left[\mathbf{X}_v^{(m)}\right]_i = \begin{cases} \left[\mathbf{X}^{(m)}\right]_i, & (v-1)\frac{N}{V} \leq i \leq v\frac{N}{V}, \\ 0, & \text{elsewhere}, \end{cases} \tag{5.3}$$

where $[\mathbf{X}]_i$ denotes the ith element of the vector $\mathbf{X}$. The second level of partitioning corresponds to formation of L interleaved subblocks from the two blocks that are located at the band edges,

i.e., $\mathbf{X}_{v,l}^{(m)}$, $v = 1, V$ and $l = 1, 2, \ldots, L$. Interleaved subblocks can similarly be given as

$$\left[\mathbf{X}_{v,l}^{(m)}\right]_i = \begin{cases} \left[\mathbf{X}_v^{(m)}\right]_i, & i = l + qL,\ q = 0, \ldots, \frac{N}{VL} - 1, \\ 0, & \text{elsewhere.} \end{cases} \tag{5.4}$$

5.3 Stage 1: Sidelobe Suppression with Frequency Domain Criterion

In OFDM, it is a well-known fact that edge subcarriers have more impact on the OOB radiation than inner subcarriers [120], because the envelope of each subcarrier's spectrum decreases monotonically. Hence, with the frequency domain criterion for sidelobe suppression in the first stage, we take only the leftmost and the rightmost blocks of subcarriers into account for spectral suppression. Within each edge block, subcarriers are further partitioned into L interleaved subblocks in order to maximize the cancellation effect on the combined OOB spectrum with appropriate phase rotations. In other words, by allowing independent phase shifts to successive edge subcarriers, which has the most effect on the signal spectrum, more degrees of freedom are achieved with the interleaved-subblock approach. Then, the operation in the first stage modifies the edge blocks as

$$\mathbf{Y}_v^{(m)} = \sum_{l=1}^{L} \alpha_{v,l}^{(m)} \mathbf{X}_{v,l}^{(m)}, \quad v = 1, V, \tag{5.5}$$

where $\alpha_{v,l}^{(m)}$ is the complex number with unity amplitude that shifts the phase of the lth subblock of the vth block in the mth OFDM symbol[2]. Thus, selection of the phases $\alpha_{v,l}$ is based on minimizing the combined effect of the interleaved subcarrier blocks, whose power is given as

$$P_{\mathrm{I}} = \|\boldsymbol{\mathcal{I}}_v \mathbf{Y}_v\|^2 \tag{5.6}$$

$$= \left\| \sum_{l=1}^{L} \boldsymbol{\mathcal{I}}_v \alpha_{v,l} \mathbf{X}_{v,l} \right\|^2 \tag{5.7}$$

[2]For notational convenience, we omit the symbol index for Sections 5.3 and 5.4 as the operations are done per-symbol basis in the first two stages.

where $\boldsymbol{\mathcal{I}}_v$ is an $K \times N$ interference matrix that gives the contribution of each data subcarrier at K frequency locations on the OOB spectrum whose normalized frequency indices are represented by $\mathbf{g}_1$ and $\mathbf{g}_V$ for lower and upper OOB, respectively. Thus the interference matrix yields

$$[\boldsymbol{\mathcal{I}}_v]_{p,k} = \frac{\sin\left(\pi \frac{G+N}{N}([\mathbf{g}_v]_p - k)\right)}{\pi \frac{G+N}{N}([\mathbf{g}_v]_p - k)}, \; v = 1, V. \tag{5.8}$$

By defining $\boldsymbol{\alpha}_v = [\alpha_{v,1}, \ldots, \alpha_{v,L}]^T$, the OOB power that needs to be minimized can be written in matrix form as

$$P_{\mathrm{I}} = \|\boldsymbol{\mathcal{I}}_v \boldsymbol{\mathcal{X}}_v \boldsymbol{\alpha}_v\|^2 \tag{5.9}$$

$$= \boldsymbol{\alpha}_v^H \underbrace{\boldsymbol{\mathcal{X}}_v{}^H \boldsymbol{\mathcal{I}}_v^H \boldsymbol{\mathcal{I}}_v \boldsymbol{\mathcal{X}}_v}_{\boldsymbol{\mathcal{A}}_v} \boldsymbol{\alpha}_v \tag{5.10}$$

where $\mathbf{X}^H$ denotes the Hermitian transpose of the matrix/vector $\mathbf{X}$, and $\boldsymbol{\mathcal{X}}_v = [\mathbf{X}_{v,1}, \mathbf{X}_{v,2}, \ldots, \mathbf{X}_{v,L}]$. Therefore, finding the phase vector $\boldsymbol{\alpha}_v$ corresponds to an optimization problem as

$$\begin{aligned} &\text{minimize} \quad \boldsymbol{\alpha}_v^H \boldsymbol{\mathcal{A}}_v \boldsymbol{\alpha}_v \\ &\text{subject to} \quad |[\boldsymbol{\alpha}_v]_l|^2 = 1, \quad l = 1, \ldots, L. \end{aligned} \tag{5.11}$$

The problem in (5.11) falls under the family of *quadratically constraint quadratic problem (QCQP)*. There exists efficient solutions to solve this optimization problem, e.g., semidefinite relaxation [136].

It is worth noting that one can also select $L = N/V$, i.e., independent phase rotation for each subcarrier, to achieve the maximum degree of freedom for minimizing the combined effects of the edge subcarriers, albeit with the penalty of increased complexity and number of phases to be sent to the receiver side. However as discussed in Section 5.6, our results show that $L > 8$ does not give remarkable additional spectral suppression.

After determining the phase vectors and combining the subblocks for the edge-blocks as in (5.5), data blocks are converted to time-domain blocks with inverse discrete Fourier transform (IDFT). Thus, the input of the PAPR reduction stage becomes V time-vectors that can be written

as

$$\mathbf{y}_v = \begin{cases} \mathbf{F}^H \mathbf{Y}_v, & v = 1, V \\ \mathbf{F}^H \mathbf{X}_v, & v = 2, 3, \ldots, V-1 \end{cases} \tag{5.12}$$

where $\mathbf{F}^H$ is $\rho(N+G) \times N$ IDFT matrix that generates time domain CP-OFDM symbol.

5.4 Stage 2: PAPR Reduction with PTS

As in Figure 5.1, the time-domain vectors that are obtained from (5.12), two of which are the output of the first stage, naturally become the input for partitioning-based PAPR reduction technique: PTS [133]. The main idea of PTS technique is based on shifting the phases of the partitions of the OFDM data vector in such a way that the resulting symbol will have a reduced PAPR. In other words, as $\mathbf{y}_v$ being the partial sequences in our notation, aim in PTS technique is to

$$\text{minimize} \quad \max_{0 \le i < \rho N} \left(\rho N \frac{|[\mathbf{z}]_i|^2}{\mathbf{z}^H \mathbf{z}} \right), \tag{5.13}$$

where $\mathbf{z}$ is the output vector of the PAPR reduction stage given as

$$\mathbf{z} = \sum_{v=1}^{V} \beta_v \mathbf{y}_v \tag{5.14}$$

and $\beta_v,\ v = 1, \ldots, V$ is the phase rotation to be performed on vth block with the objective in (5.13). Indeed, both PTS and SLM techniques can be represented by (5.13) and (5.14) but the difference emerges in implementation. That is, phase rotations for partial sequences, $\mathbf{y}_v$, are computed in PTS, while in SLM, only a number of candidate phase rotations are first performed in the frequency domain, then they are converted to the time domain and the one that has the minimum PAPR is selected for transmission. We herein adopt the PTS technique considering this fact as well as the following motivations:

- Time domain partial sequences are already computed in the first stage and can directly be used for PTS stage.
- PTS encompasses SLM in terms of range of solutions including the optimum.
- PTS can be more efficient when the fact that the majority of the input vector of IDFT operations in (5.12) consists of zeros is exploited in implementation [137].
- Optimization of the phase values as well as efficient suboptimal solutions for PTS has been extensively studied in the literature [137–141].

Thus, we adopt a simple quantized-PTS algorithm in which finite set of quantized phases is considered, i.e., $\beta_v \in \left\{1, e^{j2\pi\frac{1}{Q}}, \ldots, e^{j2\pi\frac{Q-1}{Q}}\right\}$ as also given in [133].

Note that in the PTS stage, phase rotations of the edge blocks, i.e., multiplication of $\mathbf{y}_1$ and $\mathbf{y}_V$ by β_1 and β_V, does not affect the performance of sidelobe suppression because the power level of the combined interleaved subblocks is maintained after the corresponding phase shifts.

5.5 Stage 3: Sidelobe Suppression with Time Domain Criterion

Similar to the fact that phase rotation of the blocks for PAPR reduction does not affect the sidelobe suppression performance, applying a constant phase shift to the whole OFDM block does not change the performance of the per symbol-basis operations that are carried out in the first two stages. This additional degree of freedom allows us to consider the transition between consecutive symbols to further improve the spectral suppression. In other words, after the frequency domain criterion, the phase transition between consecutive OFDM symbols is improved with a second update on the phase vector without affecting the performance of the previous stages, which corresponds to a time domain criterion of reducing the OOB. As illustrated in Figure 5.2, the symbol boundary where the sharp transitions occur is *phase-smoothed* after shifting the phase of the current symbol adaptively.

By restoring the symbol index, we denote the phase shift to be applied on the output of the second stage, $\mathbf{z}^{(m)}$, as $\gamma^{(m)}$. Thus, $\boldsymbol{\mu}^{(m)} = \gamma^{(m)}\mathbf{z}^{(m)}$ becomes the mth OFDM symbol to be transmitted. Given the previous symbol $\mathbf{z}^{(m-1)}$, the phase shift that provides the best phase

transition between the end of the $(m-1)$th symbol and the start of the mth symbol also minimizes the sidelobe power of the concatenated time domain vector defined as

$$P_{\mathrm{I}}^{(m)} = \left\| \boldsymbol{\mathcal{F}}_{K,\zeta} \begin{bmatrix} \mathbf{z}^{(m-1)} \\ \gamma^{(m)}\mathbf{z}^{(m)} \end{bmatrix} \right\|^2 \tag{5.15}$$

where $\zeta = 2\rho(N+G)$ and $\boldsymbol{\mathcal{F}}_{K,\zeta}$ is an $K \times \zeta$ interference matrix that projects the ζ-length time vector to the K frequency locations in the OOB, i.e., subset of the $\zeta \times \zeta$ discrete Fourier transform (DFT) matrix containing only the rows corresponding to the sidelobe frequencies whose power is to be minimized. By substituting $\gamma^{(m)} = e^{j\theta_m}$ and using the linearity of matrix multiplication, we rewrite (5.15) as

$$P_{\mathrm{I}}^{(m)} = \left\| \mathbf{a} + e^{j\theta_m}\mathbf{b} \right\|^2 \tag{5.16}$$

where $\mathbf{a} = \boldsymbol{\mathcal{F}}_{K,\zeta} \begin{bmatrix} \mathbf{z}^{(m-1)} \\ [\mathbf{0}]_{(N+G)\times 1} \end{bmatrix}$ and $\mathbf{b} = \boldsymbol{\mathcal{F}}_{K,\zeta} \begin{bmatrix} [\mathbf{0}]_{(N+G)\times 1} \\ \mathbf{z}^{(m)} \end{bmatrix}$. The optimum angle that minimizes $P_{\mathrm{I}}^{(m)}$ is the angle that corresponds to the global minimum of (5.16). Thus, the desired angle is the solution of

$$\frac{\partial}{\partial \theta_m} \left\| \mathbf{a} + e^{j\theta_m}\mathbf{b} \right\|^2 = 0, \tag{5.17}$$

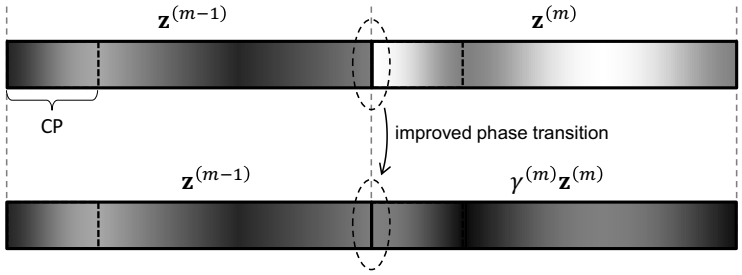

Figure 5.2 Phase rotation of the OFDM symbol to make the transition smoother.

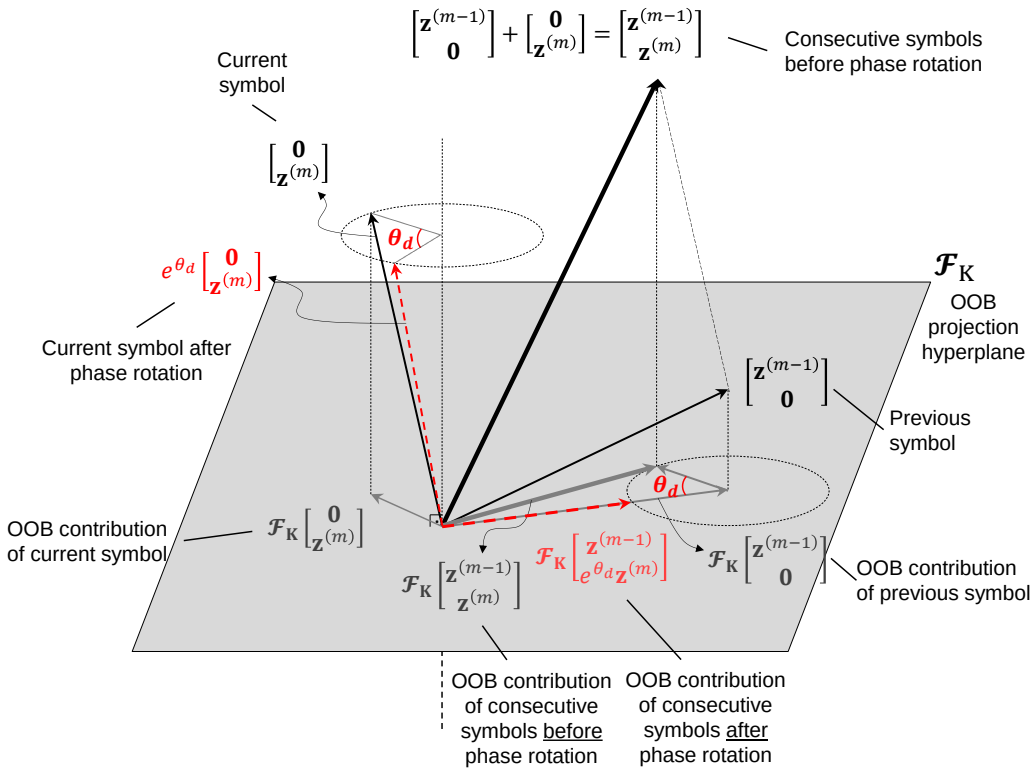

Figure 5.3 A vector space representation of symbols and their OOB contributions. Appropriate phase rotation for the current symbol reduces the length of the vector corresponding to OOB contribution of consecutive symbols.

which yields

$$e^{j2\theta_m} = \frac{\mathbf{b}^H\mathbf{a}}{\mathbf{a}^H\mathbf{b}}. \tag{5.18}$$

The phase angle in (5.16) turns out to be the angle of the inner product of the sidelobe vectors obtained from the previous symbol and the current symbol, i.e., $\theta_m = \angle\langle\mathbf{b},\mathbf{a}\rangle$. This can also be seen in Figure 5.3 where the shaded plane is the hyperplane where the projection of symbols corresponds to OOB contribution.

Although the phases are computed independently in all stages, each stage updates the phase information of the previous stage rather than increasing the number of phases to be transmitted, that is, $\beta_v^{(m)}$ updates $\boldsymbol{\alpha}_v^{(m)}$ for $v = 1, V$, and $\gamma_{(m)}$ updates $\beta_v^{(m)}$. Therefore, the number of total phases remains as $2L + V - 2$. Also, since we restricted the set of complex numbers to a smaller

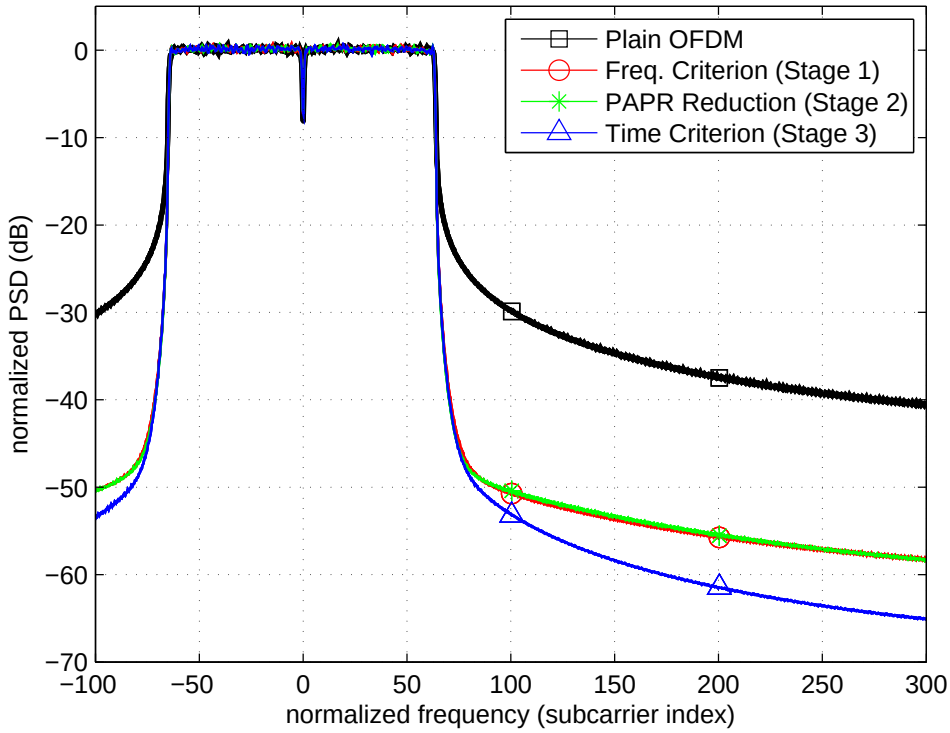

Figure 5.4 PSDs of signals after each stage showing the individual impacts on sidelobe suppression. $V = 2$ and $L = 8$.

subset, i.e., unity amplitude, complexity of the techniques in all stages reduces. Although we considered arbitrary phase shifts for the first and the third stages, more efficient implementations can be achieved by quantizing the phases into finite size of alphabet. By doing so, smaller number of bits are enough to represent the phase information for jointly performing the PAPR reduction and the sidelobe suppression for the OFDM symbol.

5.6 Simulation Results

Performance of the proposed scheme is investigated via computer simulations. An OFDM system with $N = 128$, $G = 16$, and disabled DC-subcarrier is considered. As oversampling ratio, $\rho = 8$ is adopted to better approximate[3] the true PAPR and four quantized phase shift are considered in PTS. For each simulation, 10 000 symbols are generated. We first investigate the

[3]It has been shown that an oversampling ratio greater than four is sufficient to tightly bound the peak of the continuous envelope [142].

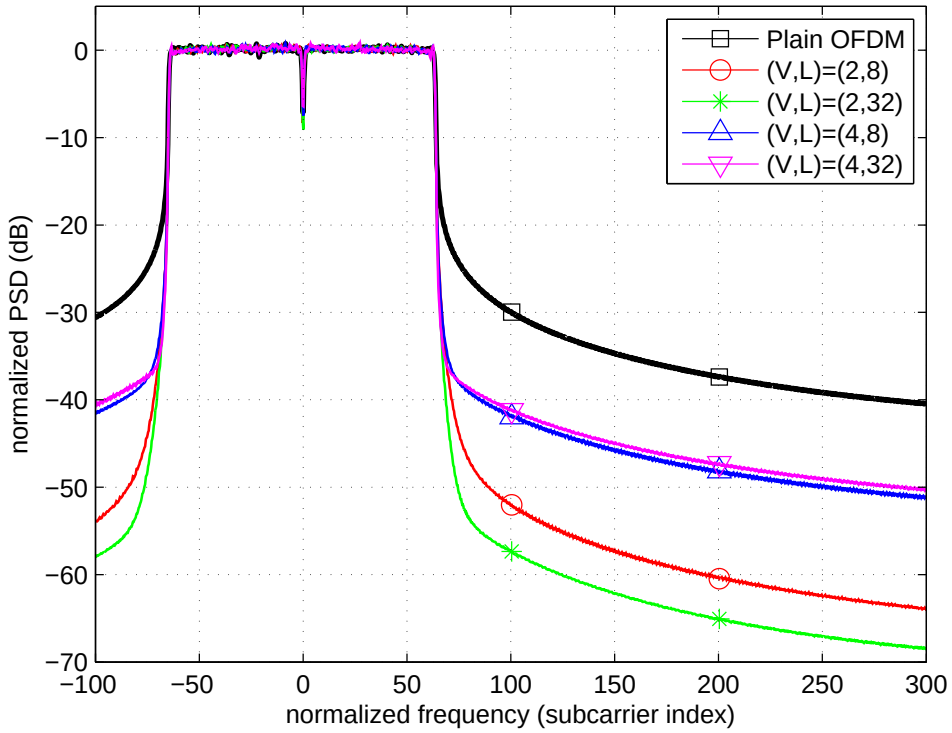

Figure 5.5 The effect of block sizes on power spectrum.

power spectral density (PSD) of the signals at the output of each stage in order to observe the impact of individual techniques on the sidelobe suppression. Figure 5.4 presents the normalized power spectra for the signal after the first, second, and third stages for $V = 2$ and $L = 8$. The distances of OOB frequency locations to the band edges are set as $\mathbf{g} = [20, 22, \ldots, 40]$ from both sides. Conventional OFDM, i.e., input signal of the proposed system, is also given as reference. The frequency domain criterion solely achieves 20 dB better suppression at the $N/4$ subcarrier distance from the band-edge compared to conventional OFDM. Note that the PSD after the second stage remains unchanged confirming the independence of the proposed sidelobe suppression and PAPR reduction. After applying the time domain criterion in the third stage, further improvement of $4 - 6$ dB on OOB suppression performance is observed in Figure 5.4.

The effect of the size and number of contiguous blocks and interleaved subblocks on the spectrum and PAPR is also investigated. Smaller V increases the size of edge blocks. Thus, increasing the number of subcarriers that are taken into account for sidelobe suppression provides better

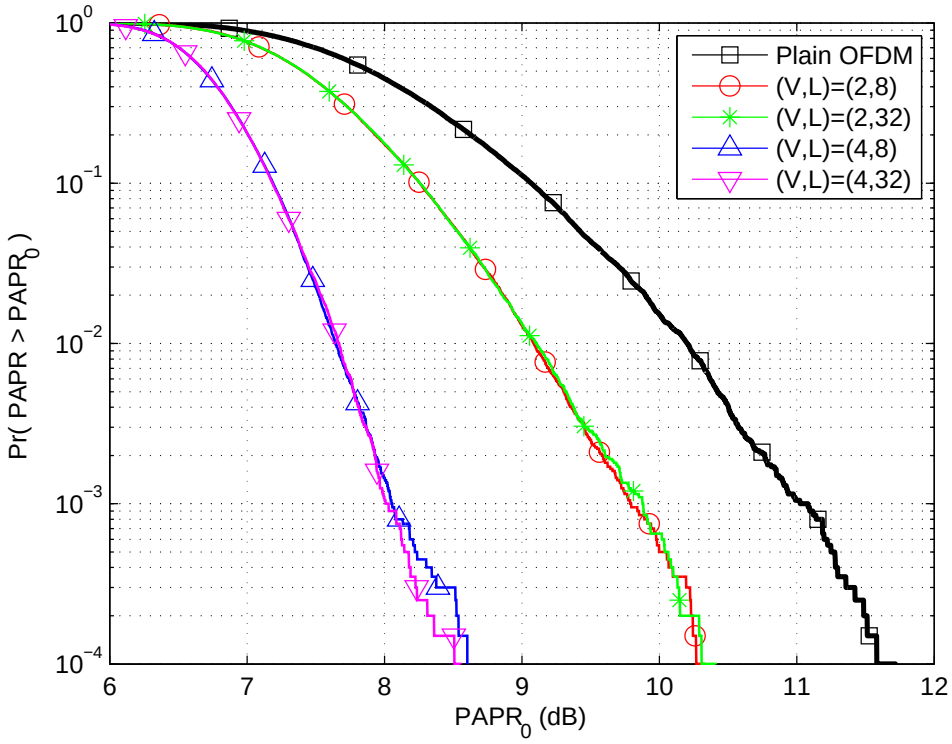

Figure 5.6 The effect of block sizes on PAPR.

performance. Similarly, for a given V, increasing L enhances the performance due to the increased degree of freedom in selecting the independent phase rotations for successive edge subcarriers. These effects are illustrated in Figure 5.5 with various block and subblock sizes. $(V, L) = (2, 32)$ gives the best result since the size of edge blocks and the number of independent phase rotations are greater than the others. Similarly, since the inner subcarriers that are not taken into account in the first stage constitute the OOB spectrum floor, $(V, L) = (4, 32)$ provides a marginal suppression gain over $(V, L) = (4, 8)$.

Finally, with the same set of block parameters, we investigate the PAPR reduction performances of the proposed method. Figure 5.6 shows the complementary cumulative distribution function (CCDF) of the PAPR of the OFDM signal with various partitioning scenarios. For a CCDF of 10^{-3}, $L = 8$ gives 1.1 dB and 3 dB less PAPR for $V = 8$ and $V = 32$, respectively, compared to conventional OFDM. Since phase rotation of the edge subcarriers are independent from the PAPR reduction, subblock size L has no observable effect on peak power reduction performance.

5.7 Conclusions

Spectral sidelobes and PAPR drawbacks in OFDM-based systems are jointly addressed by a PTS-based transmission scheme. After phase rotation of edge subcarriers in an interleaved manner for the sake of suppressing the spectral emissions, PTS is performed using the phase rotated blocks as an input for PAPR reduction. Finally, with a phase rotation of the whole OFDM symbol in time, the phase transition between the current and the previous symbol is smoothed, leading to further improvement in the spectral suppression. The proposed scheme reduces the PAPR while suppressing the OOB radiation, therefore minimizing the possibility of the spectral regrowth problem in practice. Since the main operation of the proposed algorithm involves only phase rotation of blocks, both complexity and side information are kept minimal.

Future work constitutes the investigation of the system performance in real systems including various PA simulations and measurements as well as investigating the optimum block sizes that matches the PA model with the sidelobe suppression.

CHAPTER 6:
CP-ALIGNED OFDM WITH JOINT OOB AND PAPR REDUCTION WITH PHY SECURITY

6.1 Introduction

As a prevalent multicarrier transmission scheme, orthogonal frequency-division multiplexing (OFDM) is used in most of existing communication standards such as Wi-Fi, WiMAX, LTE, and IEEE 802.20 WRAN some of which also been considered for military communications along with wideband networking waveform (WNW) [143][1]. The widespread adoption of OFDM has also expanded to the military communications This is because of its prominent features, e.g., robustness against multipath delay spread, high spectral efficiency, single-tap frequency domain equalization, and notable flexibility in spectrum usage. Despite its numerous advantages, the use of rectangular pulse shape introduces high spectral out-of-band (OOB) leakage due to sharp transitions between consecutive symbols.

In the literature, many methods have been proposed to reduce OOB leakage of OFDM based systems. Among many others, windowing [96, 100, 145] is one of the most known methods that shapes the spectral shape of the individual subcarriers. However, the extension of effective symbol duration not to allow sharp transitions between OFDM symbols reduces the spectral efficiency. In [96], the authors introduces different transition durations for inner and edge subcarriers by taking the dominant contribution of the edge subcarriers into account. In [100], a time-asymmetric windowing method is introduced which exploits some part of the cyclic prefix (CP) by considering the decaying profile of multipath channel. Different from the methods that manipulate the transmit filter for improved symbol transitions, there are other techniques that actively manipulate the data

[1]The content of this chapter is published in [144]. Copyright notice for this publication can be found in Appendix C.

subcarriers for achieving better transitions for reduced OOB leakage. In this direction, one of the elegant solutions is N-continuous OFDM [130] where each data subcarrier is exposed to a small interference so that the consecutive OFDM symbols become continuous for their first N derivatives. However, N-continuous OFDM requires a modified receiver to cancel the impact of interference. Recently, a novel approach which allows non-interfering components transmitted along with OFDM symbols has been introduced [77, 146–148]. The main idea is to cancel the superposed component on the data symbols by exploiting inevitable redundancy of OFDM symbols, i.e., CP duration. In [77], the component is generated as an artificial noise for physical-layer security. The same method is utilized for wireless power transfer in OFDM [146] and orthogonal frequency-division multiple access (OFDMA) [147] scenarios, which propose self-sustainable receiver via utilizing the power harvested from the CP duration. The idea of alignment has recently been used for the purpose of spectral suppression over a certain OOB frequency band [148], via utilizing a quadratic optimization for computation of the suppression component.

In this chapter, we introduce an OFDM transmission scheme by taking the advantages of maintaining the continuity of OFDM symbols and the idea of CP alignment. By keeping the distortion effect of the multipath channel unchanged, the proposed method yields no additional disturbance on the received data subcarriers after passing through channel, CP removal, and discrete Fourier transform (DFT) operations. This is achieved by designing the additional correction component, which maintains the continuity of OFDM symbols, such that it aligns with the CP part at the receiver. In other words, the correction component falls into the CP duration after passing through the channel. By doing so, the correction component does not induce any interference on the data subcarriers while achieving the symbol continuity. Thus, the proposed scheme is backward compatible to the conventional OFDM receivers since there is no need for a change in the reception such as decision-feedback implementation as given in conventional N-continuous OFDM [130].

The notation is given as follows. Matrices [columns vectors] are denoted with upper [lower] case boldface letters (e.g., $\mathbf{A}$ [$\mathbf{a}$]); denotes the convolution operation; superscripts T and H denote transpose, and conjugate transpose, respectively; $\overline{x}$ denotes the conjugate of a scalar number x; $j = \sqrt{-1}$ is the imaginary unit; $\mathbb{E}_x[y(x)]$ denotes the expectation of $y(x)$ over the random argument

x; $\|\mathbf{x}\|_\infty$ denotes the uniform norm (infinity norm) of vector $\mathbf{x}$; and $\frac{d^n}{dt^n}$ is the nth derivative operator with respect to t.

6.2 System Model

We consider an OFDM system where the transmitted signal is composed of two components as

$$s_i(t) = x_i(t) + a_i(t), \tag{6.1}$$

where $x_i(t)$ is the data component for ith OFDM symbol and $a_i(t)$ is its correction component which controls the spectral characteristics with symbol continuity. The complex envelope representations for two components are given as

$$x_i(t) = \frac{1}{\sqrt{N_\mathrm{d}}} \sum_{k \in \mathcal{N}_\mathrm{d}} d_{i,k} e^{j \frac{2\pi k}{T_\mathrm{d}} t}, \qquad -T_\mathrm{g} \leq t < T_\mathrm{d}, \tag{6.2}$$

where N_d is the number of OFDM subcarriers, $\mathcal{N}_\mathrm{d} = \{k_1, \ldots, k_{N_\mathrm{d}}\}$ is the corresponding subcarrier index set, and T_d and T_g are the main symbol and CP durations for the OFDM data signal, respectively.

In order to control the OOB leakage via managing the transitions between consecutive symbols, correction component is configured to be in OFDM form similar to data part. That is, the correction component is also composed of some subcarriers which are populated by optimized correction values. By defining $a_i(t)$ in the same format with rectangular pulse shape, spectral control can be achieved by considering only the symbol transitions. As it is shown in the time domain representations in Figure 6.1, T_d determines the duration in which the OFDM signal can take arbitrary value as a function of the data subcarriers, and T_g is the duration that carry the same information as last part of the main duration, i.e., redundant part. For the proposed scheme, in order to achieve sufficient degrees-of-freedom for canceling the distortion at receiver, the correction component is generated for a larger symbol period than T_d. The signal structure considered in this sequel is illustrated in Figure 6.1. As opposed to conventional N-continuous OFDM where the

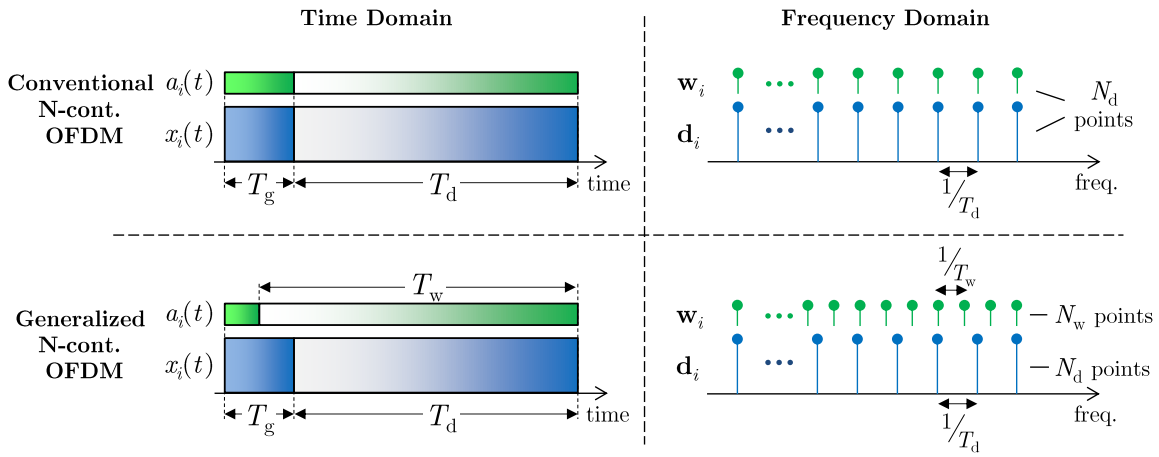

Figure 6.1 Time and frequency domain illustrations of two components that the transmitted signal consists of. Larger symbol duration for the correction component $a_i(t)$ yields to more points in frequency than that of number of data subcarriers.

data and the correction component have the same durations, the proposed structure offers larger number of subcarriers with smaller subcarrier spacing.

$$a_i(t) = \frac{1}{\sqrt{N_{\mathrm{w}}}} \sum_{l \in \mathcal{N}_{\mathrm{w}}} w_{i,l} e^{j\frac{2\pi l}{T_{\mathrm{w}}}(t-(T_{\mathrm{d}}-T_{\mathrm{w}}))}, \quad -T_{\mathrm{g}} \leq t < T_{\mathrm{d}} \tag{6.3}$$

where N_{w} is the number of frequency bins for correction component, $\mathcal{N}_{\mathrm{w}} = \{l_1, \ldots, l_{N_{\mathrm{w}}}\}$ is corresponding subcarrier index set, and T_{w} is the main duration for the correction component. Considering the consecutive symbols, the overall signal can be written as

$$s(t) = \sum_{i=0}^{I} s_i\big(t - i(T_{\mathrm{g}} + T_{\mathrm{d}})\big) \tag{6.4}$$

where I is the number of OFDM symbols in the transmitted frame.

The continuous time expression of OFDM frame in (6.4) are given for the representation of continuity at the symbol boundaries that will be maintained by the design of the correction component in discrete domain. Then, based on the OFDM formulation in (6.2) and (6.3), the discrete-time signal is given by

$$\mathbf{s}_i = \mathbf{x}_i + \mathbf{a}_i = \mathbf{A}_{\mathrm{d}}\mathbf{F}_{\mathrm{d}}^{\mathrm{H}}\mathbf{d}_i + \mathbf{A}_{\mathrm{w}}\mathbf{F}_{\mathrm{w}}^{\mathrm{H}}\mathbf{w}_i \tag{6.5}$$

where $\mathbf{d}_i = \left[d_{i,-N_\mathrm{d}/2}, \ldots, d_{i,N_\mathrm{d}/2-1}\right]^\mathrm{T} \in \mathbb{C}^{N_\mathrm{d}\times 1}$ and $\mathbf{w}_i = \left[w_{i,-N_\mathrm{w}/2}, \ldots, w_{i,N_\mathrm{w}/2-1}\right]^\mathrm{T} \in \mathbb{C}^{N_\mathrm{w}\times 1}$. In (6.5), $\mathbf{F}_\mathrm{d} \in \mathbb{C}^{N_\mathrm{d}\times N_\mathrm{d}}$ and $\mathbf{F}_\mathrm{w} \in \mathbb{C}^{N_\mathrm{w}\times N_\mathrm{w}}$ denote N_d- and N_w-point DFT matrices. The CP insertion matrices for the data and the correction parts are defined as

$$\mathbf{A}_\mathrm{d} \triangleq \begin{bmatrix} \mathbf{0}_{G_\mathrm{d}\times(N_\mathrm{d}-G_\mathrm{d})} & \mathbf{I}_{G_\mathrm{d}} \\ & \mathbf{I}_{N_\mathrm{d}} \end{bmatrix} \in \{0,1\}^{(N_\mathrm{d}+G_\mathrm{d})\times N_\mathrm{d}} \quad \text{and}$$

$$\mathbf{A}_\mathrm{w} \triangleq \begin{bmatrix} \mathbf{0}_{G_\mathrm{w}\times(N_\mathrm{w}-G_\mathrm{w})} & \mathbf{I}_{G_\mathrm{w}} \\ & \mathbf{I}_{N_\mathrm{w}} \end{bmatrix} \in \{0,1\}^{(N_\mathrm{w}+G_\mathrm{w})\times N_\mathrm{w}},$$

where G_d and G_w are corresponding CP sizes, respectively.

We assume that the transmitted signal passes through a Rayleigh fading multipath channel. The channel impulse response is represented by the vector $\mathbf{h} = \begin{bmatrix} h_0, \ldots, h_{L-1} \end{bmatrix}$ where L is the number of channel taps. We then express the received signal for the ith OFDM symbol as

$$\mathbf{r}_i = \begin{bmatrix} \mathbf{H}_\mathrm{p} & \mathbf{H}_\mathrm{c} \end{bmatrix} \begin{bmatrix} \mathbf{s}_{i-1} \\ \mathbf{s}_i \end{bmatrix} + \mathbf{n}_i, \tag{6.6}$$

where $\mathbf{n}_i \in \mathbb{C}^{(N_\mathrm{d}+G_\mathrm{d})\times 1}$ is the additive white Gaussian noise (AWGN) vector, $\mathbf{H}_\mathrm{c} \in \mathbb{C}^{(N_\mathrm{d}+G_\mathrm{d})\times(N_\mathrm{d}+G_\mathrm{d})}$ and $\mathbf{H}_\mathrm{p} \in \mathbb{C}^{(N_\mathrm{d}+G_\mathrm{d})\times(N_\mathrm{d}+G_\mathrm{d})}$ are the convolution matrices which are explicitly given by

$$\mathbf{H}_\mathrm{c} = \begin{bmatrix} h_0 & 0 & \cdots & \cdots & \cdots & 0 \\ \vdots & \ddots & \ddots & \ddots & \ddots & \vdots \\ h_{L-1} & \cdots & h_0 & \ddots & \ddots & \vdots \\ 0 & \ddots & \ddots & \ddots & \ddots & \vdots \\ \vdots & \ddots & \ddots & \ddots & \ddots & 0 \\ 0 & \cdots & 0 & h_{L-1} & \cdots & h_0 \end{bmatrix},$$

and

$$\mathbf{H}_{\mathrm{p}} = \begin{bmatrix} 0 & \cdots & 0 & h_{L-1} & \cdots & h_1 \\ \vdots & \ddots & \ddots & \ddots & \ddots & \vdots \\ \vdots & \ddots & \ddots & \ddots & \ddots & h_{L-1} \\ \vdots & \ddots & \ddots & \ddots & \ddots & 0 \\ \vdots & \ddots & \ddots & \ddots & \ddots & \vdots \\ 0 & \cdots & \cdots & \cdots & \cdots & 0 \end{bmatrix}.$$

In (6.6), $\mathbf{H}_{\mathrm{c}}$ and $\mathbf{H}_{\mathrm{p}}$ denotes the mapping from previous transmitted symbol $\mathbf{s}_{i-1}$ to the receiver window of ith symbol. That is, it characterizes the inter-symbol interference (ISI) falling into the CP duration. Then, the receiver discards the CP portion and performs DFT to convert the signal into frequency domain as

$$\begin{aligned} \mathbf{y}_i &= \mathbf{F}_{\mathrm{d}}\mathbf{B}\mathbf{r}_i \\ &= \mathbf{F}_{\mathrm{d}}\mathbf{B}\mathbf{H}_{\mathrm{c}}\mathbf{s}_i + \mathbf{F}_{\mathrm{d}}\mathbf{B}\mathbf{H}_{\mathrm{p}}\mathbf{s}_{i-1} + \mathbf{F}_{\mathrm{d}}\mathbf{B}\mathbf{n}_i, \end{aligned} \tag{6.7}$$

where $\mathbf{B} = \begin{bmatrix} \mathbf{0}_{N_{\mathrm{d}} \times G_{\mathrm{d}}} & \mathbf{I}_{N_{\mathrm{d}}} \end{bmatrix}$ denotes the CP removal operation by nullifying the first G_{d} rows of the matrix/vector that is multiplied from the right. Hence, it follows that $\mathbf{B}\mathbf{H}_{\mathrm{p}} = \mathbf{0}$, representing the elimination of the ISI with CP removal. Therefore, the received symbol in the frequency domain becomes

$$\mathbf{y}_i = \mathbf{F}_{\mathrm{d}}\mathbf{B}\mathbf{H}_{\mathrm{c}}\mathbf{s}_i + \mathbf{F}_{\mathrm{d}}\mathbf{B}\mathbf{n}_i. \tag{6.8}$$

6.3 Generalized N-Continuous OFDM

In this section, we establish the generalization of N-continuity in OFDM transmission to address the design of correction component with larger symbol duration. This generalization enables distortion-free reception which will be discussed in the next section. Similar to conventional N-continuous OFDM [130], the correction term is designed to satisfy the equality of the first N derivatives at the symbol boundary. As shown in Figure 6.1, the correction component and the

data subcarriers have the same size N_{d}. In the proposed scheme, the number of subcarriers for the correction component, N_{w}, is not necessarily equal to the number of data subcarriers i.e., N_{d}. Considering this relaxation for the dimension of the correction component, we call this scheme as *generalized N-continuous OFDM*.

The continuity condition at the boundary between the $(i-1)$th and ith symbols is represented via system of differential equations as

$$\frac{d^n}{dt^n} s_i(t)\Big|_{t=-T_{\mathrm{g}}} = \frac{d^n}{dt^n} s_{i-1}(t)\Big|_{t=T_{\mathrm{d}}}, \tag{6.9}$$

$$\frac{d^n}{dt^n}\big(x_i(t)+a_i(t)\big)\Big|_{t=-T_{\mathrm{g}}} = \frac{d^n}{dt^n}\big(x_{i-1}(t)+a_{i-1}(t)\big)\Big|_{t=T_{\mathrm{d}}}, \tag{6.10}$$

for $n = 0, \ldots, N-1$. The set of equations represented in (6.10) are due to substitution of (6.1) into (6.9). Then substituting (6.2) and (6.3) into (6.10), and characterizing the derivations yield

$$\begin{aligned}\frac{1}{\sqrt{N_{\mathrm{d}}}T_{\mathrm{d}}^n}\sum_{k\in\mathcal{N}_{\mathrm{d}}} k^n d_{i,k} e^{j\phi_{\mathrm{d}}k} + \frac{1}{\sqrt{N_{\mathrm{w}}}T_{\mathrm{w}}^n}\sum_{l\in\mathcal{N}_{\mathrm{w}}} l^n w_{i,l} e^{j\phi_{\mathrm{w}}l} \\ = \frac{1}{\sqrt{N_{\mathrm{d}}}T_{\mathrm{d}}^n}\sum_{k\in\mathcal{N}_{\mathrm{d}}} k^n d_{i-1,k} + \frac{1}{\sqrt{N_{\mathrm{w}}}T_{\mathrm{w}}^n}\sum_{l\in\mathcal{N}_{\mathrm{w}}} l^n w_{i-1,l}, \quad n = 0, \ldots, N\end{aligned} \tag{6.11}$$

where $\phi_{\mathrm{d}} = -2\pi T_{\mathrm{d}}/T_{\mathrm{g}}$ and $\phi_{\mathrm{w}} = -2\pi\left(T_{\mathrm{g}}+T_{\mathrm{d}}\right)/T_{\mathrm{w}}$ are the phase offset coefficient at the beginning of symbol for each subcarrier of data and correction components, respectively. The matrix equivalent of the system in (6.11) is given as

$$\mathbf{K}\boldsymbol{\Phi}_{\mathrm{d}}\mathbf{d}_i + \mathbf{L}\boldsymbol{\Phi}_{\mathrm{w}}\mathbf{w}_i = \mathbf{K}\mathbf{d}_{i-1} + \mathbf{L}\mathbf{w}_{i-1} \tag{6.12}$$

where $\boldsymbol{\Phi}_{\mathrm{d}} \triangleq \mathrm{diag}\left(e^{j\phi_{\mathrm{d}}k_1}, \ldots, e^{j\phi_{\mathrm{d}}k_{N_{\mathrm{d}}}}\right) \in \mathbb{C}^{N_{\mathrm{d}}\times N_{\mathrm{d}}}$ and $\boldsymbol{\Phi}_{\mathrm{w}} \triangleq \mathrm{diag}\left(e^{j\phi_{\mathrm{w}}l_1}, \ldots, e^{j\phi_{\mathrm{w}}l_{N_{\mathrm{w}}}}\right) \in \mathbb{C}^{N_{\mathrm{w}}\times N_{\mathrm{w}}}$ are the diagonal matrices corresponding to the phase terms, and the matrices $\mathbf{K} \in \mathbb{R}^{(N+1)\times N_{\mathrm{d}}}$ and

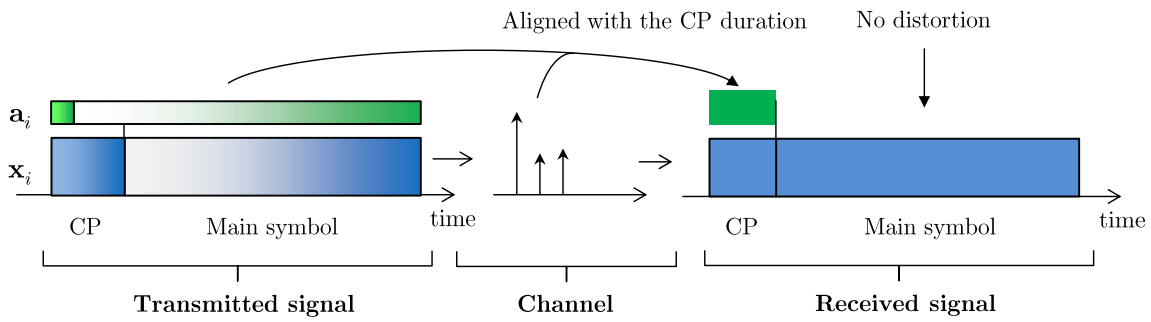

Figure 6.2 The correction component is aligned with the CP duration of OFDM symbol after it passes through multipath channel.

$\mathbf{L} \in \mathbb{R}^{(N+1)\times N_{\mathrm{w}}}$ are given as

$$\mathbf{K} \triangleq \frac{1}{\sqrt{N_{\mathrm{d}}}}\mathrm{diag}\left(\frac{1}{T_{\mathrm{d}}^0},\ldots,\frac{1}{T_{\mathrm{d}}^N}\right)\begin{bmatrix} 1 & 1 & \cdots & 1 \\ k_1 & k_2 & \cdots & k_{N_{\mathrm{d}}} \\ \vdots & \vdots & \vdots & \vdots \\ k_1^N & k_2^N & \cdots & k_{N_{\mathrm{d}}}^N \end{bmatrix},$$

and

$$\mathbf{L} \triangleq \frac{1}{\sqrt{N_{\mathrm{w}}}}\mathrm{diag}\left(\frac{1}{T_{\mathrm{w}}^0},\ldots,\frac{1}{T_{\mathrm{w}}^N}\right)\begin{bmatrix} 1 & 1 & \cdots & 1 \\ l_1 & l_2 & \cdots & l_{N_{\mathrm{w}}} \\ \vdots & \vdots & \vdots & \vdots \\ l_1^N & l_2^N & \cdots & l_{N_{\mathrm{w}}}^N \end{bmatrix}.$$

Hence, any vector $\mathbf{w}_i$ satisfying

$$\mathbf{L}\mathbf{\Phi}_{\mathrm{w}}\mathbf{w}_i = \mathbf{b}_i \tag{6.13}$$

where $\mathbf{b}_i = -\mathbf{K}\mathbf{\Phi}_{\mathrm{d}}\mathbf{d}_i + \mathbf{K}\mathbf{d}_{i-1} + \mathbf{L}\mathbf{w}_{i-1}$, achieves the N-continuity. Equation (6.13) constructs the condition for the generalized N-continuous OFDM where $N_{\mathrm{w}} \geq N_{\mathrm{d}}$, i.e., the correction component has more dimensions than the data component. Since $N+1 < N_{\mathrm{w}}$, (6.13) is an under-determined system of equations and has infinitely many solutions. Without posing any other requirement on

$\mathbf{w}_i$, we are interested in minimizing the distortion of the correction component on the data signal. We then select the solution that has minimum norm via Moore-Penrose pseudoinverse of $\mathbf{L}\mathbf{\Phi}_{\mathrm{w}}$ [130, 149], defined as $(\mathbf{L}\mathbf{\Phi}_{\mathrm{w}})^{\dagger} = \mathbf{\Phi}_{\mathrm{w}}^{\mathrm{H}}\mathbf{L}^{\mathrm{H}}\left(\mathbf{L}\mathbf{L}^{\mathrm{H}}\right)^{-1}$. Hence, the solution is obtained in frequency domain as

$$\mathbf{w}_i^{\mathrm{mn}} = \mathbf{\Phi}_{\mathrm{w}}^{\mathrm{H}}\mathbf{L}^{\mathrm{H}}\left(\mathbf{L}\mathbf{L}^{\mathrm{H}}\right)^{-1}\mathbf{b}_i, \tag{6.14}$$

which provides N-continuity with an arbitrary number of dimension for the correction component. After establishing the generalization, the distortion-free reception is presented in the sequel.

6.4 CP-Alignment

In the conventional N-continuous OFDM configuration where $N_{\mathrm{w}} = N_{\mathrm{d}}$, each data subcarrier has one correction component because both components have same symbol and CP durations. Thus, the data subcarriers are distorted even though the power of correction component is minimized. In addition, removing the distortion from the data subcarriers necessitates a modified receiver structure, e.g., with decision feedback equalizer [130].

As we have more degrees-of-freedom on the correction component, i.e., $N_{\mathrm{w}} > N_{\mathrm{d}}$, it is possible to remove the distortion caused by the correction component considering the idea of CP-alignment. As illustrated in Figure 6.2, the dimensions of the signal space of OFDM symbols reduces from $N_{\mathrm{d}} + G_{\mathrm{d}}$ to N_{d} with CP removal after the multipath channel. This difference leaves a room for no-distortion transmission by aligning the correction component with the CP duration at the receiver. The overall picture of the proposed method, including the N-continuity and component alignment, is represented as functional block diagram in Figure 6.3.

The substitution of (6.5) into (6.8) yields the frequency domain received signal without the noise as

$$\mathbf{y}_i = \mathbf{F}_{\mathrm{d}}\mathbf{B}\mathbf{H}_{\mathrm{c}}\mathbf{A}_{\mathrm{d}}\mathbf{F}_{\mathrm{d}}^{\mathrm{H}}\mathbf{d}_i + \mathbf{F}_{\mathrm{d}}\mathbf{B}\mathbf{H}_{\mathrm{c}}\mathbf{A}_{\mathrm{w}}\mathbf{F}_{\mathrm{w}}^{\mathrm{H}}\mathbf{w}_i, \tag{6.15}$$

where the first term is the desired OFDM data symbol vector and the second term is the correction component that falls into the DFT window for the ith symbol. In order to cancel the correction

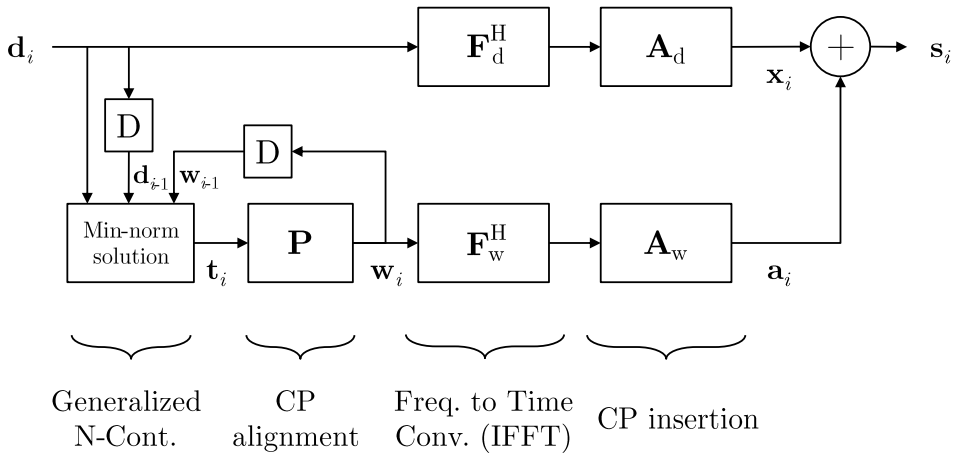

Figure 6.3 Block diagram of the proposed scheme representing the mathematical flow. The block named as "D" introduces one symbol duration delay.

component in the OFDM reception, one needs to satisfy

$$\mathbf{F}_{\mathrm{d}}\mathbf{B}\mathbf{H}_{\mathrm{c}}\mathbf{A}_{\mathrm{w}}\mathbf{F}_{\mathrm{w}}^{\mathrm{H}}\mathbf{w}_i = \mathbf{0}, \tag{6.16}$$

which implies that $\mathbf{w}_i$ should be in the nullspace of $\mathbf{F}_{\mathrm{d}}\mathbf{B}\mathbf{H}_{\mathrm{c}}\mathbf{A}_{\mathrm{w}}\mathbf{F}_{\mathrm{w}}^{\mathrm{H}} \in \mathbb{C}^{N_{\mathrm{d}} \times N_{\mathrm{w}}}$. The enabling factor for canceling the correction component after the channel and CP-removal is having a nonzero nullspace for the system in (6.16). We know from the rank-nullity theorem [149] that

$$\begin{aligned} \dim\left(\mathrm{null}\left(\mathbf{F}_{\mathrm{d}}\mathbf{B}\mathbf{H}_{\mathrm{c}}\mathbf{A}_{\mathrm{w}}\mathbf{F}_{\mathrm{w}}^{\mathrm{H}}\right)\right) &= N_{\mathrm{w}} - \mathrm{rank}\left(\mathbf{F}_{\mathrm{d}}\mathbf{B}\mathbf{H}_{\mathrm{c}}\mathbf{A}_{\mathrm{w}}\mathbf{F}_{\mathrm{w}}^{\mathrm{H}}\right) \\ &= N_{\mathrm{w}} - N_{\mathrm{d}}, \end{aligned} \tag{6.17}$$

which dictates selecting smaller CP size for the correction component, i.e., $N_{\mathrm{w}} > N_{\mathrm{d}}$ to have a non-injective system for (6.16). Thus, the dimension of the nullspace will be nonzero. The solution space for (6.16) can be realized by

$$\mathbf{w}_i = \mathbf{P}\mathbf{t}_i \tag{6.18}$$

where $\mathbf{P} \in \mathbb{C}^{N_\mathrm{w} \times (N_\mathrm{w} - N_\mathrm{d})}$ is the precoder matrix that maps an arbitrary vector $\mathbf{t}_i \in \mathbb{C}^{(N_\mathrm{w} - N_\mathrm{d}) \times 1}$ into the nullspace of $\mathbf{F}_\mathrm{d}\mathbf{B}\mathbf{H}_\mathrm{c}\mathbf{A}_\mathrm{w}\mathbf{F}_\mathrm{w}^\mathrm{H}$. In other words, the columns of $\mathbf{P}$ spans the nullspace as

$$\mathrm{range}\left(\mathbf{P}\right) = \mathrm{null}\left(\mathbf{F}_\mathrm{d}\mathbf{B}\mathbf{H}_\mathrm{c}\mathbf{A}_\mathrm{w}\mathbf{F}_\mathrm{w}^\mathrm{H}\right), \tag{6.19}$$

and can be computed via singular value decomposition (SVD) by

$$\mathbf{F}_\mathrm{d}\mathbf{B}\mathbf{H}_\mathrm{c}\mathbf{A}_\mathrm{w}\mathbf{F}_\mathrm{w}^\mathrm{H} = \mathbf{U}\mathbf{\Sigma}\mathbf{V}^\mathrm{H} \tag{6.20}$$

where $\mathbf{U} \in \mathbb{C}^{N_\mathrm{d} \times N_\mathrm{d}}$ and $\mathbf{V} \in \mathbb{C}^{N_\mathrm{w} \times N_\mathrm{w}}$ are orthonormal matrices and $\mathbf{\Sigma} \in \mathbb{C}^{N_\mathrm{d} \times N_\mathrm{w}}$ is the diagonal matrix containing the singular values in decreasing order along its diagonal. Then, $\mathbf{P}$ is found by importing the last $N_\mathrm{w} - N_\mathrm{d}$ columns of $\mathbf{V}$ [149, Ch. 6.3], given as

$$\mathbf{P} = \left[\mathbf{v}_{N_\mathrm{d}}, \ldots, \mathbf{v}_{N_\mathrm{w}-1}\right]. \tag{6.21}$$

After the presenting the correction component alignment with nullspace preconditioning, substituting (6.18) into the main equation (6.13) yields

$$\mathbf{L}\mathbf{\Phi}_\mathrm{w}\mathbf{P}\mathbf{t}_i = \mathbf{b}_i. \tag{6.22}$$

Equation (6.22) explains how the correction component simultaneously provides $N-$continuity between consecutive signals at the transmitter and the alignment into the CP portion at the receiver. It is worth noting that the system in (6.22) is under-determined as well since we maintain $N + 1 < N_\mathrm{w} - N_\mathrm{d}$. Similar to previous case, one can select the minimum-norm solution for (6.22) even though the effect on the OFDM reception is readily canceled with component alignment. The solution for $\mathbf{t}_i$ is found by using the pseudoinverse of $\mathbf{L}\mathbf{\Phi}_\mathrm{w}\mathbf{P}$ as

$$\mathbf{t}_i^\mathrm{mn} = \left(\mathbf{L}\mathbf{\Phi}_\mathrm{w}\mathbf{P}\right)^\dagger \mathbf{b}_i, \tag{6.23}$$

which is substituted into (6.18) to obtain the minimum norm frequency domain correction component that satisfies N-continuity and is aligned with CP at the same time.

6.5 PAPR Reduction

In this section, we introduce the peak-to-average power ratio (PAPR) reduction into the overall design of the correction component. Since both cases given in (6.13) and (6.22) have systems of underdetermined linear equations, the solution is not unique. Among many possible solutions, the ones with minimum length are selected in (6.14) and (6.23), respectively. The availability of selecting arbitrary vector for $\mathbf{t}_i$ promises the use of this component for further improvements on the transmitted signal without a sacrifice from other benefits[2]. The PAPR reduction comes at this stage as a suitable objective in finding a particular $\mathbf{t}_i$ rather than $\mathbf{t}_i^{\mathrm{mn}}$. Hence, the correction component will also reduce the PAPR of transmitted signal while achieving the symbol continuity and CP alignment properties.

Any typical solution vector of an underdetermined system can be represented by a combination of a vector in the row space and a vector in its nullspace [149, Ch. 3.1]. In our case, a solution for (6.22) can be written as

$$\mathbf{t}_i = \underbrace{\mathbf{t}_i^{\mathrm{mn}}}_{\substack{\text{row space}\\ \text{component}}} + \underbrace{\mathbf{t}_i^{\mathrm{ns}}}_{\substack{\text{nullspace}\\ \text{component}}} \tag{6.24}$$

where the first component is the minimum-norm solution laying in the row space of $\mathbf{L}\mathbf{\Phi}_{\mathrm{w}}\mathbf{P}$ as given in (6.23) and the second component is selected from the nullspace of $\mathbf{L}\mathbf{\Phi}_{\mathrm{w}}\mathbf{P}$. By considering the decomposition in (6.24) the main equation can be rewritten as

$$\mathbf{L}\mathbf{\Phi}_{\mathrm{w}}\mathbf{P}\mathbf{t}_i = \mathbf{L}\mathbf{\Phi}_{\mathrm{w}}\mathbf{P}\mathbf{t}_i^{\mathrm{mn}} + \mathbf{L}\mathbf{\Phi}_{\mathrm{w}}\mathbf{P}\mathbf{t}_i^{\mathrm{ns}} = \mathbf{b}_i \tag{6.25}$$

[2]We note here that we construct the PAPR reduction on top of the CP alignment case in Section 6.4 although the it can also be built solely on the non-aligned case in Section 6.3, which will not have the benefit of CP-alignment property at the receiver.

which implies $\mathbf{L}\mathbf{\Phi}_{\mathrm{w}}\mathbf{P}\mathbf{t}_i^{\mathrm{ns}} = \mathbf{0}$. Similar to approach in finding the nullspace component for CP-alignment (6.18)-(6.23), we can generate the nullspace vector that satisfy the N-continuity inside the nullspace of CP-alignment as

$$\mathbf{t}_i^{\mathrm{ns}} = \mathbf{Q}\mathbf{q}_i \tag{6.26}$$

where $\mathbf{Q} \in \mathbb{C}^{(N_{\mathrm{w}}-N_{\mathrm{d}})\times((N_{\mathrm{w}}-N_{\mathrm{d}}-N-1))}$ satisfies

$$\mathrm{range}\left(\mathbf{Q}\right) = \mathrm{null}\left(\mathbf{L}\mathbf{\Phi}_{\mathrm{w}}\mathbf{P}\right), \tag{6.27}$$

and hence, maps any arbitrary vector $\mathbf{q}_i \in \mathbb{C}^{(N_{\mathrm{w}}-N_{\mathrm{d}}-N-1)\times 1}$ into the nullspace of $\mathbf{L}\mathbf{\Phi}_{\mathrm{w}}\mathbf{P}$. Columns of $\mathbf{Q}$ can be found via SVD of $\mathbf{L}\mathbf{\Phi}_{\mathrm{w}}\mathbf{P}$ similar to method in Section 6.4.

Finally, the free variable $\mathbf{q}_i$ is optimized to minimize the PAPR of the ith transmitted symbol. By representing the peak power of the transmitted signal by the infinite norm as

$$\|\mathbf{s}_i\|_\infty = \|\mathbf{x}_i + \mathbf{a}_i\|_\infty. \tag{6.28}$$

Thus, the free variable can be optimized to minimize the peak power of the overall time domain OFDM signal as

$$\begin{aligned} \mathbf{q}_i^{\mathrm{pa}} &= \arg\min_{\mathbf{q}_i} \|\mathbf{x}_i + \mathbf{A}_{\mathrm{w}}\mathbf{F}_{\mathrm{w}}^{\mathrm{H}}\mathbf{P}(\mathbf{t}_i^{\mathrm{mn}} + \mathbf{Q}\mathbf{q}_i)\|_\infty \\ \text{subject to} \quad & \|\mathbf{t}_i^{\mathrm{mn}} + \mathbf{Q}\mathbf{q}_i\|_2^2 < \alpha N_{\mathrm{d}} \end{aligned} \tag{6.29}$$

which makes the overall signal N-continuous with the correction component is aligned to the CP duration at the receiver while reducing PAPR for the transmitted signal. By substituting (6.26) into (6.24) and then (6.24) into (6.18), we can represent the frequency domain alignment vector from the reduced dimensional free variable $\mathbf{q}_i$ as

$$\mathbf{w}_i^{\mathrm{pa}} = \mathbf{P}(\mathbf{t}_i^{\mathrm{mn}} + \mathbf{Q}\mathbf{q}_i^{\mathrm{pa}}) \tag{6.30}$$

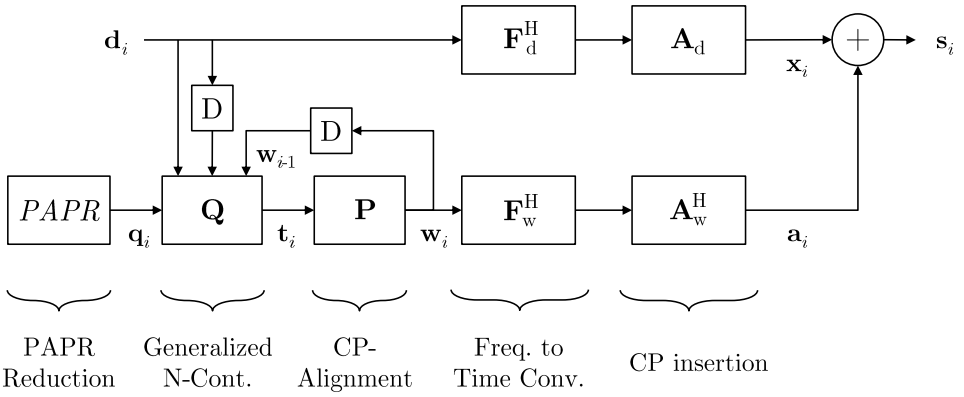

Figure 6.4 The mathematical block diagram of the overall proposed scheme including the PAPR reduction.

The overall picture including the PAPR reduction along with N-continuity and component alignment is represented as functional block diagram in Figure 6.4.

6.6 PHY Security Aspects

Inserting an additive component on top of the data signal creates distortion and degrades bit error rate (BER) at the receiver as it happens in conventional [130] and generalized N-continuous cases shown above. When the inserted component is created as a function of channel response between transmitter and receiver and aligned with the receivers nullspace after channel, i.e., CP duration, the distortion becomes invisible to the intended receiver. In contrast, this is not valid for any arbitrary receiver which experiences independently faded multipath channel. Thus, the additive component will not be aligned with the CP duration and spread over the received time domain OFDM data signal. The component can then be regarded as artificial noise (AN) [23] which also exploits the nullspace in the system for generating distortion in the unintended receivers.

By considering the communication scenario with secrecy constraints, convention on naming the nodes suggests Alice for transmitter, Bob for intended receiver, and Eve for the eavesdropper as also introduced in Chapter 2. Calculation of the additional correction term, $a_i(t)$, in CP-aligned generalized N-continuous in Section 6.4 is based on minimum norm solution similar to conventional N-continuous and generalized N-continuous cases in Section 6.3. Thus, the relative power associated to additional term has limited effect on the distortion. In contrast, the infinite

norm minimization in (6.29) along with upper power limit enables to have sufficient distortion on the data symbols at the unintended receiver Eve. The power allocated to the correction, α, ensures a maximum SINR that Eve can achieve. By rewriting (6.15) for Eve with the noise term for a particular subcarrier k as

$$y_{i,k} = H_k d_{i,k} + H_k w_{i,k} + v_{i,k}, \tag{6.31}$$

we can determine the SINR for a given channel as

$$\gamma = \frac{|H_k|^2}{\alpha|H_k|^2 + \sigma_v^2} \tag{6.32}$$

$$< \frac{1}{\alpha}. \tag{6.33}$$

Thus, the transmitter ensures an error floor at eavesdropper with the level determined by the allocated power α, as it will be shown in the results section.

6.7 Numerical Results

In this section, we present the performance results of the proposed scheme with the following OFDM parameters. $N_{\mathrm{d}} = 300$ data subcarriers with 16 QAM modulation are active with $T_{\mathrm{g}} = \frac{1}{4}T_{\mathrm{d}}$. The DC subcarrier is disabled. The duration of the main part for the correction component is selected as $T_{\mathrm{w}} = \frac{9}{8}T_{\mathrm{d}}$ unless otherwise stated. For each simulation result, 100 independent channel realizations are considered and 1000 OFDM symbols are evaluated for each channel realization. We assume block fading 6-tap Rayleigh multipath channel with uniform power delay profile (PDP).

6.7.1 Power Spectrum

We first present the OOB emission performances of conventional and proposed schemes. The power spectrum for $N = 0$ and $N = 1$ are given in Figure 6.5. Regardless of CP alignment, the generalized N-continuous OFDM, formulated in (6.12), offers the identical level of continuity as conventional N-continuous OFDM. Therefore, generalized N-continuous OFDM schemes achieve the same OOB emission performance as conventional N-continuous OFDM [130]. This result also

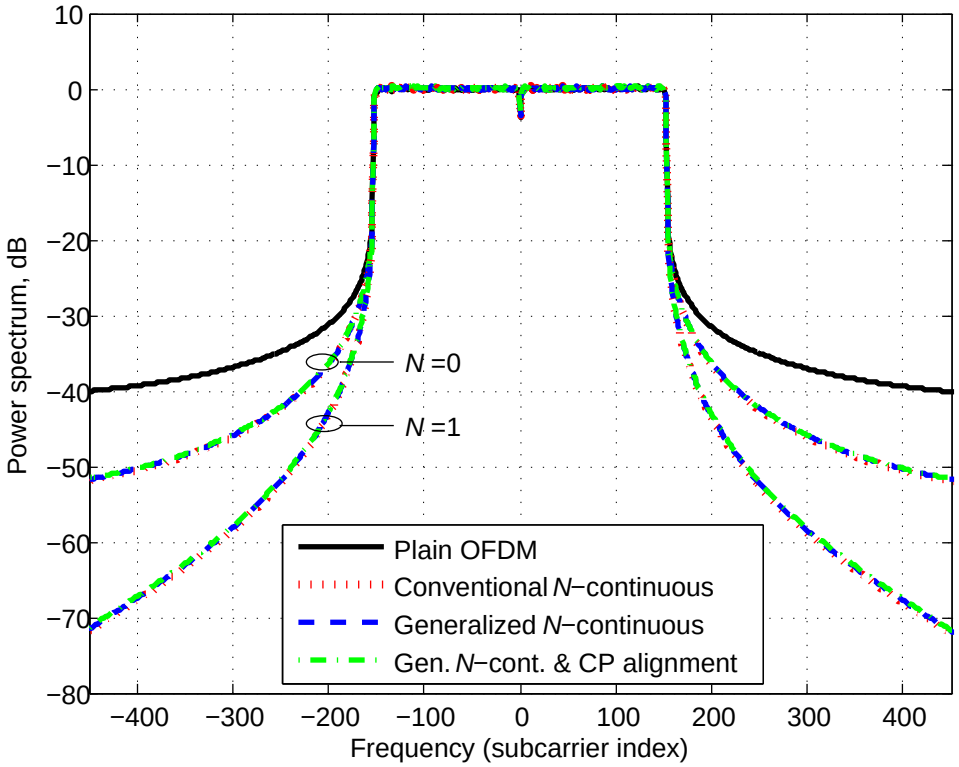

Figure 6.5 Power spectrum when $N = 0$ and $N = 1$.

shows that the OOB performance is solely a function of the level of continuity rather than the symbol duration of the correction component.

6.7.2 PAPR Performance

Given that the OFDM signal, as a multicarrier scheme, suffers from high dynamic range in time domain, we investigate the PAPR of the transmitted signal for each transmission scenario. Figure 6.6 shows the CCDF of PAPR of all cases. The scenarios without PAPR reduction including plain, conventional, generalized, and generalized CP-aligned N-continuous OFDM experience very similar PAPR performance as it can be seen from the figure. When we have active PAPR reduction on top of the other properties, N-continuous OFDM there is a substation in the peak power statistics.

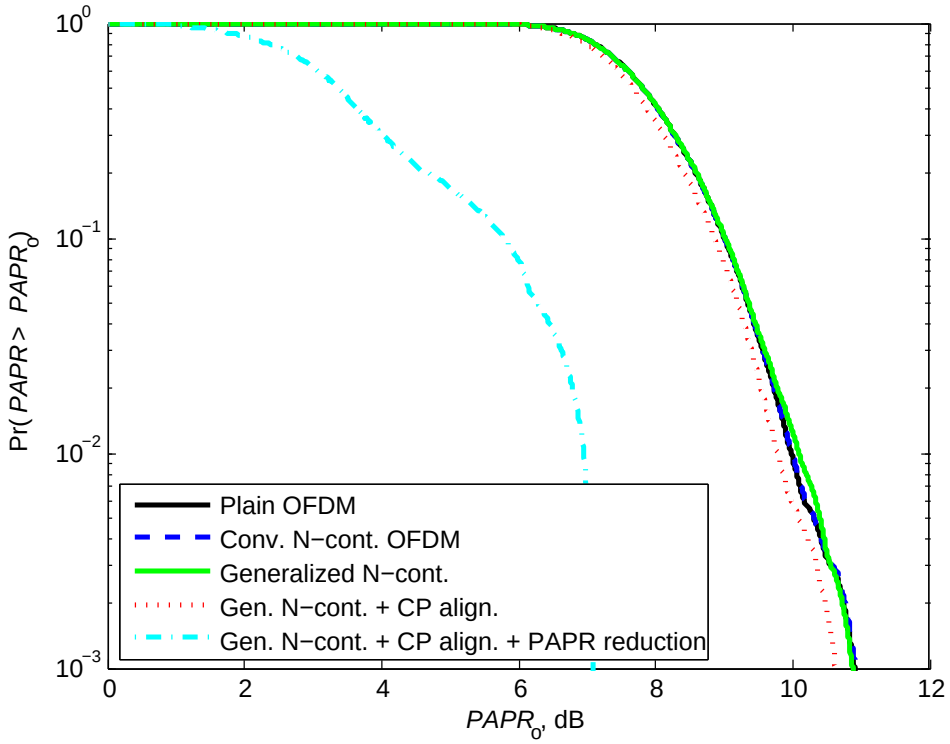

Figure 6.6 PAPR results for all cases.

6.7.3 Bit Error Rate

The uncoded BER performance is evaluated for each case with both QPSK and 16QAM modulation types. It is worth noting that conventional and generalized N-continuous OFDM both suffer from the interference caused by the correction component without a modified receiver [130]. Since we do not necessitate any change at the receiver for the sake of receiver backward compatibility, we present the error rates with conventional OFDM reception without any modification. The results for BER are shown in Figure 6.7. Although the correction component in the first case of the generalized N-continuous is not aligned with the CP, its distortion is slightly less compared to the conventional N-continuous OFDM. The reason is considered as the fact that the larger number of free variable in generalized case helps achieving the continuity with slightly smaller distortion on the modulation symbols. On the other hand, the proposed CP-aligned N-continuous OFDM does not have a distortion effect in the receiver BER performance as shown in Figure 6.7. The offset between the plain OFDM and the proposed scheme in the BER results is due to the fact

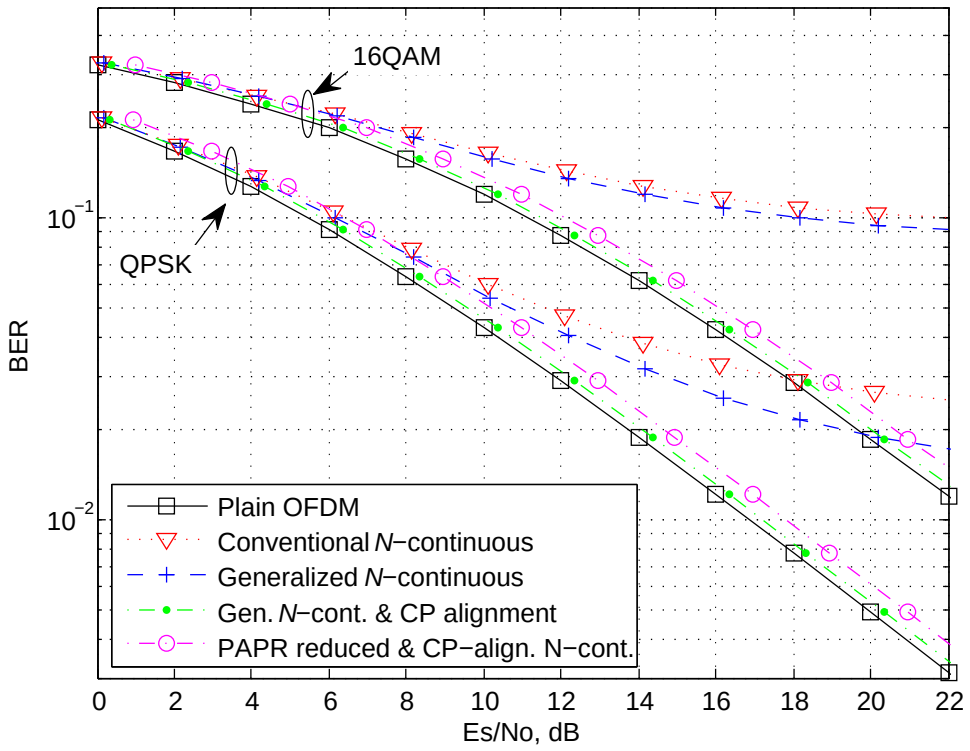

Figure 6.7 BER results for QPSK and 16QAM modulation types.

that the signal power in the signal-to-noise ratio (SNR) calculation includes the power of correction component along with the data signal. Except from this small price, the receiver enjoys the distortion-free subcarriers without a need in a modification in the OFDM demodulation as the correction component is aligned with CP duration.

6.8 Conclusions

In this chapter, we propose an OFDM scheme which offers the continuity between consecutive symbols without causing any distortion on data subcarriers at the receiver. This is achieved by exploiting the room left by the CP removal operation at the receiver. Therefore, three main goals are achieved with the proposed scheme: 1) closed form solution for the OOB reduction without loss in spectral efficiency, 2) no BER degradation due to distortion, and 3) no modification in the conventional OFDM receivers. As a future work, we will investigate the joint PAPR and the OOB

leakage reduction together, performance evaluation and compensation for the imperfect channel state knowledge and multiple accessing scenarios into account.

CHAPTER 7:
SECURE COMMUNICATION IN FREQUENCY SELECTIVE CHANNELS WITH FADE-AVOIDING SUBCHANNEL USAGE

7.1 Introduction

In consequence of the broadcast nature of the radio waves, privacy and security have become essential issues with the increasing number of applications and devices that employ wireless connection[1]. Transmission of data has traditionally been secured via cryptographic techniques. Recent considerations in security of communication system aim to take advantage of the randomness of the wireless channel between the nodes to provide a security layer in the physical domain [150]. Fundamentally, physical layer techniques prevent malicious nodes from capturing information via eavesdropping, rather than relying solely on the upper layer countermeasures to make the decoding of the captured signal a harder task for the eavesdropper.

Foundations of the secure communication has been laid by Shannon and Wyner from the information theoretic perspective. In [16], the secrecy capacity is shown to be positive only when the entropy of the secret key is equal or larger than the entropy of the message itself without any assumption on the computational resources of the malicious node. Then, the wire-tap channel, which has different noise statistics than the main channel, is introduced, and the trade-off between the secrecy capacity and information rate is revealed in [20]. Parallel fading Gaussian broadcast channels are studied in [151] considering the secrecy capacity when the transmitter has common information for all receivers as well as confidential information for the legitimate receiver. In [152], Wyner's work is extended to the single-input multiple-outputs (SIMO) scenario. Usefulness of fading in the information-theoretic security is emphasized in [25] by achieving positive secrecy even

[1]The content of this chapter is published in [78]. Copyright notice for this publication can be found in Appendix C.

when the eavesdropper's channel has better signal-to-noise ratio (SNR) than the main channel. Optimal power allocation with full channel state information (CSI) is given for slow fading channels in [153]. Also, authors showed that an on/off transmission scheme approaches the optimal performance when the transmitter does not possess CSI of the eavesdropper. A more aggressive technique while exploiting the wireless channel for secrecy is proposed in [23] for multiple-input multiple-output (MIMO) scenarios. Transmitter distorts the reception of possible eavesdroppers by inserting artificial noise (AN) to the useful data without an effect on the legitimate receiver performance. This is achieved by selecting the noise vector from the nullspace of the MIMO channel between the legitimate nodes. In [154], nulls of the frequency selective channel of the eavesdropper is exploited to hide information, albeit with the requirement of full CSI knowledge.

In this study, we propose the usage of the artificial noise in frequency selective (i.e., time dispersive) single-input single-output (SISO) channels to degrade the reception of the eavesdroppers. Unlike MIMO case, the nullspace of SISO channel is considered to be along frequency domain. In other words, deep-faded subchannels are taken as the best candidate set for nulls of the channel between legitimate nodes, and not used for information transmission. By excluding the subchannels that are already in fade, channel capacity reduction of legitimate link is minimized. However, a reduction proportional to the percentage of unused subchannels in eavesdropper's channel capacity is maintained. Besides the secrecy gain with provided by the difference between channel capacity reductions, the insertion of fade-filler noise further degrades the reception quality of the unintended receivers. Thus, outcomes of the proposed technique can be considered as two folds. First, without considering the AN, higher probability of achieving nonzero secrecy capacity by channel-specific subchannel usage of the legitimate nodes is provided. Second, the AN integrated into the transmitted signal provides distortion on the eavesdropper's reception, including an error floor for high SNR regimes.

The remainder of this chapter is organized as follows: In Section 4.2, the system model is introduced. Then, the proposed technique is presented in Section 7.3 including the communication secrecy analysis and discussion on threshold selection. AN insertion is given in Section 7.4. Nu-

merical results are presented in Section 7.5 and finally, we wrap up the chapter in Section 7.6 with concluding remarks.

7.2 System Model

We consider a scenario as depicted in Figure 7.1. A legitimate transmitter, Alice, wants to send message to legitimate receiver, Bob. The message $x(n)$ is transmitted over a discrete time wireless multipath fading channel whose output at Bob's side is

$$y_{\mathrm{B}}(n) = \sum_{m=0}^{L_{\mathrm{B}}-1} h_{\mathrm{B}}(n,m)x(n-m) + w_{\mathrm{B}}(n), \tag{7.1}$$

where $h_{\mathrm{B}}(n,m)$ is time-varying complex gain of the mth tap of the main multipath channel with maximum excess delay of L_{B}, and $w_{\mathrm{B}}(n)$ is the zero-mean complex additive white Gaussian noise (AWGN).

An eavesdropper, named as Eve, intends to receive the signal transmitted by Alice. Likewise, the signal received by Eve is given as

$$y_{\mathrm{E}}(n) = \sum_{m=0}^{L_{\mathrm{E}}-1} h_{\mathrm{E}}(m,n)x(n-m) + w_{\mathrm{E}}(n). \tag{7.2}$$

where $h_{\mathrm{E}}(m,n)$, L_{E}, and $w_{\mathrm{E}}(n)$ are the complex response, maximum excess delay, and AWGN of eavesdropper channel, respectively. Block transmission is considered where each block constitutes N information symbols. The frequency-selective fading channel can be considered as combination of orthogonal flat-fading sub-channels when a cyclic prefix (CP) longer than the multipath channel excess delay is added to signal [155]. Thus, transmission blocks consist of G-size CP as well as the main block of size N. We assume the channel fading coefficients are quasi-static during one transmission block, i.e., $h_{\mathrm{B}}(m,n) = h_{\mathrm{B}}(m)$, and $h_{\mathrm{E}}(m,n) = h_{\mathrm{E}}(m)$ for $n = -G, \ldots, N-1$. Therefore, $G \geq L_{\mathrm{B}} - 1$ provides circular channel convolution allowing simple frequency domain equalization (FDE) for Bob. Note that, we do not take into account the effect of a possible

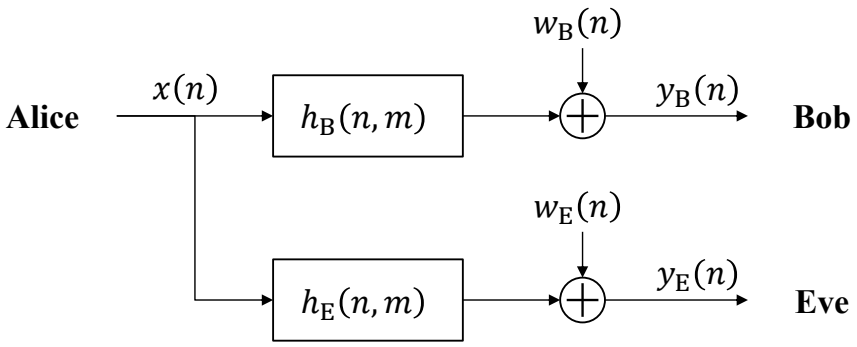

Figure 7.1 System model consisting of legitimate transmitter (Alice) and receiver (Bob), and eavesdropper (Eve) with multipath fading channels.

interference between transmission blocks on Eavesdropper's reception due to insufficient CP size. Thus, we also assume that $G \geq L_{\mathrm{E}} - 1$.

Multipath response of the main channel, $h_{\mathrm{B}}(m)$, is assumed to be known by the legitimate users Alice and Bob. This can be realized by utilizing the channel reciprocity [155]. Since Eve is a passive node, we assume that Alice has no information about CSI for the eavesdropper channel, $h_{\mathrm{E}}(m)$. This practical assumption is also motivated by the results that additional knowledge of eavesdropper's channel does not provide gain in terms of secrecy in fading channels [153], especially for high SNR regimes. As a final notice, we assume that Eve does not posses any information about the main channel because the frequency selective response of the wireless channel is unique to the locations of the transmitter and receiver as well as the environment. Therefore, $h_{\mathrm{B}}(m)$ and $h_{\mathrm{E}}(m)$ are uncorrelated.[2]

Since the security related tasks are considered via frequency domain adaptations such as subchannel nulling and noise insertion, we adopt frequency domain channel and signal representations. It is worth noting that the techniques proposed in this study are applicable to any system that has the ability of adaptive frequency usage[3]. Then, the received signals for Bob and Eve can

[2]Multipath components decorrelate from one transmit-receive path to another if the paths are separated by the order of an RF wavelength or more [156].

[3]Specifically, single-carrier frequency-domain-equalization (SC-FDE) and orthogonal frequency-division multiplexing (OFDM)-based systems are well known examples enabling dynamic spectrum usage with discrete Fourier transform (DFT) implementation [157].

be defined in frequency domain as

$$Y_{\mathrm{B}}(k) = H_{\mathrm{B}}(k)X(k) + W_{\mathrm{B}}(k), \text{ and} \tag{7.3}$$

$$Y_{\mathrm{E}}(k) = H_{\mathrm{E}}(k)X(k) + W_{\mathrm{E}}(k), \tag{7.4}$$

where $H_{\mathrm{B}}(k)$ and $H_{\mathrm{E}}(k)$ are complex channel gains for kth sub-channel, i.e., kth element of N-point discrete Fourier transforms (DFT) of $h_{\mathrm{B}}(m)$ and $h_{\mathrm{E}}(m)$, respectively. Similarly, $X(k)$, $W_{\mathrm{B}}(k)$, and $W_{\mathrm{E}}(k)$ are DFTs of $x(n)$, $w_{\mathrm{B}}(n)$, and $w_{\mathrm{E}}(n)$, for $n = 0, \ldots, N-1$, respectively.

In the following, we present secrecy capacity for given channels, which is defined as the difference between the capacities of the Alice-Bob (main) and Alice-Eve (eavesdropper) channels as

$$C_{\mathrm{s}} = C_{\mathrm{B}} - C_{\mathrm{E}}, \tag{7.5}$$

where

$$C_{\mathrm{B}} = \sum\nolimits_{k=1}^{N} \Delta f \log\left(1 + g_{\mathrm{B}}(k)\right) \quad \text{and} \tag{7.6}$$

$$C_{\mathrm{E}} = \sum\nolimits_{k=1}^{N} \Delta f \log\left(1 + g_{\mathrm{E}}(k)\right) \tag{7.7}$$

denote the capacities for the main and the eavesdropper channels, respectively. In (7.6) and (7.7), Δf is the sub-channel bandwidth, $g_{\mathrm{B}}(k) = \gamma_{\mathrm{B}} \left|H_{\mathrm{B}}(k)\right|^2$ and $g_{\mathrm{E}}(k) = \gamma_{\mathrm{E}} \left|H_{\mathrm{E}}(k)\right|^2$ are combined subchannel gains where γ_{B} and γ_{E} denoting the mean SNRs of the main and eavesdropper channels, respectively. In other words, the first term in combined gains represents the large scale effects, i.e., path loss and shadowing, while the second term corresponds to normalized channel gain for the kth sub-channel denoting the small-scale multipath effect, i.e., frequency selectivity.

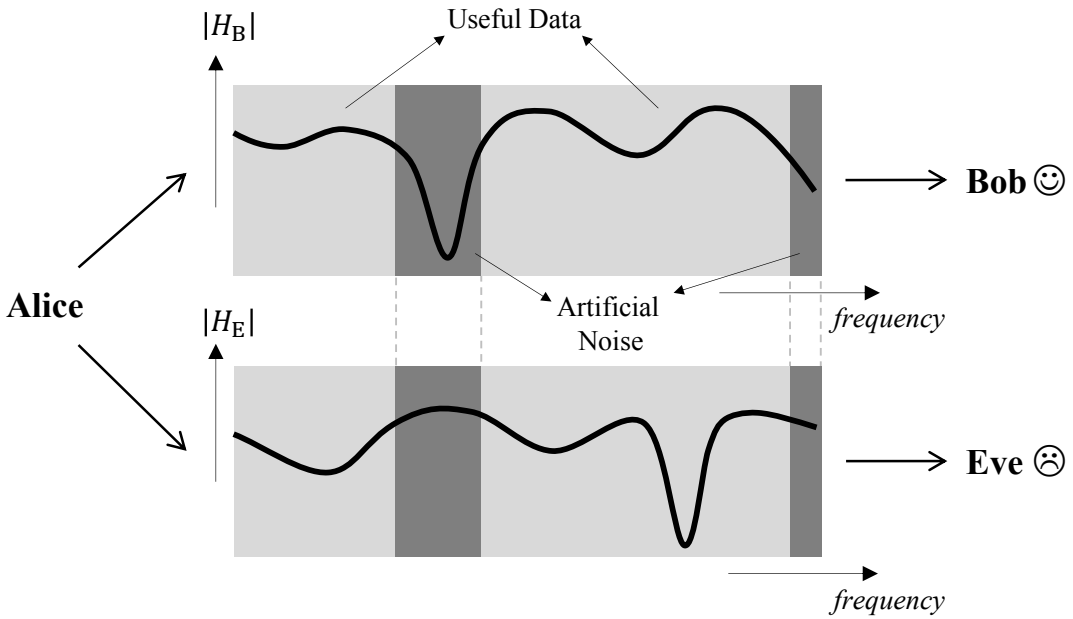

Figure 7.2 Intelligent sub-channel usage between Alice and Bob deteriorating the signal quality captured by Eve.

7.3 Adaptive Subchannel Usage

Three main mechanisms; reflection, diffraction, and scattering construct small scale effects in wireless propagation medium [158]. Therefore, multipath channel, i.e., frequency selectivity, is a random function of the physical environment.

We herein consider this phenomena to be able to provide nonzero secrecy capacity via fade-avoiding sub-channel utilization as illustrated in Figure 7.2. Returning to our notation, Alice employs the sub-channels on which she experiences relatively good channel gains for the transmission of useful information[4]. Since the contribution of faded subchannels on total capacity is the smallest among others, sacrificing these subcarriers provides the minimum reduction in the capacity of the main channel. However, the same conclusion cannot be drawn for the capacity of eavesdropper channel, C_E. Therefore, the reduction in eavesdropper channel's capacity becomes linearly proportional to the subchannel sacrifice ratio. Since the main and eavesdropper channels are statistically independent, the unused subcarrier locations and the channel response of Eve are

[4]Since only the amount of fading is required for subchannel allocation, it is enough for Alice to know only the magnitude of the channel frequency response rather than CSI with phase information.

uncorrelated. The difference between the capacity reductions provides nonzero secrecy capacity even when the mean SNRs at Eve is better than Bob for sufficient sacrifice ratios, which will be discussed in the section 7.5.

In the following, we reformulate the capacities of the main and eavesdropper channels in the presence of intelligent subchannel usage by the legitimate pair. Given a channel realization, the main channel capacity becomes

$$C_{\mathrm{B}} = \sum\nolimits_{k=1}^{N} \Delta f \log\left(1 + \mathbf{1}_{\mathcal{R}}(g_{\mathrm{B}}(k)) g_{\mathrm{B}}(k)\right) \tag{7.8}$$

where $\mathbf{1}_{\mathcal{R}}(x)$ is indicator function defined as

$$\mathbf{1}_{\mathcal{R}}(x) = \begin{cases} 1, & x \in \mathcal{R} = [r, \infty), \\ 0, & \text{elsewhere}, \end{cases}$$

with r denoting the channel power threshold for determining sub-channels that will be populated with useful information or AN. Similarly, we can rewrite eavesdropper channel capacity as

$$C_{\mathrm{E}} = \sum\nolimits_{k=0}^{N-1} \Delta f \log\left(1 + \mathbf{1}_{\mathcal{R}}(g_{\mathrm{B}}(k)) g_{\mathrm{E}}(k)\right). \tag{7.9}$$

Note that utilizing the subchannels that have greater power than a threshold corresponds to manipulating the distribution of the activated subchannel gains. For instance, although the channel between Alice and Bob experiences Rayleigh fading, active subchannels will not be Rayleigh-distributed when the subchannels are selected as a function of channel frequency response. In addition, we assume that the amount of frequency selectivity is sufficient such that all realizations of the sub-channel powers are observed along the band under consideration [22], even if there exist some correlation between close-by subchannels. In other words, N is large enough to consider channel as ergodic in frequency. Therefore, the main channel capacity can be rewritten as

$$C_{\mathrm{B}} = (1 - F_{g_{\mathrm{B}}}(r)) N \Delta f \log\left(1 + \tilde{g}_{\mathrm{B}}\right), \tag{7.10}$$

where $F_{g_{\mathrm{B}}}(r)$ is cumulative distribution function (CDF) of g_{B} at r. Thus, $(1-F_{g_{\mathrm{B}}}(r))N$ corresponds to the number of active subchannels with gains denoted by $\tilde{g}_{\mathrm{B}}$. For a constant threshold r, the modified channel gain follows a distribution which is truncated distribution of g_{B}. Probability density function (PDF) of $\tilde{g}_{\mathrm{B}}$ is then becomes

$$f_{\tilde{g}_{\mathrm{B}}}(x) = \begin{cases} \frac{f_{g_{\mathrm{B}}}(x)}{1-F_{g_{\mathrm{B}}}(r)}, & x \geq r, \\ 0, & x < r \end{cases} \tag{7.11}$$

where $f_{g_{\mathrm{B}}}(x)$ is the PDF of g_{B}.

For the reception of Eve, it is known that random variables $\mathbf{1}_{\mathcal{R}}(g_{\mathrm{B}}(k))$ and g_{B} are uncorrelated. That is, the effect of fade-avoiding subchannel usage by Alice is nothing but reduced number of subchannels with same statistical characteristics. Therefore, the distribution of the channel gains of active subchannels observed by Eve follows the same distribution of $f_{\tilde{g}_{\mathrm{B}},g_{\mathrm{E}}}$, assuming that small reduction in the number of subcarriers does not affect the ergodic assumption. Then, the channel capacity of Eve turns out to be

$$C_{\mathrm{E}} = (1 - F_{g_{\mathrm{B}}}(r))N\Delta f \log\left(1 + g_{\mathrm{E}}\right), \tag{7.12}$$

where $(1 - F_{g_{\mathrm{B}}}(r))N$ is the number of active subchannels populated with useful information.

7.3.1 Outage Probability

As opposed to ideal condition where noise is the only channel effect, the capacities given in (7.10) and (7.12) are random variables in fading channels. In other words, besides the frequency ergodicity that makes the total channel capacity over frequency deterministic value, the time variation of channel fading is not high enough to assume that the channel is ergodic in time. Thus, we adopt the statistical measures for the information theoretic secrecy, without considering the effect of AN. Probability of achieving nonzero secrecy capacity and the outage probability for a target secrecy rate are analyzed. Considering the channel capacities given in (7.10) and (7.12), the probability that the secrecy capacity is nonzero yields

$$
\begin{aligned}
\mathcal{P}\left(C_{\mathrm{s}}>0\right) &= \mathcal{P}\Big(\big(1-F_{g_{\mathrm{B}}}(r)\big)N\Delta f\log\left(1+\tilde{g}_{\mathrm{B}}\right) > \big(1-F_{g_{\mathrm{B}}}(r)\big)N\Delta f\log\left(1+g_{\mathrm{E}}\right)\Big) \\
&= \mathcal{P}\big(\log\left(1+\tilde{g}_{\mathrm{B}}\right) > \log\left(1+g_{\mathrm{E}}\right)\big) \\
&= \mathcal{P}\big(\tilde{g}_{\mathrm{B}} > g_{\mathrm{E}}\big) \\
&= \int_0^{\infty}\int_0^{u} f_{\tilde{g}_{\mathrm{B}},g_{\mathrm{E}}}(u,v)\ \mathrm{d}v\mathrm{d}u \\
&= \int_0^{\infty}\int_0^{u} f_{\tilde{g}_{\mathrm{B}}}(u)f_{g_{\mathrm{E}}}(v)\ \mathrm{d}v\mathrm{d}u \\
&= \int_0^{\infty} f_{\tilde{g}_{\mathrm{B}}}(u)F_{g_{\mathrm{E}}}(u)\ \mathrm{d}u
\end{aligned} \tag{7.13}
$$

where $f_{g_{\mathrm{E}}}(x)$ and $F_{g_{\mathrm{E}}}(x) = \int_{-\infty}^{x} f_{g_{\mathrm{E}}}(u)\ \mathrm{d}u$ denote PDF and CDF of g_{E}, respectively. When we assume that both channels experience Rayleigh fading, the power of the channel gains, g_{B} and g_{E} follow exponential distribution with mean value γ_{B} and γ_{E} [155]. That is, $f_{g_{\mathrm{B}}}(x) = \frac{1}{\gamma_{\mathrm{B}}}e^{-\frac{1}{\gamma_{\mathrm{B}}}x}$ and $f_{g_{\mathrm{E}}}(x) = \frac{1}{\gamma_{\mathrm{E}}}e^{-\frac{1}{\gamma_{\mathrm{E}}}x}$ for $x \geq 0$, and 0 otherwise. After obtaining the modified PDF for $\tilde{g}_{\mathrm{B}}$ by using (7.11), substituting the distributions into (7.13) yields

$$
\begin{aligned}
\mathcal{P}\left(C_{\mathrm{s}}>0\right) &= \mathcal{P}\big(\tilde{g}_{\mathrm{B}} > g_{\mathrm{E}}\big) \\
&= \int_r^{\infty} \frac{e^{\frac{r}{\gamma_{\mathrm{B}}}}}{\gamma_{\mathrm{B}}} e^{-\frac{1}{\gamma_{\mathrm{B}}}u}\left(1-e^{-\frac{1}{\gamma_{\mathrm{E}}}u}\right)\ \mathrm{d}u \\
&= \frac{\gamma_{\mathrm{B}}+\left(1-e^{-\frac{1}{\gamma_{\mathrm{E}}}r}\right)\gamma_{\mathrm{E}}}{\gamma_{\mathrm{B}}+\gamma_{\mathrm{E}}}.
\end{aligned} \tag{7.14}
$$

Note that when all the subchannels are used for useful data transmission, i.e., $r = 0$, existence of the nonzero secrecy capacity reduces to the ratio of the SNR of main channel to the total SNR of the two channels, which is also shown in [25]. Introducing intelligent subchannel usage increases the probability of achieving nonzero secrecy in (7.14) as a function of γ_{E} and r.

In the following, we present the outage probability, which is defined as the probability that the secrecy capacity drops below a target secrecy rate, R_{s}. Using the law of total probability, the

outage probability can be written as

$$\begin{aligned}\mathcal{P}_{\text{out}}(R_{\text{s}}) &= \mathcal{P}\left(C_{\text{s}} < R_{\text{s}}\right) \\ &= \mathcal{P}\left(C_{\text{s}} < R_{\text{s}} \mid \tilde{g}_{\text{B}} > g_{\text{E}}\right)\mathcal{P}\left(\tilde{g}_{\text{B}} > g_{\text{E}}\right) \\ &\quad + \mathcal{P}\left(C_{\text{s}} < R_{\text{s}} \mid \tilde{g}_{\text{B}} \leq g_{\text{E}}\right)\mathcal{P}\left(\tilde{g}_{\text{B}} \leq g_{\text{E}}\right) \end{aligned} \tag{7.15}$$

Elaborating the individual components of (7.15), we have

$$\begin{aligned}&\mathcal{P}(\, C_{\text{s}} < R_{\text{s}} \mid \tilde{g}_{\text{B}} > g_{\text{E}}) \\ &= \mathcal{P}\left(\log\left(1+\tilde{g}_{\text{B}}\right) - \log\left(1+g_{\text{E}}\right) < R_{\text{s}} \mid \tilde{g}_{\text{B}} > g_{\text{E}}\right) \\ &= \mathcal{P}\left(\tilde{g}_{\text{B}} < e^{R_{\text{s}}}\left(1+g_{\text{E}}\right) - 1 \mid \tilde{g}_{\text{B}} > g_{\text{E}}\right) \\ &= \int_0^{\infty}\int_v^{e^{R_{\text{s}}}(1+v)-1} \frac{f_{\tilde{g}_{\text{B}},g_{\text{E}}}(u,v)}{\mathcal{P}\left(\tilde{g}_{\text{B}} > g_{\text{E}}\right)}\,\mathrm{d}v\mathrm{d}u \\ &= \int_0^{\infty}\int_v^{e^{R_{\text{s}}}(1+v)-1} \frac{f_{\tilde{g}_{\text{B}}}(u) f_{g_{\text{E}}}(v)}{\mathcal{P}\left(\tilde{g}_{\text{B}} > g_{\text{E}}\right)}\,\mathrm{d}v\mathrm{d}u. \end{aligned} \tag{7.16}$$

Substituting the PDF of the channel gains, i.e., $f_{\tilde{g}_{\text{B}}}(x)$ and $f_{g_{\text{E}}}(x)$, into (7.16) yields

$$\mathcal{P}(C_{\text{s}} < R_{\text{s}} |\, \tilde{g}_{\text{B}} > g_{\text{E}}) = \frac{1}{\gamma_{\text{B}}\gamma_{\text{E}}}\int_0^{\infty}\int_{\lambda}^{e^{R_{\text{s}}}(1+v)-1} \frac{e^{\frac{r}{\gamma_{\text{B}}}} e^{-\frac{u}{\gamma_{\text{B}}}} e^{-\frac{v}{\gamma_{\text{E}}}}}{\mathcal{P}\left(\tilde{g}_{\text{B}} > g_{\text{E}}\right)}\,\mathrm{d}u\mathrm{d}v \tag{7.17}$$

where $\lambda = \max(v, r)$. Then, computing the integrations follows that

$$
\begin{aligned}
&\mathcal{P}(C_{\mathrm{s}} < R_{\mathrm{s}} \mid \tilde{g}_{\mathrm{B}} > g_{\mathrm{E}}) \\
=&\frac{(\gamma_{\mathrm{B}}+\gamma_{\mathrm{E}})\, e^{\frac{r}{\gamma_{\mathrm{B}}}}}{\gamma_{\mathrm{B}}\gamma_{\mathrm{E}}\left(\gamma_{\mathrm{B}}+\left(1-e^{-\frac{1}{\gamma_{\mathrm{E}}}r}\right)\gamma_{\mathrm{E}}\right)}\int_0^{\infty}\int_{\lambda}^{e^{R_{\mathrm{s}}}(1+v)-1} e^{-\frac{u}{\gamma_{\mathrm{B}}}} e^{-\frac{v}{\gamma_{\mathrm{E}}}}\,\mathrm{d}u\mathrm{d}v \\
=&\frac{(\gamma_{\mathrm{B}}+\gamma_{\mathrm{E}})\, e^{\frac{r}{\gamma_{\mathrm{B}}}}}{\gamma_{\mathrm{E}}\left(\gamma_{\mathrm{B}}+\left(1-e^{-\frac{1}{\gamma_{\mathrm{E}}}r}\right)\gamma_{\mathrm{E}}\right)}\int_0^{\infty}\left(-e^{\frac{1-e^{R_{\mathrm{s}}}(1+v)}{\gamma_{\mathrm{B}}}}+e^{-\frac{\lambda}{\gamma_{\mathrm{B}}}}\right)e^{-\frac{v}{\gamma_{\mathrm{E}}}}\,\mathrm{d}v \\
=&\frac{(\gamma_{\mathrm{B}}+\gamma_{\mathrm{E}})\, e^{\frac{r}{\gamma_{\mathrm{B}}}}}{\gamma_{\mathrm{E}}\left(\gamma_{\mathrm{B}}+\left(1-e^{-\frac{1}{\gamma_{\mathrm{E}}}r}\right)\gamma_{\mathrm{E}}\right)}\left(\int_0^{\infty} -e^{\frac{1-e^{R_{\mathrm{s}}}}{\gamma_{\mathrm{B}}}} e^{-\left(\frac{e^{R_{\mathrm{s}}}}{\gamma_{\mathrm{B}}}+\frac{1}{\gamma_{\mathrm{E}}}\right)v}\,\mathrm{d}v\right. \\
&\qquad\left.+e^{-\frac{r}{\gamma_{\mathrm{B}}}}\int_0^{r} e^{-\frac{v}{\gamma_{\mathrm{E}}}}\,\mathrm{d}v+\int_r^{\infty} e^{-\left(\frac{1}{\gamma_{\mathrm{B}}}+\frac{1}{\gamma_{\mathrm{E}}}\right)v}\,\mathrm{d}v\right) \\
=&\frac{(\gamma_{\mathrm{B}}+\gamma_{\mathrm{E}})\, e^{\frac{r}{\gamma_{\mathrm{B}}}}}{\gamma_{\mathrm{B}}+\left(1-e^{-\frac{1}{\gamma_{\mathrm{E}}}r}\right)\gamma_{\mathrm{E}}}\left(-\frac{\gamma_{\mathrm{B}}}{\gamma_{\mathrm{B}}+e^{R_{\mathrm{s}}}\gamma_{\mathrm{E}}}e^{-\frac{e^{R_{\mathrm{s}}}-1}{\gamma_{\mathrm{B}}}}\right. \\
&\qquad\left.+e^{-\frac{r}{\gamma_{\mathrm{B}}}}\left(1-e^{-\frac{r}{\gamma_{\mathrm{E}}}}\right)+\frac{\gamma_{\mathrm{B}}}{\gamma_{\mathrm{B}}+\gamma_{\mathrm{E}}}e^{-\frac{\gamma_{\mathrm{B}}+\gamma_{\mathrm{E}}}{\gamma_{\mathrm{B}}\gamma_{\mathrm{E}}}r}\right),
\end{aligned}
\tag{7.18}
$$

which reduces to

$$
\begin{aligned}
&\mathcal{P}(C_{\mathrm{s}} < R_{\mathrm{s}} \mid \tilde{g}_{\mathrm{B}} > g_{\mathrm{E}}) \\
&\qquad= \frac{\gamma_{\mathrm{B}}+\gamma_{\mathrm{E}}}{\gamma_{\mathrm{B}}+\left(1-e^{-\frac{r}{\gamma_{\mathrm{E}}}}\right)\gamma_{\mathrm{E}}}\left(1-\frac{\gamma_{\mathrm{B}}}{\gamma_{\mathrm{B}}+e^{R_{\mathrm{s}}}\gamma_{\mathrm{E}}}e^{\frac{r-e^{R_{\mathrm{s}}}+1}{\gamma_{\mathrm{B}}}}-\left(1-\frac{\gamma_{\mathrm{B}}}{\gamma_{\mathrm{B}}+\gamma_{\mathrm{E}}}\right)e^{-\frac{r}{\gamma_{\mathrm{E}}}}\right).
\end{aligned}
\tag{7.19}
$$

Then for the other terms, we know that

$$
\mathcal{P}(C_{\mathrm{s}} < R_{\mathrm{s}} \mid \tilde{g}_{\mathrm{B}} \leq g_{\mathrm{E}}) = 1 \tag{7.20}
$$

and

$$
\mathcal{P}\left(\tilde{g}_{\mathrm{B}} \leq g_{\mathrm{E}}\right) = 1 - \mathcal{P}\left(\tilde{g}_{\mathrm{B}} > g_{\mathrm{E}}\right). \tag{7.21}
$$

Then, substituting (7.19), (7.14), (7.20), and (7.21) into (7.15) yields the outage probability as a function of mean SNRs and channel threshold as

$$\mathcal{P}_{\text{out}}(R_{\text{s}}) = 1 - \frac{\gamma_{\text{B}}}{\gamma_{\text{B}} + e^{R_{\text{s}}}\gamma_{\text{E}}} e^{\frac{r - e^{R_{\text{s}}} + 1}{\gamma_{\text{B}}}} \tag{7.22}$$

when both main and eavesdropper channels experience Rayleigh-distributed fading.

7.3.2 Discussion on Threshold Selection

For a given distribution for the main channel gain g_{B} and a threshold level, the percentage of the unused subchannels to the total, i.e., sacrifice ratio, is given as

$$\eta = F_{g_{\text{B}}}(r). \tag{7.23}$$

Therefore, the power threshold can be determined as a function of the sacrifice ratio, that is, $r = F^{-1}_{g_{\text{B}}}(\eta)$. However, Alice and Bob might experience some difficulties in distribution-based threshold selection. Although r is driven by a desired bandwidth sacrifice ratio η, ergodicity over frequency for the channel might not be valid at all time. That is, number of subchannels might not be enough to determine the threshold based on a theoretical distribution function as in (7.23). For example, when high number of subcarriers experience low channel gain due to slow fading, zero or few subchannels might exceed the power threshold r, which negatively effects the latency of the communication. On the other extreme, when most of the subchannels are above the threshold, secrecy requirements would not be satisfied. Also, the distribution of the channel gain might be different than the distribution that is considered in determining the threshold. For instance, having a strong line-of-sight component corresponds Rician distribution instead of Rayleigh [155].

Considering the aforementioned issues, a practical subchannel selection technique is introduced. Instead of setting a fixed threshold, Alice selects the best $\lceil (1-\eta)N \rceil$ subchannels for the transmission of useful data. By doing so, the two extreme cases regarding to latency and security are moderated. That is, fixed number of subchannel usage guarantees a constant bandwidth usage for legitimate transmission without introducing random latency. Also, maintaining the fixed num-

ber of subchannels with AN guarantees a minimum disturbance onto Eve's reception, which will be discussed in the next section.

7.4 Fade-Filler Artificial Noise

In addition to the intelligent subchannel usage for data transmission that creates a gap between the main and eavesdropper channel capacities, we propose populating the unused subchannels with AN so that an additional uncertainty is introduced into the reception of Eve. In particular, $\lfloor \eta N \rfloor$ independently distributed Gaussian random samples with zero mean and unit variance are assigned to $\lfloor \eta N \rfloor$ subchannels that are not selected for information bearing.

Aforementioned subchannel usage can be considered as the worst case scenario of the scheme with the AN. That is, when Eve has the CSI of Alice-Bob channel, she can discard the inserted noise components but still suffers from the reduction in the channel capacity. Therefore, additional secrecy gain via AN depends on the modulation/coding scheme and the computational abilities of the eavesdropper. Although the concept of fade-filler noise is given to show the possible improvement on secure communication, theoretical analysis and the effect of signal structure is the subject of future research. Besides that, substitution of the faded subchannels with AN instead of leaving empty maintains the covertness of the technique. In other words, AN insertion is also motivated for its benefit of preventing eavesdropper from detecting the exact location of used subchannels via observation of spectral gaps.

7.5 Results

Effectiveness of the proposed technique is presented in two stages. First, existence of nonzero secrecy capacity and outage probability are presented without the effect of AN. Then by taking the AN into account, the outcomes of the proposed technique are presented from communications viewpoint via Monte Carlo simulations. In a simple single-carrier frequency-domain-equalization system, error vector magnitude (EVM) results are given for the signals captured by Bob and Eve. We assume that all nodes experience Rayleigh-distributed fading.

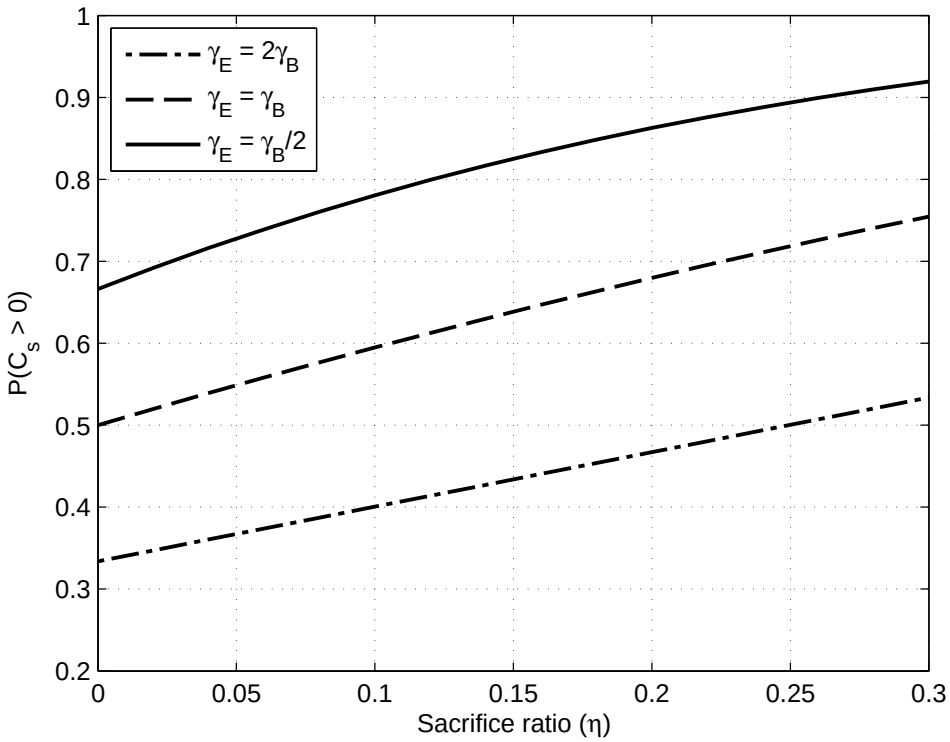

Figure 7.3 Probability of having nonzero secrecy capacity vs. sacrifice ratio for different relative SNR cases for Eve. $\gamma_{\mathrm{B}} = 1/2$.

Figure 7.3 depicts the probability of achieving nonzero secrecy capacity, $\mathcal{P}(C_{\mathrm{s}} > 0)$ as a function of sacrifice ratio, η. We set $\gamma_{\mathrm{B}} = 1/2$, and investigate different γ_{E} cases. For the symmetric case where Eve and Bob has same mean SNR, i.e., $\gamma_{\mathrm{B}} = \gamma_{\mathrm{E}}$, achieving nonzero secrecy capacity becomes highly probable as the sacrifice ratio increases. Increasing trend in probability also applies for asymmetric SNR scenarios. It is worth noting that even eavesdropper's SNR doubles the SNR of the main channel, the same secrecy performance of the symmetric case is achieved for $\eta = 0.25$. Performance for a broader SNR range can be observed in Figure 7.4 where the outage probabilities are depicted. We set a normalized[5] target secrecy rate of $R_{\mathrm{s}} = 0.1$. For $\eta = 0.1$, we achieve lower outage probabilities compared to conventional usage of the subchannels ($\eta = 0$). For instance, when $\gamma_{\mathrm{B}} = 14$ dB, SNR requirement for Eve to achieve an outage probability of $\mathcal{P}_{\mathrm{out}}(R_{\mathrm{s}}) = 6 \times 10^{-2}$ is increased from -10 dB to 0 dB with the proposed technique for $\eta = 0.1$.

[5]Normalization is done over the main channel capacity when there is no subchannel sacrifice.

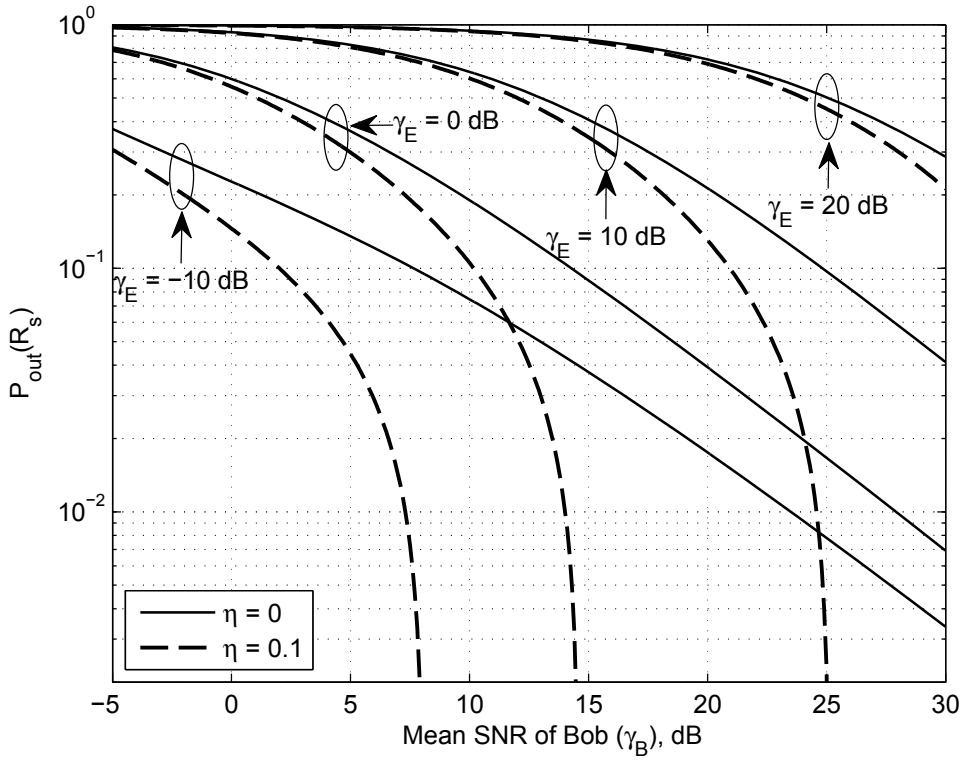

Figure 7.4 Outage probabilities as a function main channel SNR. $R_{\rm s} = 0.1$ is the normalized to the main channel capacity.

In the following, error performance is investigated for $\gamma_{\rm B} = \gamma_{\rm E}$. It is worth noting that the impact of AN on the useful symbols at unintended receiver depends on the waveform and coding schemes as well as the receiver algorithms that Eve performs. That is, various parameters, which are out of the scope of this study, have impact on the ultimate bit error rate (BER) performance. Therefore, we adopt EVM results that shows the normalized error between the ideal and the received signal. Basic modulation schemes are set to illustrate the impact of the proposed technique on the secrecy. Δf is set to 15 kHz. We generate $1,000$ data blocks with size $N = 512$ for each multipath channel realization, and the output from 100 channel realizations are averaged for the final result. Vehicular-A model [159] is used for realization of the main and the eavesdropper channel responses. Practical threshold selection is implemented as discussed in Section 7.3.2. Alice performs $\lceil (1-\eta)N \rceil$ size DFT to QPSK-modulated data symbols, then maps the output to the used subchannels locations. Depending on the scenario, the unused subchannels are nulled or populated

with zero-mean Gaussian noise with unit power. Finally, performing N-size inverse DFT and CP insertion construct the time domain block to be transmitted. Both receivers employ minimum mean square error (MMSE)-FDE by using their own CSI.

Two scenarios, i.e., solely nulling the selected subchannels and putting AN on the nulled subchannels, are considered to illustrate the effects of fade-avoiding subchannel usage and the AN separately. Figure 7.5 shows rms EVM that is measured after equalization. In nulling case, the difference between the error magnitudes for the received signals of Bob and Eve is due to difference in capacity reductions. Eve suffers from a signal power problem that cannot be solved with additional processing. As observed from Figure 7.5, EVM difference reduces with increasing SNRs. When AN is present, although the gain in EVM is moderate at low SNR regime, the reduction in performance with increasing SNR is mitigated since the distortion in received signal is a function of η rather than background noise in high SNR region. Indeed, artificially generated disturbance, which is possibly weighed with a good channel gain due to uncorrelated locations with the channel response (refer to Figure 7.2), introduces an error floor for eavesdropper.

7.6 Conclusions

Uniqueness of the wireless channel to the location of users and the unpredictability are considered for achieving communication secrecy. It is shown that without the need for CSI knowledge of the eavesdroppers, careful utilization of the resources provides improved secrecy in frequency selective channels. By avoiding the use of faded subchannels for data transmission, a gap in the channel capacity reductions for main and eavesdropper channels is achieved corresponding to positive secrecy capacity. Also, by populating the unused subchannels with artificial disturbance, further degradation for eavesdropper's reception is achieved.

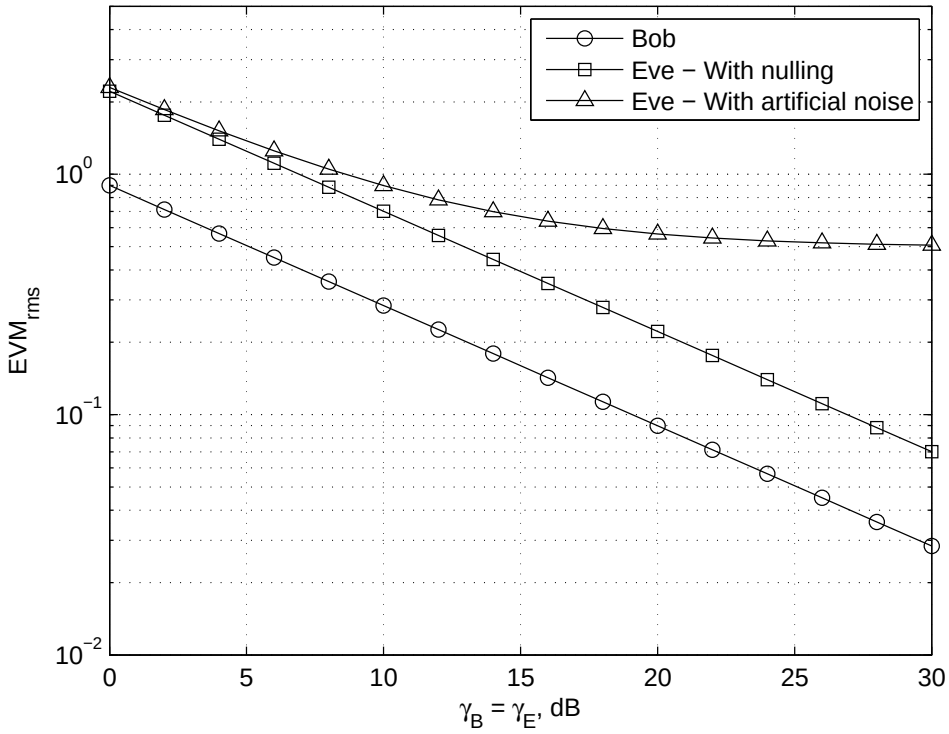

Figure 7.5 EVM for the signals received by Bob and Eve for the symmetric SNR scenario. $\eta = 0.1$.

CHAPTER 8:

CONCLUSIONS

Achieving high information transfer rates with limited spectral resources has been a long-standing challenge in wireless communications. The physical layer of the communication stack is responsible for the conversion of the information from digital binary sequences to RF signals at transmitter and the vice versa at the receiver. In this stage where various aspects such as multipath fading channel, hardware impairments and multiuser environment, waveform design plays critical role. Besides improving the signal reception at the intended receivers, securing the information content from unintended entities becomes essential in wireless transmission. In this dissertation, novel methods for improving the signal in different domains are proposed. Rather than coping with a single issue, the signal processing techniques studied in this dissertation includes OFDM-based waveform design in multiple perspectives such as OOB emission reduction, PAPR reduction, and secure transmission with minimum or no effect at the receiver side. Various concepts are coherently exploited while achieving aforementioned goals with minimal cost such as unexplored spaces in the signal space like CP, guard band, multipath fading; multivariate nature of the multicarrier signals; time spreading and location uniqueness of the wireless channels. The proposed techniques are analyzed theoretically and performance results are presented including related previous works in the literature. It is worth noting that the methods presented in the dissertation can be easily applicable to conventional orthogonal frequency-division multiplexing (OFDM) systems thanks to having no or minimal change in the receiver structure.

The author believes that there are still unexplored spaces in wireless signal space that are utilized for only a single purpose or not utilized effectively. For the future research, exploring new spaces that the multiple domains can commonly benefit and activating new opportunities by connecting these gaps with available priors such as wireless channel, multiple antennas, reference

signals, and user behavior can open new dimensions in enhancing wireless communication signal quality and physical layer information security.

REFERENCES

[1] J. W. Orton, *The Story of Semiconductors*. Oxford University Press, Feb. 2009.

[2] C. E. Shannon, "Communication in the presence of noise," *Proc. IRE*, vol. 37, pp. 10–21, Jan. 1949.

[3] H. F. Harmuth, "On the transmission of information by orthogonal time functions," *AIEE Transactions, Part I: Communication and Electronics*, vol. 79, no. 3, pp. 248–255, July 1960.

[4] R. W. Chang, "Synthesis of band-limited orthogonal signals for multichannel data transmission," *Bell System Technical Journal*, vol. 45, pp. 1775–1796, Dec. 1966.

[5] B. Saltzberg, "Performance of an efficient parallel data transmission system," *IEEE Transactions on Communication Technology*, vol. 15, no. 6, pp. 805–811, Dec. 1967.

[6] R. Chang and R. Gibby, "A theoretical study of performance of an orthogonal multiplexing data transmission scheme," *IEEE Transactions on Communication Technology*, vol. 16, no. 4, pp. 529–540, Aug. 1968.

[7] J. W. T. James W. Cooley, "An algorithm for the machine calculation of complex Fourier series," *Math. Comput.*, vol. 19, pp. 297–301, 1965.

[8] *Radio Broadcasting Systems; Digital Audio Broadcasting (DAB) to mobile, portable and fixed receivers*, ETSI - European Telecommunications Standards Institute EN 300 401 Std., Rev. 1.4.1, Aug. 2006.

[9] *Digital Video Broadcasting (DVB); Frame structure channel coding and modulation for a second generation digital terrestrial television broadcasting system (DVB-T2)*, ETSI - European Telecommunications Standards Institute EN 302 755 Std., Apr. 2012.

[10] *Very high speed digital subscriber line transceivers 2 (VDSL2)*, ITU - International Telecommunication Union - T G.993.2 Std., Dec. 2011.

[11] *IEEE Standard for Broadband over Power Line Networks: Medium Access Control and Physical Layer Specifications*, IEEE 1901 Std., 2010.

[12] *IEEE Standard for Information technology-Telecommunications and information exchange between systems Local and metropolitan area networks-Specific requirements Part 11: Wireless LAN Medium Access Control (MAC) and Physical Layer (PHY) Specifications*, IEEE 802.11 Std., 2012.

[13] *IEEE Standard for Air Interface for Broadband Wireless Access Systems*, IEEE 802.16 Std., 2012.

[14] *3rd Generation Partnership Project; Technical Specification Group Radio Access Network; Evolved Universal Terrestrial Radio Access (E-UTRA); Physical Channels and Modulation (Release 11)* , 3GPP TS 36.211 Std., Rev. 11.1.0, Dec. 2012.

[15] *IEEE Standard for Information Technology-Telecommunications and information exchange between systems Wireless Regional Area Networks (WRAN)-Specific requirements Part 22: Cognitive Wireless RAN Medium Access Control (MAC) and Physical Layer (PHY) Specifications: Policies and Procedures for Operation in the TV Bands*, IEEE 802.22 Std., 2011.

[16] C. E. Shannon, "Communication theory of secrecy systems," *Bell Syst. Tech. J.*, vol. 28, pp. 656–715, Oct. 1949.

[17] S. M. Bellovin, "Frank miller: Inventor of the one-time pad," *Cryptologia*, vol. 35, no. 3, pp. 203–222, 2011.

[18] J. Massey, "An introduction to contemporary cryptology," *Proceedings of the IEEE*, vol. 76, no. 5, pp. 533–549, 1988.

[19] U. Maurer, "Secret key agreement by public discussion from common information," *IEEE Transactions on Information Theory*, vol. 39, no. 3, pp. 733–742, 1993.

[20] A. D. Wyner, "The wire-tap channel," *Bell Syst. Tech. J.*, vol. 54, pp. 1355–1387, 1975.

[21] T. Yucek and H. Arslan, "A survey of spectrum sensing algorithms for cognitive radio applications," *IEEE Commun. Surveys Tuts.*, vol. 11, no. 1, pp. 116–130, 2009.

[22] E. Biglieri, J. Proakis, and S. Shamai, "Fading channels: information-theoretic and communications aspects," *IEEE Trans. Inf. Theory*, vol. 44, no. 6, pp. 2619–2692, 1998.

[23] S. Goel and R. Negi, "Guaranteeing secrecy using artificial noise," *IEEE Trans. Wireless Commun.*, vol. 7, no. 6, pp. 2180–2189, 2008.

[24] C. E. Shannon, "A mathematical theory of communication," *Bell Syst. Tech. J.*, vol. 27, pp. 379–423, 623–656, July, Oct. 1948.

[25] J. Barros and M. R. D. Rodrigues, "Secrecy capacity of wireless channels," in *Proc. IEEE Int. Symp. Information Theory*, 2006, pp. 356–360.

[26] I. Csiszar and J. Korner, "Broadcast channels with confidential messages," *IEEE Trans. Inf. Theory*, pp. 339–348, 1978.

[27] D. Klinc, J. Ha, S. McLaughlin, J. Barros, and B.-J. Kwak, "LDPC codes for physical layer security," in *IEEE Global Telecommunications Conference (GLOBECOM)*, Nov. 2009, pp. 1–6.

[28] ——, "LDPC codes for the Gaussian wiretap channel," *IEEE Transactions on Information Forensics and Security*, vol. 6, no. 3, pp. 532–540, Sep. 2011.

[29] M. Baldi, M. Bianchi, and F. Chiaraluce, "Non-systematic codes for physical layer security," in *IEEE Information Theory Workshop (ITW)*, Aug. 2010, pp. 1–5.

[30] ——, "Increasing physical layer security through scrambled codes and ARQ," in *IEEE International Conference on Communications Workshops (ICC)*, June 2011, pp. 1–5.

[31] ——, "Coding with scrambling, concatenation, and HARQ for the AWGN wire-tap channel: A security gap analysis," *IEEE Transactions on Information Forensics and Security*, vol. 7, no. 3, pp. 883–894, June 2012.

[32] N. Maturo, M. Baldi, M. Bianchi, and F. Chiaraluce, "Security gap assessment for the fast fading wiretap channel," in *20th International Conference on Telecommunications (ICT)*, May 2013, pp. 1–5.

[33] J. G. Proakis and M. Salehi, *Digital Communications*, 5th ed. New York: McGraw-Hill, 2008.

[34] M. Daly and J. Bernhard, "Directional modulation technique for phased arrays," *IEEE Transactions on Antennas and Propagation*, vol. 57, no. 9, pp. 2633–2640, Sep. 2009.

[35] M. Daly, E. Daly, and J. Bernhard, "Demonstration of directional modulation using a phased array," *IEEE Transactions on Antennas and Propagation*, vol. 58, no. 5, pp. 1545–1550, May 2010.

[36] R. Scholtz, "The origins of spread-spectrum communications," *IEEE Transactions on Communications*, vol. 30, no. 5, pp. 822–854, 1982.

[37] G. Prescott, "Performance metrics for low probability of intercept-communication system," Air Force Office of Scientific Research, Tech. Rep., 1993.

[38] A. Hero, "Secure space-time communication," *IEEE Transactions on Information Theory*, vol. 49, no. 12, pp. 3235–3249, Dec. 2003.

[39] F. A. P. Petitcolas, R. Anderson, and M. Kuhn, "Information hiding-a survey," *Proceedings of the IEEE*, vol. 87, no. 7, pp. 1062–1078, Jul. 1999.

[40] E. Ghashghai, "Communications networks to support integrated intelligence, surveillance, reconnaissance, and strike operations," RAND Corporation, Tech. Rep., 2004.

[41] A. F. Molisch, *Wireless Communications*, 2nd ed. Wiley, Dec. 2010.

[42] R. Pickholtz, D. Schilling, and L. Milstein, "Theory of spread-spectrum communications–A tutorial," *IEEE Transactions on Communications*, vol. 30, no. 5, pp. 855–884, 1982.

[43] X. Li, J. Hwu, and E. P. Ratazzi, "Using antenna array redundancy and channel diversity for secure wireless transmissions," *Journal of Communications*, vol. 2, no. 3, pp. 24–32, 2007.

[44] G. Burel, C. Bouder, and O. Berder, "Detection of direct sequence spread spectrum transmissions without prior knowledge," in *IEEE Global Telecommunications Conference (GLOBECOM)*, vol. 1, 2001, pp. 236–239.

[45] C. Hill, V. Comley, and E. Adams, "Techniques for detecting and characterising covert communication signals," in *IEEE Military Communications Conference (MILCOM)*, vol. 3, 1997, pp. 1361–1365.

[46] Z. Shen, B. Tang, Y. Lv, and X. Zhu, "Multiple parameters estimation simultaneously for DS-SS/BPSK signal based on fourth-order cumulant 2D slice," in *International Conference on Communications, Circuits and Systems (ICCCAS)*, vol. 2, 2004, pp. 867–870.

[47] S. Ghavami and B. Abolhassani, "Detection of DS-SS signals over fading channels without prior knowledge of spreading sequence by measuring signal nongaussianity," in *IEEE 17th International Symposium on Personal, Indoor and Mobile Radio Communications (PIMRC)*, 2006, pp. 1–5.

[48] ——, "Blind detection of DS-SS signals over fading channels using negentropy or kurtosis without any prior knowledge," in *IEEE 18th International Symposium on Personal, Indoor and Mobile Radio Communications (PIMRC)*, 2007, pp. 1–5.

[49] M. J. Mihaljevic and J. D. Golic, "Convergence of a bayesian iterative error-correction procedure on a noisy shift register sequence," in *Advances in Cryptology.* Springer Berlin Heidelberg, 1993, vol. 658, pp. 124–137.

[50] T. Hong, M.-Z. Song, and Y. Liu, "Dual-beam directional modulation technique for physical-layer secure communication," *IEEE Antennas Wireless Propag. Lett.*, vol. 10, pp. 1417–1420, 2011.

[51] *Standard for Information technology - Local and metropolitan area networks - Specific requirements - Part 11: Wireless LAN Medium Access Control (MAC)and Physical Layer (PHY) Specifications Amendment 5: Enhancements for Higher Throughput*, Std., Oct. 2009.

[52] H. Yagi and S. Uda, "Projector of the sharpest beam of electric waves," *Proc. of the Imperial Academy of Japan*, vol. 2, pp. 49–52, 1926.

[53] C. A. Balanis, *Antenna Theory: Analysis and Design.* John Wiley & Sons, 2012.

[54] K. F. Braun, "Electrical oscillations and wireless telegraphy," Nobel Lecture delivered in Dec., 1909, Reprinted in *Nobel Lectures in Physics,* Elsevier Publishing Co., Amsterdam, 1967, Available: http://www.nobelprize.org/nobel_prizes/physics/laureates/1909/braun-lecture.html.

[55] D. H. Johnson and D. E. Dudgeon, *Array Signal Processing: Concepts and Techniques.* Prentice Hall, 1993.

[56] O. Alrabadi and G. Pedersen, "Directional space-time modulation: A novel approach for secured wireless communication," in *IEEE International Conference on Communications (ICC)*, June 2012, pp. 3554–3558.

[57] E. J. Baghdady, "Directional signal modulation by means of switched spaced antennas," *IEEE Trans. Commun.*, vol. 38, no. 4, pp. 399–403, Apr. 1990.

[58] A. Babakhani, D. Rutledge, and A. Hajimiri, "Transmitter architectures based on near-field direct antenna modulation," *IEEE J. Solid-State Circuits*, vol. 43, no. 12, pp. 2674–2692, Dec. 2008.

[59] ——, "A near-field modulation technique using antenna reflector switching," in *Proc. IEEE Int. Solid State Circuits Conf.*, Feb. 2008, pp. 188–189.

[60] M. Daly and J. Bernhard, "Beamsteering in pattern reconfigurable arrays using directional modulation," *IEEE Transactions on Antennas and Propagation*, vol. 58, no. 7, pp. 2259–2265, July 2010.

[61] T. Hong, M.-Z. Song, and Y. Liu, "RF directional modulation technique using a switched antenna array for physical layer secure communication applications," *Progress In Electromagnetics Research*, vol. 116, pp. 363–379, 2011.

[62] C. Elam and D. Leavy, "Secure communication using array transmitter," US Patent 6 275 679, Aug. 14, 2001.

[63] N. Valliappan, A. Lozano, and R. Heath, "Antenna subset modulation for secure millimeter-wave wireless communication," *IEEE Trans. Commun.*, vol. 61, no. 8, pp. 3231–3245, Aug. 2013.

[64] X. Li, M. Chen, and E. P. Ratazzi, "A randomized spacetime transmission scheme for secret-key agreement," in *Conference on Information Sciences and Systems (CISS)*, 2005.

[65] ——, "Space-time transmissions for wireless secret-key agreement with information-theoretic secrecy," in *IEEE 6th Workshop Signal Processing Advances in Wireless Communications (SPAWC)*, June 2005, pp. 811–815.

[66] X. Li and E. Ratazzi, "MIMO transmissions with information-theoretic secrecy for secret-key agreement in wireless networks," in *IEEE Military Communications Conference*, Oct. 2005, pp. 1353–1359 Vol. 3.

[67] X. Li, J. Hwu, and E. P. Ratazzi, "Array redundancy and diversity for wireless transmissions with low probability of interception," in *IEEE International Conference on Acoustics, Speech and Signal Processing (ICASSP)*, vol. 4, May 2006.

[68] Q. Zhu, S. Yang, R. Yao, and Z. Nie, "Directional modulation based on 4-D antenna arrays," *IEEE Transactions on Antennas and Propagation*, vol. 62, no. 2, pp. 621–628, Feb. 2014.

[69] R. Negi and S. Goel, "Secret communication using artificial noise," in *IEEE Vehicular Technology Conference*, vol. 3, Sep. 2005, pp. 1906–1910.

[70] S. Goel and R. Negi, "Secret communication in presence of colluding eavesdroppers," in *IEEE Military Communications Conference (MILCOM)*, vol. 3, Oct. 2005, pp. 1501–1506.

[71] A. Swindlehurst, "Fixed SINR solutions for the MIMO wiretap channel," in *IEEE International Conference on Acoustics, Speech and Signal Processing (ICASSP)*, 2009, pp. 2437–2440.

[72] X. Zhou and M. McKay, "Secure transmission with artificial noise over fading channels: Achievable rate and optimal power allocation," *IEEE Transactions on Vehicular Technology*, vol. 59, no. 8, pp. 3831–3842, Oct. 2010.

[73] P.-H. Lin, S.-H. Lai, S.-C. Lin, and H.-J. Su, "On secrecy rate of the generalized artificial-noise assisted secure beamforming for wiretap channels," *IEEE Journal on Selected Areas in Communications*, vol. 31, no. 9, pp. 1728–1740, 2013.

[74] T. Hong, M.-Z. Song, and Y. Liu, "Directional sensitive modulation signal transmitted by monopulse cassegrain antenna for physical layer secure communication," *Progress In Electromagnetics Research*, vol. 17, pp. 167–181, 2011.

[75] W.-C. Liao, T.-H. Chang, W.-K. Ma, and C.-Y. Chi, "QoS-based transmit beamforming in the presence of eavesdroppers: An optimized artificial-noise-aided approach," *IEEE Transactions on Signal Processing*, vol. 59, no. 3, pp. 1202–1216, 2011.

[76] Z. Li, R. Yates, and W. Trappe, "Achieving secret communication for fast Rayleigh fading channels," *IEEE Transactions on Wireless Communications*, vol. 9, no. 9, pp. 2792–2799, 2010.

[77] H. Qin, Y. Sun, T.-H. Chang, X. Chen, C.-Y. Chi, M. Zhao, and J. Wang, "Power allocation and time-domain artificial noise design for wiretap OFDM with discrete inputs," *IEEE Transactions on Wireless Communications*, vol. 12, no. 6, pp. 2717–2729, 2013.

[78] E. Guvenkaya and H. Arslan, "Secure communication in frequency selective channels with fade-avoiding subchannel usage," in *IEEE International Conference on Communications Workshops (ICC)*, June 2014, pp. 813–818.

[79] W. Jakes, "Mobile radio propagation," in *Microwave Mobile Communications*. Wiley-IEEE Press, 1974.

[80] J. Hershey, A. Hassan, and R. Yarlagadda, "Unconventional cryptographic keying variable management," *IEEE Transactions on Communications*, vol. 43, no. 1, pp. 3–6, 1995.

[81] A. A. Hassan, W. E. Stark, J. E. Hershey, and S. Chennakeshu, "Cryptographic key agreement for mobile radio," *Digital Signal Processing*, vol. 6, no. 4, pp. 207–212, 1996.

[82] H. Koorapaty, A. A. Hassan, and S. Chennakeshu, "Secure information transmission for mobile radio," *IEEE Communications Letters*, vol. 4, no. 2, pp. 52–55, Feb. 2000.

[83] Y. Chen, W. Xu, W. Trappe, and Y. Zhang, "Securing wireless systems via lower layer enforcements," in *Securing Emerging Wireless Systems*. Springer, 2009, pp. 1–20.

[84] M. Di Renzo and M. Debbah, "Wireless physical-layer security: The challenges ahead," in *International Conference on Advanced Technologies for Communications (ATC)*, 2009, pp. 313–316.

[85] E. Guvenkaya, A. Sahin, E. Bala, R. Yang, and H. Arslan, "A windowing technique for optimal time-frequency concentration & ACI rejection in OFDM-based systems," *IEEE Transactions on Communications*, vol. PP, no. 99, to be published, early Access.

[86] A. Sahin, I. Guvenc, and H. Arslan, "A survey on multicarrier communications: Prototype filters, lattice structures, and implementation aspects," *IEEE Commun. Surveys Tuts.*, no. 99, pp. 1–27, Dec. 2013.

[87] B. Farhang-Boroujeny, "OFDM versus filter bank multicarrier," *IEEE Signal Processing Magazine*, vol. 28, no. 3, pp. 92–112, 2011.

[88] A. Vahlin and N. Holte, "Optimal finite duration pulses for OFDM," *IEEE Trans. Commun.*, vol. 44, no. 1, pp. 10–14, 1996.

[89] T. Ihalainen, T. Hidalgo Stitz, M. Rinne, and M. Renfors, "Channel equalization in filter bank based multicarrier modulation for wireless communications," *EURASIP J. Advances in Signal Process.*, 2007.

[90] T. Ihalainen, A. Ikhlef, J. Louveaux, and M. Renfors, "Channel equalization for multi-antenna FBMC/OQAM receivers," *IEEE Trans. Veh. Technol.*, vol. 60, no. 5, pp. 2070–2085, 2011.

[91] N. Michailow, M. Matthe, I. Gaspar, A. Caldevilla, L. Mendes, A. Festag, and G. Fettweis, "Generalized frequency division multiplexing for 5th generation cellular networks," *IEEE Trans. Commun.*, vol. 62, no. 9, pp. 3045–3061, 2014.

[92] G. Fettweis, M. Krondorf, and S. Bittner, "GFDM - Generalized Frequency Division Multiplexing," in *Proc. IEEE Veh. Technol. Conf. (VTC)*, 2009, pp. 1–4.

[93] T. Weiss, J. Hillenbrand, A. Krohn, and F. Jondral, "Mutual interference in OFDM-based spectrum pooling systems," in *Proc. IEEE Veh. Technol. Conf. (VTC)*, vol. 4, May 2004, pp. 1873–1877.

[94] B. Farhang-Boroujeny and R. Kempter, "Multicarrier communication techniques for spectrum sensing and communication in cognitive radios," *IEEE Communications Magazine*, vol. 46, no. 4, pp. 80–85, 2008.

[95] P. Sutton, B. Ozgul, I. Macaluso, and L. Doyle, "OFDM Pulse-Shaped Waveforms for Dynamic Spectrum Access Networks," in *Proc. IEEE Symp. New Frontiers in Dynamic Spectrum (DySPAN)*, 2010, pp. 1–2.

[96] A. Sahin and H. Arslan, "Edge windowing for OFDM based systems," *IEEE Communications Letters*, vol. 15, no. 11, pp. 1208–1211, 2011.

[97] ——, "The impact of scheduling on edge windowing," in *Proc. IEEE Global Telecommun. Conf.*, 2011, pp. 1–5.

[98] E. Bala, J. Li, and R. Yang, "Shaping spectral leakage: A novel low-complexity transceiver architecture for cognitive radio," *IEEE Veh. Technol. Mag.*, vol. 8, no. 3, pp. 38–46, Sep. 2013.

[99] I. Macaluso, B. Ozgul, T. Forde, P. Sutton, and L. Doyle, "Spectrum and energy efficient block edge mask-compliant waveforms for dynamic environments," *IEEE J. Sel. Areas Commun.*, vol. 32, no. 2, pp. 307–321, Feb. 2014.

[100] E. Guvenkaya, E. Bala, R. Yang, and H. Arslan, "Time-asymmetric and subcarrier-specific pulse shaping in OFDM-based waveforms," *IEEE Trans. Veh. Technol.*, pp. 1–1, Dec. 2014.

[101] *Wireless LAN Medium Access Control (MAC) and Physical Layer (PHY) Specification*, IEEE Std. 802.11, 2012.

[102] *Cognitive Wireless RAN Medium Access Control (MAC) and Physical Layer (PHY) Specifications: Policies and Procedures for Operation in the TV Bands*, IEEE Std. 802.22, 2011.

[103] H. Lin and P. Siohan, "Multi-carrier modulation analysis and WCP-COQAM proposal," *EURASIP J Adv Signal Process*, vol. 2014, no. 1, p. 79, 2014. [Online]. Available: http://dx.doi.org/10.1186/1687-6180-2014-79

[104] M. Benedicks, "On fourier transforms of functions supported on sets of finite Lebesgue measure," *Journal of mathematical analysis and applications*, vol. 106, no. 1, pp. 180–183, 1985.

[105] D. Slepian, "Prolate spheroidal wave functions, Fourier analysis and uncertainty-V: The discrete case," *Bell Syst. Tech. J.*, vol. 57, pp. 1371–1430, May 1978.

[106] A. Sahin, E. Bala, I. Guvenc, R. Yang, and H. Arslan, "Partially overlapping tones for uncoordinated networks," *IEEE Trans. Commun.*, vol. 62, no. 9, pp. 3363–3375, Sep. 2014.

[107] B. N. Parlett, *The Symmetric Eigenvalue Problem (Classics in Applied Mathematics)*. Society for Industrial and Applied Mathematics, 1 1987.

[108] R. A. Horn and C. R. Johnson, *Matrix Analysis*, 2nd ed. Cambridge University Press, 10 2012.

[109] C. Muschallik, "Improving an OFDM reception using an adaptive Nyquist windowing," *IEEE Trans. Consum. Electron.*, vol. 42, no. 3, pp. 259–269, 1996.

[110] J. Armstrong, "Analysis of new and existing methods of reducing intercarrier interference due to carrier frequency offset in OFDM," *IEEE Trans. Commun.*, vol. 47, no. 3, pp. 365–369, 1999.

[111] S. Muller-Weinfurtner, "Optimum Nyquist windowing in OFDM receivers," *IEEE Trans. Commun.*, vol. 49, no. 3, pp. 417–420, 2001.

[112] A. Seyedi and G. Saulnier, "General ICI self-cancellation scheme for OFDM systems," *IEEE Trans. Veh. Technol.*, vol. 54, no. 1, pp. 198–210, 2005.

[113] N. Beaulieu and P. Tan, "On the effects of receiver windowing on OFDM performance in the presence of carrier frequency offset," *IEEE Trans. Wireless Commun.*, vol. 6, no. 1, pp. 202–209, 2007.

[114] J. F. Kaiser, "Digital filters," in *System Analysis by Digital Computer*, F. F. Kuo and J. F. Kaiser, Eds. New York: Wiley, 1966, pp. 218–285.

[115] C. Murphy, "Low-complexity FFT structures for OFDM transceivers," *IEEE Trans. Commun.*, vol. 50, no. 12, pp. 1878–1881, 2002.

[116] H. Mahmoud, T. Yucek, and H. Arslan, "OFDM for cognitive radio: Merits and challenges," *IEEE Wireless Communications*, vol. 16, no. 2, pp. 6–15, Apr. 2009.

[117] C.-L. Liu and K. Feher, "An asymmetrical pulse shaping technique to combat delay spread," *IEEE Trans. Veh. Technol.*, vol. 42, no. 4, pp. 425–433, 1993.

[118] V. Erceg, D. Michelson, S. Ghassemzadeh, L. Greenstein, J. Rustako, A.J., P. Guerlain, M. Dennison, R. Roman, D. Barnickel, S. Wang, and R. Miller, "A model for the multipath delay profile of fixed wireless channels," *IEEE J. Sel. Areas Commun.*, vol. 17, no. 3, pp. 399–410, Mar. 1999.

[119] K. M. Anstreicher, "On convex relaxations for quadratically constrained quadratic programming," *Mathematical Programming*, vol. 136, no. 2, pp. 233–251, Dec 2012.

[120] A. Tom, A. Sahin, and H. Arslan, "Mask Compliant Precoder for OFDM Spectrum Shaping," *IEEE Communications Letters*, vol. 17, no. 3, pp. 447–450, 2013.

[121] L. Greenstein, V. Erceg, Y. Yeh, and M. Clark, "A new path-gain/delay-spread propagation model for digital cellular channels," *IEEE Trans. Veh. Technol.*, vol. 46, no. 2, pp. 477–485, May 1997.

[122] J. van de Beek, "Sculpting the multicarrier spectrum: a novel projection precoder," *IEEE Communications Letters*, vol. 13, no. 12, pp. 881–883, 2009.

[123] W. Jiang and M. Schellmann, "Suppressing the out-of-band power radiation in multi-carrier systems: A comparative study," in *Proc. IEEE Global Telecommun. Conf.*, 2012, pp. 1477–1482.

[124] P. Kryszkiewicz, H. Bogucka, and A. M. Wyglinski, "Protection of primary users in dynamically varying radio environment: Practical solutions and challenges," *EURASIP J. on wireless commun. and networking*, no. 1, pp. 1–20, 2012.

[125] K. Cho and D. Yoon, "On the general BER expression of one- and two-dimensional amplitude modulations," *IEEE Trans. Commun.*, vol. 50, no. 7, pp. 1074–1080, July 2002.

[126] E. Guvenkaya, A. Tom, and H. Arslan, "Joint sidelobe suppression and PAPR reduction in OFDM using partial transmit sequences," in *IEEE Military Communications Conference*, 2013, pp. 95–100.

[127] S. Brandes, I. Cosovic, and M. Schnell, "Reduction of out-of-band radiation in OFDM systems by insertion of cancellation carriers," *IEEE Communications Letters*, vol. 10, no. 6, pp. 420–422, Jun. 2006.

[128] I. Cosovic and T. Mazzoni, "Suppression of sidelobes in OFDM systems by multiple-choice sequences," *Eur. Trans. Telecomms.*, vol. 17, pp. 623–630, 2006.

[129] H. Mahmoud and H. Arslan, "Sidelobe suppression in OFDM-based spectrum sharing systems using adaptive symbol transition," *IEEE Communications Letters*, vol. 12, no. 2, pp. 133–135, Feb. 2008.

[130] J. van de Beek and F. Berggren, "N-continuous OFDM," *IEEE Communications Letters*, vol. 13, no. 1, pp. 1–3, Jan. 2009.

[131] E. Costa, M. Midrio, and S. Pupolin, "Impact of amplifier nonlinearities on OFDM transmission system performance," *IEEE Communications Letters*, vol. 3, no. 2, pp. 37–39, 1999.

[132] S. H. Han and J. H. Lee, "An overview of peak-to-average power ratio reduction techniques for multicarrier transmission," *IEEE Wireless Communications*, vol. 12, no. 2, pp. 56–65, 2005.

[133] S. H. Muller and J. B. Huber, "OFDM with reduced peak-to-average power ratio by optimum combination of partial transmit sequences," *Electron. Lett.*, vol. 33, no. 5, pp. 368–369, Feb. 1997.

[134] R. Bauml, R. F. H. Fischer, and J. Huber, "Reducing the peak-to-average power ratio of multicarrier modulation by selected mapping," *Electron. Lett.*, vol. 32, no. 22, pp. 2056–2057, Oct. 1996.

[135] A. Ghassemi, L. Lampe, A. Attar, and T. Gulliver, "Joint sidelobe and peak power reduction in ofdm-based cognitive radio," in *Proc. IEEE Vehic. Tech. Conf.*, Sept. 2010, pp. 1–5.

[136] Z.-Q. Luo, W.-K. Ma, A.-C. So, Y. Ye, and S. Zhang, "Semidefinite Relaxation of Quadratic Optimization Problems," *IEEE Signal Processing Magazine*, vol. 27, no. 3, pp. 20–34, 2010.

[137] L. J. Cimini and N. R. Sollenberger, "Peak-to-average power ratio reduction of an OFDM signal using partial transmit sequences," *IEEE Commun. Lett.*, vol. 4, no. 3, pp. 86–88, 2000.

[138] A. D. S. Jayalath and C. Tellambura, "Adaptive PTS approach for reduction of peak-to-average power ratio of OFDM signal," *Electron. Lett.*, vol. 36, no. 14, pp. 1226–1228, 2000.

[139] C. Tellambura, "Improved phase factor computation for the PAR reduction of an OFDM signal using PTS," *IEEE Communications Letters*, vol. 5, no. 4, pp. 135–137, 2001.

[140] S. H. Han and J. H. Lee, "PAPR reduction of OFDM signals using a reduced complexity PTS technique," *IEEE Signal Process. Lett.*, vol. 11, no. 11, pp. 887–890, 2004.

[141] T. T. Nguyen and L. Lampe, "On partial transmit sequences for PAR reduction in OFDM systems," *IEEE Trans. Wireless Commun.*, vol. 7, no. 2, pp. 746–755, 2008.

[142] M. Sharif, M. Gharavi-Alkhansari, and B. Khalaj, "New results on the peak power of OFDM signals based on oversampling," in *IEEE International Conference on Communications*, vol. 2, 2002, pp. 866–871 vol.2.

[143] K. Osborn, "Army demonstrating wideband waveforms," *The United States Army*, April 1, 2011. [Online]. Available: http://www.army.mil/article/54285/army-demonstrating-wideband-waveforms

[144] E. Guvenkaya, A. Sahin, and H. Arslan, "N-continuous OFDM with cp alignment," in *IEEE Military Communications Conference*, Oct. 2015.

[145] T. Weiss and F. Jondral, "Spectrum pooling: an innovative strategy for the enhancement of spectrum efficiency," *IEEE Communications Magazine*, vol. 42, no. 3, pp. S8 – 14, mar 2004.

[146] M. Maso, S. Lakshminarayana, T. Quek, and H. Poor, "A composite approach to self-sustainable transmissions: Rethinking OFDM," *IEEE Transactions on Communications*, vol. 62, no. 11, pp. 3904–3917, Nov. 2014.

[147] ——, "The price of self-sustainability for block transmission systems," *IEEE Journal on Selected Areas in Communications*, to be published, early Access.

[148] A. Tom, A. Sahin, and H. Arslan, "Suppressing alignment: An approach for out-of-band interference reduction in OFDM systems," in *Proc. IEEE International Conference on Communications (ICC)*, London, UK, June 2015, accepted.

[149] G. Strang, *Linear Algebra and Its Applications*, 4th ed. Cengage Learning, 7 2005.

[150] Y.-S. Shiu, S.-Y. Chang, H.-C. Wu, S.-H. Huang, and H.-H. Chen, "Physical layer security in wireless networks: A tutorial," *IEEE Wireless Communications*, vol. 18, no. 2, pp. 66–74, 2011.

[151] Y. Liang, H. Poor, and S. Shamai, "Secure communication over fading channels," *IEEE Trans. Inf. Theory*, vol. 54, no. 6, pp. 2470–2492, 2008.

[152] P. Parada and R. Blahut, "Secrecy capacity of simo and slow fading channels," in *Proc. IEEE Int. Symp. Information Theory*, 2005, pp. 2152–2155.

[153] P. K. Gopala, L. Lai, and H. El-Gamal, "On the secrecy capacity of fading channels," *IEEE Trans. Inf. Theory*, vol. 54, no. 10, pp. 4687–4698, 2008.

[154] M. Kobayashi, M. Debbah, and S. S. (Shitz), "Secured communication over frequency-selective fading channels: A practical vandermonde precoding," *EURASIP Journal on Wireless Communications and Networking*, 2009.

[155] D. Tse and P. Viswanath, *Fundamentals of Wireless Communication*. Cambridge University Press, 2005.

[156] L. Xiao, L. Greenstein, N. B. Mandayam, and W. Trappe, "Using the physical layer for wireless authentication in time-variant channels," *IEEE Transactions on Wireless Communications*, vol. 7, pp. 2571–2579, 2008.

[157] D. Falconer, S. Ariyavisitakul, A. Benyamin-Seeyar, and B. Eidson, "Frequency domain equalization for single-carrier broadband wireless systems," *IEEE Communications Magazine*, vol. 40, no. 4, pp. 58–66, 2002.

[158] T. S. Rappaport, *Wireless Communications: Principles and Practice (2nd Edition)*. Prentice Hall, 2002.

[159] "Rec. ITU-R M.1225: Guidelines for Evaluation of Radio Transmission Technologies for IMT-2000," International Telecommunication Union, Tech. Rep., 1997.

APPENDICES

Appendix A: Derivation Steps

By defining $\hat{w}_k^{(i)}(t) = w_{ki}^{(i)}(t + iT)$ and $\hat{q}_l^{(\epsilon)}(t) = q_{lu}^{(\epsilon)}(t + uT)$, we can make the pulse shape function variables independent of i and u by taking the symbol indexes into the argument of the functions. By substituting the above definitions, (3.30) is rewritten as

$$I_{lu}^{(i)} = \frac{\alpha_i}{T} \sum_{k=-\frac{N_i}{2}}^{\frac{N_i}{2}-1} \sum_{i\in\mathbb{Z}} \int_{-T/2}^{T/2} \left| \langle \hat{w}_k^{(i)}(t + \Delta t_i - iT), \hat{q}_l^{(\epsilon)}(t - uT) \rangle \right|^2 \mathrm{d}\Delta t_i. \tag{A.1}$$

Then by making the necessary change of variables for Δt_i we can update the limits of integration. Also, by considering the summation over symbol index i, the region of the integrals for each summation combines and spans the whole real number set. In other words, the inner summation and the integration in (A.1) combines into one integration as

$$I_{lu}^{(i)} = \frac{\alpha_i}{T} \sum_{k=-\frac{N_i}{2}}^{\frac{N_i}{2}-1} \int_{-\infty}^{\infty} \left| \langle \hat{w}_k^{(i)}(t + \Delta t_i - uT), \hat{q}_l^{(\epsilon)}(t - uT) \rangle \right|^2 \mathrm{d}\Delta t_i \tag{A.2}$$

where the time shift uT is added in transmitter pulse function which will be used to omit common uT terms in the next step. Note that since the integration runs over infinity, any shift in Δt_i does not have an impact on the result. From open form of the correlator operation and the definition of the convolution, we can rewrite the (A.2) as

$$\begin{aligned} I_{lu}^{(i)} &= \frac{\alpha_i}{T} \sum_{k=-\frac{N_i}{2}}^{\frac{N_i}{2}-1} \int_{-\infty}^{\infty} \left| \int_t \hat{w}_k^{(i)}(t + \Delta t_i) \overline{\hat{q}_l^{(\epsilon)}(t)} \mathrm{d}t \right|^2 \mathrm{d}\Delta t_i \\ &= \frac{\alpha_i}{T} \sum_{k=-\frac{N_i}{2}}^{\frac{N_i}{2}-1} \int_{-\infty}^{\infty} \left| \left(\hat{w}_k^{(i)} * \overline{\hat{q}_l^{(\epsilon)}} \right)(\Delta t_i) \right|^2 \mathrm{d}\Delta t_i. \end{aligned} \tag{A.3}$$

Appendix A (Continued)

Then by using the convolution theorem and the inverse Fourier transform (FT), we can represent (A.3) by the frequency domain functions as

$$\begin{aligned} I_{lu}^{(i)} &= \frac{\alpha_i}{T} \sum_{k=-\frac{N_i}{2}}^{\frac{N_i}{2}-1} \int_{-\infty}^{\infty} \left| \int_f \hat{W}_k^{(i)}(f) \overline{\hat{Q}_l^{(\epsilon)}(f)} e^{j2\pi f \Delta t_i} \mathrm{d}f \right|^2 \mathrm{d}\Delta t_i \\ &= \frac{\alpha_i}{T} \sum_{k=-\frac{N_i}{2}}^{\frac{N_i}{2}-1} \int_f \left| W_k^{(i)}(f - k\Delta f - \Delta f_i) \overline{Q_l^{(\epsilon)}(f - l\Delta f)} \right|^2 \mathrm{d}f \end{aligned} \tag{A.4}$$

where $\hat{W}_k^{(i)}(f)$, $\hat{Q}_l^{(\epsilon)}(f)$, $W_k^{(i)}(f)$, and $Q_l^{(\epsilon)}(f)$ are the FTs of $\hat{w}_k^{(i)}(t)$, $\hat{q}_l^{(\epsilon)}(t)$, $w_k^{(i)}(t)$, and $q_l^{(\epsilon)}(t)$, respectively.

Appendix B: List of Acronyms

Acronym	Description
3G	third generation
4G	fourth generation
ACI	adjacent-channel interference
ADSL	asymmetric digital subscriber line
AN	artificial noise
AWGN	additive white Gaussian noise
BER	bit error rate
BPL	Broadband over Power Line
BS	base station
CCDF	complementary cumulative distribution function
CDF	cumulative distribution function
CFO	carrier frequency offset
CIR	channel impulse response
CP	cyclic prefix
CR	cognitive radio
CSI	channel state information
DAB	Digital Audio Broadcasting
DFT	discrete Fourier transform
DSA	dynamic spectrum access
DTFT	discrete-time Fourier transform
DVB-T2	Terrestrial Digital Video Broadcasting
DPSS	discrete prolate spheroidal sequences
E-UTRA	Evolved Universal Terrestrial Radio Access
EVM	error vector magnitude

Appendix B (Continued)

FBMC	filter bank multicarrier
FDE	frequency domain equalization
FFT	fast Fourier transform
FT	Fourier transform
GA	genetic algorithm
GFDM	generalized frequency-division multiplexing
GKW	generalized Kaiser window
ICI	inter-carrier interference
IDFT	inverse discrete Fourier transform
IFFT	inverse fast Fourier transform
i.i.d.	independent and identically distributed
ISI	inter-symbol interference
LDPC	low-density parity-check
LFSR	linear-feedback shift register
LOS	line-of-sight
LPD	low-probability-of-detection
LPI	low-probability-of-interception
LTE	Long Term Evolution
MAN	metropolitan-area networks
MCS	multiple-choice sequences
MED	maximum excess delay
MIMO	multiple-input multiple-output
MISO	multiple-input single-output
ML	maximum likelihood
MMSE	minimum mean square error
MSE	mean-squared error

Appendix B (Continued)

NLOS	non-LOS
NP	non-polynomial
OFDM	orthogonal frequency-division multiplexing
OFDMA	orthogonal frequency-division multiple access
OQAM	offset-QAM
OOB	out-of-band
OTP	One-time pad
PA	power amplifier
PAPR	peak-to-average power ratio
per-SC	per-subcarrier
PDF	Probability density function
PDP	power delay profile
PHY	physical layer
PN	pseudo-noise
PPM	pulse position modulation
PSD	power spectral density
PSWF	prolate spheroidal wave function
PTS	partial transmit sequences
QAM	quadrature amplitude modulation
QCQP	quadratically constraint quadratic problem
QPSK	quadrature phase-shift keying
RB	resource block
RC	raised-cosine
RF	radio frequency
rms	root mean square
SC-FDE	single-carrier frequency-domain-equalization

Appendix B (Continued)

SE	spectral efficiency
SIMO	single-input multiple-outputs
SINR	signal to interference plus noise ratio
SISO	single-input single-output
SISOSE	single-input single-output single-eavesdropper
SLM	selected mapping
SNR	signal-to-noise ratio
SS	spread spectrum
SVD	singular value decomposition
TDE	time domain equalization
VDSL2	Very-high-speed digital subscriber line 2
WiMAX	Worldwide Interoperability for Microwave Access
WLAN	wireless local area network
WNW	wideband networking waveform
ZF	zero forcing

Appendix C: Copyright Notices

The following notice is for the material in Chapter 3.

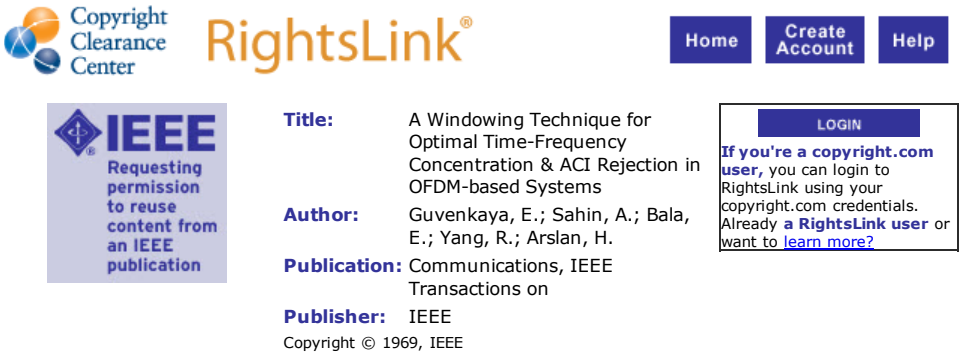

Copyright Clearance Center RightsLink®

Home | Create Account | Help

IEEE Requesting permission to reuse content from an IEEE publication

Title: A Windowing Technique for Optimal Time-Frequency Concentration & ACI Rejection in OFDM-based Systems

Author: Guvenkaya, E.; Sahin, A.; Bala, E.; Yang, R.; Arslan, H.

Publication: Communications, IEEE Transactions on

Publisher: IEEE

Copyright © 1969, IEEE

LOGIN

If you're a copyright.com user, you can login to RightsLink using your copyright.com credentials. Already **a RightsLink user** or want to learn more?

Thesis / Dissertation Reuse

The IEEE does not require individuals working on a thesis to obtain a formal reuse license, however, you may print out this statement to be used as a permission grant:

Requirements to be followed when using any portion (e.g., figure, graph, table, or textual material) of an IEEE copyrighted paper in a thesis:

1) In the case of textual material (e.g., using short quotes or referring to the work within these papers) users must give full credit to the original source (author, paper, publication) followed by the IEEE copyright line © 2011 IEEE.
2) In the case of illustrations or tabular material, we require that the copyright line © [Year of original publication] IEEE appear prominently with each reprinted figure and/or table.
3) If a substantial portion of the original paper is to be used, and if you are not the senior author, also obtain the senior author's approval.

Requirements to be followed when using an entire IEEE copyrighted paper in a thesis:

1) The following IEEE copyright/ credit notice should be placed prominently in the references: © [year of original publication] IEEE. Reprinted, with permission, from [author names, paper title, IEEE publication title, and month/year of publication]
2) Only the accepted version of an IEEE copyrighted paper can be used when posting the paper or your thesis on-line.
3) In placing the thesis on the author's university website, please display the following message in a prominent place on the website: In reference to IEEE copyrighted material which is used with permission in this thesis, the IEEE does not endorse any of [university/educational entity's name goes here]'s products or services. Internal or personal use of this material is permitted. If interested in reprinting/republishing IEEE copyrighted material for advertising or promotional purposes or for creating new collective works for resale or redistribution, please go to http://www.ieee.org/publications_standards/publications/rights/rights_link.html to learn how to obtain a License from RightsLink.

If applicable, University Microfilms and/or ProQuest Library, or the Archives of Canada may supply single copies of the dissertation.

BACK | CLOSE WINDOW

Appendix C (Continued)

The following notice is for the material in Chapter 4.

Title: Time-Asymmetric and Subcarrier-Specific Pulse Shaping in OFDM-Based Waveforms

Author: Guvenkaya, E.; Bala, E.; Yang, R.; Arslan, H.

Publication: Vehicular Technology, IEEE Transactions on

Publisher: IEEE

Copyright © 1969, IEEE

LOGIN

If you're a copyright.com user, you can login to RightsLink using your copyright.com credentials. Already **a RightsLink user** or want to learn more?

Thesis / Dissertation Reuse

The IEEE does not require individuals working on a thesis to obtain a formal reuse license, however, you may print out this statement to be used as a permission grant:

Requirements to be followed when using any portion (e.g., figure, graph, table, or textual material) of an IEEE copyrighted paper in a thesis:

1) In the case of textual material (e.g., using short quotes or referring to the work within these papers) users must give full credit to the original source (author, paper, publication) followed by the IEEE copyright line © 2011 IEEE.
2) In the case of illustrations or tabular material, we require that the copyright line © [Year of original publication] IEEE appear prominently with each reprinted figure and/or table.
3) If a substantial portion of the original paper is to be used, and if you are not the senior author, also obtain the senior author's approval.

Requirements to be followed when using an entire IEEE copyrighted paper in a thesis:

1) The following IEEE copyright/ credit notice should be placed prominently in the references: © [year of original publication] IEEE. Reprinted, with permission, from [author names, paper title, IEEE publication title, and month/year of publication]
2) Only the accepted version of an IEEE copyrighted paper can be used when posting the paper or your thesis on-line.
3) In placing the thesis on the author's university website, please display the following message in a prominent place on the website: In reference to IEEE copyrighted material which is used with permission in this thesis, the IEEE does not endorse any of [university/educational entity's name goes here]'s products or services. Internal or personal use of this material is permitted. If interested in reprinting/republishing IEEE copyrighted material for advertising or promotional purposes or for creating new collective works for resale or redistribution, please go to http://www.ieee.org/publications_standards/publications/rights/rights_link.html to learn how to obtain a License from RightsLink.

If applicable, University Microfilms and/or ProQuest Library, or the Archives of Canada may supply single copies of the dissertation.

BACK CLOSE WINDOW

Appendix C (Continued)

The following notice is for the material in Chapter 5.

Home | Create Account | Help

Title: Joint Sidelobe Suppression and PAPR Reduction in OFDM Using Partial Transmit Sequences

Conference Proceedings: Military Communications Conference, MILCOM 2013 - 2013 IEEE

Author: Guvenkaya, E.; Tom, A.; Arslan, H.

Publisher: IEEE

Date: 18-20 Nov. 2013

Copyright © 2013, IEEE

LOGIN

If you're a copyright.com user, you can login to RightsLink using your copyright.com credentials. Already **a RightsLink user** or want to learn more?

Thesis / Dissertation Reuse

The IEEE does not require individuals working on a thesis to obtain a formal reuse license, however, you may print out this statement to be used as a permission grant:

Requirements to be followed when using any portion (e.g., figure, graph, table, or textual material) of an IEEE copyrighted paper in a thesis:

1) In the case of textual material (e.g., using short quotes or referring to the work within these papers) users must give full credit to the original source (author, paper, publication) followed by the IEEE copyright line © 2011 IEEE.
2) In the case of illustrations or tabular material, we require that the copyright line © [Year of original publication] IEEE appear prominently with each reprinted figure and/or table.
3) If a substantial portion of the original paper is to be used, and if you are not the senior author, also obtain the senior author's approval.

Requirements to be followed when using an entire IEEE copyrighted paper in a thesis:

1) The following IEEE copyright/ credit notice should be placed prominently in the references: © [year of original publication] IEEE. Reprinted, with permission, from [author names, paper title, IEEE publication title, and month/year of publication]
2) Only the accepted version of an IEEE copyrighted paper can be used when posting the paper or your thesis on-line.
3) In placing the thesis on the author's university website, please display the following message in a prominent place on the website: In reference to IEEE copyrighted material which is used with permission in this thesis, the IEEE does not endorse any of [university/educational entity's name goes here]'s products or services. Internal or personal use of this material is permitted. If interested in reprinting/republishing IEEE copyrighted material for advertising or promotional purposes or for creating new collective works for resale or redistribution, please go to http://www.ieee.org/publications_standards/publications/rights/rights_link.html to learn how to obtain a License from RightsLink.

If applicable, University Microfilms and/or ProQuest Library, or the Archives of Canada may supply single copies of the dissertation.

BACK | CLOSE WINDOW

Appendix C (Continued)

The following notice is for the material in Chapter 6.

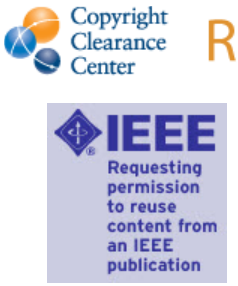

Appendix C (Continued)

The following notice is for the material in Chapter 7.

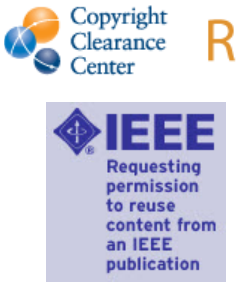

ABOUT THE AUTHOR

Ertuğrul Güvenkaya received the B.Sc. (summa cum laude) degree in Electrical and Electronics Engineering from Middle East Technical University (METU), Turkey in 2011; and M.S. in Electrical Engineering from University of South Florida, FL. He is currently working towards the Ph.D. degree in the same department. His research interests include multicarrier waveform design and physical layer security in wireless communications.